



DELFT UNIVERSITY OF TECHNOLOGY
FACULTY OF CIVIL ENGINEERING AND GEOSCIENCES
DEPARTMENT OF GEO-ENGINEERING

Extension of Automated Parameter
Determination framework to cope
with fine-grained soils

Author

F. J. PADULI

Committee

Dr. Ir. R. B. J. BRINKGREVE, TU Delft

Prof. Dr. K. G. GAVIN, TU Delft

Ir. H. J. LENGKEEK, TU Delft

to obtain the degree of Master of Science at Delft University of Technology,
to be defended publicly on Friday September 10, 2021 at 10:30h

Abstract

The Automated Parameter Determination project aims to provide advanced geotechnical models parameters from in-situ tests in a transparent and flexible process. The framework was initially developed for coarse-grained soils, and it was needed to be expanded to all types of common soils.

This report presents the expansion of the APD database to deal with fine-grained soils, claylike soils specifically. The APD variability assessment framework is customised to deal with log-transformed correlations' uncertainty. Moreover, it is found a large dependency on Atterberg limits for claylike soils parametrisation. Only one set of correlations from CPT database is found in literature to obtain these limits, for which a new set is developed based on critical state soil mechanics and the assumption that the CPT friction sleeve is similar to the remoulded undrained shear strength.

The proposed correlation is validated with a published database, showing acceptable results with similar variability when compared to the existing equation. A first validation of the complete model parameters for fine-grained soils using Plaxis Hardening Soil with small strain stiffness model is achieved. The Plaxis Soil Test facility is used and the results are compared with triaxial and oedometer tests, showing good results in compressibility characterisation and low estimation of friction angle, possibly attributed to organic and silt content. The friction angle characterisation is discussed, and it is concluded that a better estimation for fine-grained soils is needed to be studied. Further studies on soils in between claylike and sandlike behaviour is needed, as well for organics.

Keywords: parameter determination, Atterberg Limits, cone penetration test (CPT), Plaxis Hardening Soil model, log-transformed correlations.

Acknowledgements

I decided to become an engineer before starting high school. I graduated as Civil Engineer in my hometown, Santa Fe, Argentina, and not exhausted from a six-year degree I decided to continue my studies. After an unforgettable experience overseas with my partner, Josefina, we aspired to our dream of improving our knowledge with a master's degree. I am delighted to finish this exciting adventure.

First of all, I would like to express my gratitude to my graduation committee. Mainly, I would like to thank Ronald Brinkgreve for introducing me to the exciting APD project and encouraged me to keep on the right path with his precise, sound advice. Furthermore, I am highly grateful to Arny Lengkeek for being an inspirational icon who always gave constructive feedbacks on statistics and geotechnical aspects. I am also thankful to the APD team, particularly Neethu Ragi Manoj, who has a successful professional career ahead, for the working time together.

Secondly, the last years of personal growth are unique and are the merits of wonderful people. I would like to show my gratitude to my big, lovely family, who supported and encouraged me to pursue this journey. This degree would not have been possible without my adventure partner, Josefina, who was my pillar and always had love and an ear for me.

A special thanks go to Nicolas and Sandy. They gave me precious memories when being far away from my hometown, the opportunity to work with them, and to take this adventure.

Finally, I would like to thank the friends I made in the master, from my student partners to Anesh and Paul, my flatmates. Especially to the Monicas, with whom I spent unforgettable moments and made my days in the Netherlands.

Contents

1	Introduction	6
1.1	Problem description	6
1.1.1	Motivation	6
1.1.2	Main idea of the APD project	6
1.1.3	State of APD development	7
1.2	Research Questions and Methods	8
1.3	Thesis outline	9
2	Automatic Parameter Determination framework achievements	10
2.1	Introduction	10
2.2	Graph theory in APD framework	10
2.2.1	Workflow to generate paths	11
2.2.2	External database	12
2.3	Statistical framework on APD	12
2.3.1	Parameter’s uncertainty	13
2.3.2	Method’s uncertainty	13
2.3.3	Distribution of uncertainty of in-situ measurements	14
2.3.4	Propagation of the uncertainty	14
2.3.5	Model averaging in APD	15
2.4	Circular references in fine-grained soils correlations	16
3	Literature review of fine grained	17
3.1	Introduction	17
3.2	Physical based characterisation	17
3.3	Behaviour based characterisation	18
3.3.1	CPT behaviour based characterisation	18
3.3.2	Micro-structure identification using SCPT	23
3.4	Key-parameter on fine grained soil engineering properties	25
3.4.1	Definition of key-parameter for APD framework on coarse-grained soils	25
3.4.2	Definition of key-parameter for fine grained soils	25
3.5	Conclusion on fine-grained soil characterisation on APD framework	32
4	Implementation of correlations for fine grained soils	34
4.1	Soil correlations introduction	34
4.2	Soil correlations in APD framework	34
4.2.1	Non normality variability of regression’s correlations	34
4.2.2	Logarithmic transformation	36

4.2.3	Implementation of coefficient of variation in APD program variability assessment	39
4.3	New filters on correlations	40
4.4	Verification of implemented correlations	40
4.4.1	Methods Unit Tests	40
4.5	Conclusions	41
5	From CPT measurements to clay properties	42
5.1	Clay properties introduction	42
5.2	The objective: Hardening Soil model's parameters	42
5.2.1	The Hardening Soil model with small-strain stiffness, (HSsmall)	43
5.2.2	Soft Soil model	44
5.2.3	Identification of current model parameter determination problem for fine-grained soils	44
5.3	Existing clay constants correlations and frameworks	45
5.3.1	Liquidity Index - effective stress frameworks	45
5.3.2	The undrained shear strength at plastic and liquid limits	50
5.3.3	Plasticity index - liquid limit relationships	51
5.3.4	Compressibility correlations	53
5.4	Proposition of clay parameters estimation from CPT data	55
5.5	Validation of proposed estimation of plasticity indexes	59
5.6	Additional option to estimate elasticity parameters for fine-grained soils	63
5.6.1	Constrained modulus from CPT data	63
5.6.2	Secant stiffness	65
5.6.3	Unload-reload stiffness	65
5.6.4	Shear modulus	66
5.7	Conclusion on parametrisation of clayey soils	67
6	Validation of extended APD implementations database	68
6.1	Introduction	68
6.2	The soil data	68
6.2.1	Physical description	69
6.3	Methodology of validation	70
6.4	Validation	71
6.4.1	Liquid limit	71
6.4.2	Oedometer test	72
6.4.3	CAU triaxial test	73
6.4.4	Shear modulus at small strains	75
6.5	Discussion of validation	76
6.6	Conclusion on validation	77
7	Conclusions and Recommendations	78
7.1	Conclusions	78
7.2	Recommendations	79
	Appendices	86
A	Collection of Correlations	87
A.1	Collection of Correlations	87

A.1.1	Small strain shear Modulus	87
A.1.2	Constrain elastic modulus	91
A.1.3	Rigidity Index	92
A.1.4	Overconsolidation ratio and effective preconsolidation stress	93
A.1.5	Shear wave velocity	99
A.1.6	Undrained shear strength ratio	101
A.1.7	Undrained shear strength factors	104
B	Validation of plasticity index and liquid limit proposition	106
C	Oedometer and Triaxial simulation results	111
C.1	Oedometer simulation	111
C.2	CAU simulation	113
C.3	Summary of APD's parameters output	115

List of Figures

- 1.1 Schematic representation of APD’s concept, extracted from Hauth (2020) 7
- 2.1 Representation of the Graph theory applied in APD: nodes of methods indicated in blue, nodes of parameters shown in green. Source parameters and the destination parameter are indicated by the circles and the square, respectively. In colour, the four paths. Retrieved from van Berkom (2020) 11
- 2.2 Uncertainty in APD framework, retrieved from Hauth (2020). 13
- 2.3 Upper and lower 95% bounds for a regression line where σ is the standard error. 14
- 3.1 Consistency chart according ISO 14688-2:2018 18
- 3.2 Critical state concept, including yield surfaces. Retrieved from Mayne (2007) 20
- 3.3 2016 Robertson CPT classification chart - $Q_{tn} - F_r$ update, Robertson 2016 22
- 3.4 2016 Robertson CPT classification chart - $U_2 - Q_{tn}$, Robertson 2016 23
- 3.5 Critical state soil mechanics representation on ideal soil and structured soil. Retrieved from Robertson (2016) 24
- 3.6 Roberson 2016 chart to identify soils with microstructure, Robertson 2016 24
- 3.7 Comparison of actual and predicted plasticity index I_P and liquid limit w_L by Cetin and Ozan 2009. 27
- 3.8 Robertson 2016 chart Robertson 2009 together with symbolic representation of plasticity index I_P of Cetin and Ozan 2009, equation 3.5 over different soils. $q_{t,1,net}[MPa] \approx Q_{tn} \cdot p_{atm}[MPa]$ and stress exponent $c = 1$ 28
- 3.9 Robertson 1990 chart, Robertson 1990, indicating OCR trend 30
- 3.10 Mayne 2013 graph showing no correlation between I_P and ϕ' , contrary to what is seen in many bibliographies. 31
- 3.11 Graph retrieved from Mayne 2013 showing undrained strength ratio $S = s_u/\sigma'_{v,NC}$ vs I_P . For triaxial compression, TC , no relation is found. Original publication from Ladd 1991. 31
- 3.12 Mayne 2013 confirm from independent data the trends of Ladd 1991, figure 3.11, for undrained strength ratio S to plasticity index I_P . For triaxial compression, TC , no relation is found. 32
- 4.1 Example of a distribution of Y for given values of x 35
- 4.2 Example of linear regression on transformed variables. Note the logarithmic scale of the axis and the normal distribution of $\ln Y$ scattering around the trendline. 36
- 4.3 Example of an linear regression on transformed variables, as figure 4.2. Note the regular scale of the axis, the log-normal distribution of Y scattering around the trendline and the heteroscedasticity. 37

4.4	Normal distribution of error assumption over log-transformed correlations .	38
4.5	Mayne and Rix (1995) relation for V_s from q_c . Estimated bounds for normal distribution of 95% are shown	39
4.6	Schematic example of Unit test tool operation applied to a method. The complete database of the correlation is not shown.	41
5.1	Idealized Critical State Line related to Liquidity Index LI , Schofield and Wroth 1968.	46
5.2	Ratio of vertical effective stress in one-dimensional normal compression, and undrained strength at same specific volume as function of $\Lambda = \frac{\lambda-\kappa}{\lambda}$ and friction angle ϕ' , from Wood 1990.	47
5.3	Favre 1972 and Wroth 1979, Wood 1990 Normally Consolidated Remoulded Simplified line on the $(I_L - \sigma'_v)$ plane. Wood 1990 equation is also plotted with Vardanega and Haigh 2014 proposed ratio, $R = 35$	48
5.4	Burland's Intinsic compression Line on the $I_v - \sigma'_v$ plane, Burland 1990 . .	49
5.5	Liquid limit w_L Plasticity index I_L relationships. Left graph shows a close-view for low plasticity soils.	53
5.6	Correlations for compression index (C_c) and liquid limit (w_L)	55
5.7	Correlations for compression index (C_c) and plasticity index (I_P)	55
5.8	Variation of e_0 based on G_s adoption.	56
5.9	Liquidity Index, I_L , resulted of equation 5.32 on non normalised chart of Robertson 2010	57
5.10	First proposed framework to approximate I_L from vertical effective stress and OCR, to obtain w_L ; I_P and C_c . It is not further studied for large number of assumptions.	58
5.11	Proposed framework to approximate I_L from sleeve resistance f_s , saturated volumetric weight γ_{sat} and $G_s = \gamma_{solids}/\gamma_{water}$	59
5.12	Liquidity Index, I_L , resulted of equation 5.32 on non normalised chart of Robertson 2010	60
5.13	Comparison of measured liquid limit and estimated water content. On the left, using equation 5.34. On the right, equation 5.34 is modified adding 2 kN/m^3 . Both cases assumed $G_s = 2.65$	60
5.14	Sensitivity of liquid limit w_L to the specific weight of the solids G_s . Two scenarios are considered, the first with $G_s = 2.65$ on straight line and the second, on dashed line, $G_s = 2.20$	61
5.15	Comparison of predicted plasticity index $I_{P \text{ predicted}}$ to the actual value of I_P , $I_{P \text{ actual}}$, Plotted above Cetin and Ozan 2009 graph, grey triangles. On blue is shown the back-calculated result of Cetin and Ozan 2009 equations with the provided data. Only clayey samples are used for the prediction. .	62
5.16	Comparison of predicted liquid limit $w_{L \text{ predicted}}$ to actual value of w_L , $w_{L \text{ measured}}$. Plotted above Cetin and Ozan 2009 graph, grey triangles. On blue is shown the back-calculated result of Cetin and Ozan 2009 equations with the provided data. Only clayey samples were used for the prediction.	62
5.17	Definition of $1 - D$ constrained modulus at reference stress E_{oed}^{ref} in oedometer test result. Retrieved from PLAXIS Material Model 2020.	64
5.18	Relationship for small strain stiffness E_0 and secant stiffness E_{50} , extracted from Benz et al. 2009a.	65

6.1	Classification of Calais A clay layer on Robertson 2016 chart. Representative values of CPTu data of the correspondent layer to the sample are used.	69
6.2	Classification of Calais A clay layer on Robertson 2010 chart. Representative values of CPTu data of the correspondent layer to the sample are used.	70
6.3	Measured water content compared with the existing correlation of Cetin and Ozan 2009, with proposed correlation presented in chapter 5, and the average of the two.	71
6.4	Oedometer laboratory data of Calais A clay together with simulated test using APD data.	72
6.5	Oedometer laboratory data of Calais A clay together with simulated test using APD data.	73
6.6	$q-p'$ plot of CAU data of Calais A clay together with a simulated test using APD data. The friction angle ϕ' is set to 38° due to the low-estimation of existing correlations.	74
6.7	$\varepsilon_{yy} - q$ plot of CAU data of Calais A clay together with a simulated test using APD data. The friction angle ϕ' is set to 38° due to the low-estimation of existing correlations.	74
6.8	S ratio, $S = s_u/\sigma'_v$ from CAU test compared to the provided parameter by APD methods and the simulated CAU test using adopted $\phi = 38^\circ$	75
6.9	Shear modulus G_0^{ref} from APD framework compared to the correlation of Hardin and Drnevich 1972, based on measured void ratio, plotted above graph provided by Benz 2007. The horizontal axis is enlarged to cope with sample number 3.	76
A.1	Mayne and Rix (1993) G_0 apparent relation to cone tip resistance (q_c). The CV match the lower boundary.	88
A.2	Mayne (2007) relation for the net cone resistance ($q_t - \sigma_{v0}$) to G_0	89
A.3	Simonini and Cola (2000) relation for G_0 from CPTu measurements	91
A.4	Kulhawy and Mayne (1990) relation for σ'_p from q_c	93
A.5	Kulhawy and Mayne (1990) relation for σ'_p from q_t	94
A.6	Chen and Mayne (1996) relation for σ'_p from q_t and I_P	95
A.7	Chen and Mayne (1996) relation for σ'_p from u_2 and I_P	95
A.8	Chen and Mayne (1996) relation for σ'_p from $q_t - u_2$ and I_P	96
A.9	Mayne (2014) relation for σ'_y from $q_t - \sigma_v$. Bounds for normal distribution of 95% confidence for clays ($m' = 1$) are shown.	97
A.10	Mayne (1991) relation for OCR from cavity expansion theory and critical state soil mechanics. Statistical data is not provided. Pore pressure in graph $u_m = u_2$	98
A.11	Mayne and Rix (1995) relation for V_s from q_c . Estimated bounds for normal distribution of 95% are shown	99
A.12	Mayne (2007) relation for V_s from f_s . Bounds for normal distribution of 95%	100
A.13	Mayne (2013) relation for S_{DSS} from PI . Bounds for normal distribution of 95%	102
A.14	Mayne (2013) relation for S from $\sin \phi'$. Statistical data is provided and since no transformation of the variable was used, it can be used directly.	102

A.15	Mayne (2013) relation for S from $\sin \phi'$ and OCR . Statistical data is not provided.	103
A.16	Levesque et al. (2007) relation for s_u from V_s , retrieved from Mayne 2014 . CV estimated from the provided statistics.	104
C.1	Oedometer simulation of sample number 1	111
C.2	Oedometer simulation of sample number 3	112
C.3	Oedometer simulation of sample number 3	112
C.4	Oedometer simulation of sample number 4.	113
C.5	Oedometer simulation of sample number 5.	113
C.6	CAU triaxial simulation using APD framework compared to laboratory test for sample s1.	114
C.7	CAU triaxial simulation using APD framework compared to laboratory test for sample s3.	114
C.8	CAU triaxial simulation using APD framework compared to laboratory test for sample s4.	115
C.9	CAU triaxial simulation using APD framework compared to laboratory test for sample s5.	115

List of Tables

- 5.1 Failure parameters as in Mohr-Coulomb model, PLAXIS Material Model 2020 43
- 5.2 Basic parameters for soil stiffness, PLAXIS Material Model 2020. 43
- 5.3 Alternative parameters for soil stiffness basic parameters, PLAXIS Material Model 2020. 43
- 5.4 Basic parameters, PLAXIS Material Model 2020 44
- 5.5 Brief summary of frameworks to estimate I_L from σ'_v (kPa) or s_{ur} (kPa). . . 52
- 5.6 Summary of some liquid limit w_L to plasticity index I_P correlations. 52
- 5.7 Summary of some liquid limit w_L to compression index C_c correlations. . . 54
- 5.8 Residual Standard Deviation for the back-calculated data using the published equations by Cetin and Ozan 2009 (B-C), and the proposed correlation (proposed) 63

- 6.1 Laboratory results of samples on physical characterisation. 69

- C.1 Summary of five clay Calais A layers compared to the resulted *Layer* of the stratification program and the customised layer *Local* correspondent to a small layer at the sample depth *LAB* 116

Chapter 1

Introduction

By the present document, the MSc graduation thesis' report of Francisco Paduli is presented. The topic chosen to develop the Geo-Engineering master thesis will supplement the work done in the graduation project of two former master students, Ivanka van Berkom and Matthias Hauth, including an external collaboration team. This work is within the framework of Automatic Parameter Determination (APD) for advanced constitutive soil models based on in-situ data.

1.1 Problem description

1.1.1 Motivation

Advanced constitutive models can be more representative than simple ones when implemented in numerical analysis since they include more features. However, the use of them in numerical analysis is not widely spread and simple constitutive models together with traditional methods are still used. It was stated by Brinkgreve 2019 four key reasons that might explain this: limited availability of soil data, limited knowledge, (mis)perception of cost-benefit of numerical analysis and limited confidence over "black box" software.

The idea of Automatic Parameter Determination (APD) for advanced constitutive soil models was explained by Brinkgreve et al. 2010, who determined and validated the parameters necessary for the Hardening Soil Small model from Relative Density (RD) for sands. As the RD can be correlated from in situ tests, an approach could be developed for an APD framework.

It was also stated by Brinkgreve 2019 that a transparent and flexible APD framework, based on in situ test results, could foster the practical use of advanced constitutive models in the finite element method. Apart from its better description of the soil behaviour, one main advantage of advanced models is the less subjective parameters involved.

1.1.2 Main idea of the APD project

In numerical analysis, assuming that the correct constitutive model is adopted, selecting the input parameters is decisive for correct geotechnical modelling. Typically, geotechnical engineers estimate the complete set of constitutive models' parameters from a few tests using empirical correlations. However, several correlations, equations and combinations

might exist for each parameter, and they often not have the same result. Therefore, depending on the set of correlations chosen, different constitutive models' parameters will be encountered, resulting in a decrease in the model's confidence. This spread of solutions explains the complexity of geotechnical parameter determination.

To deal with this, the APD concept aims to find from input source parameters (e.g. CPTu data) numerous ways to calculate a destination parameter through intermediate parameters. The idea is represented in figure 1.1, where all the possible paths are estimated. Each path could be the choice of one engineer; however, the APD would have its totality.

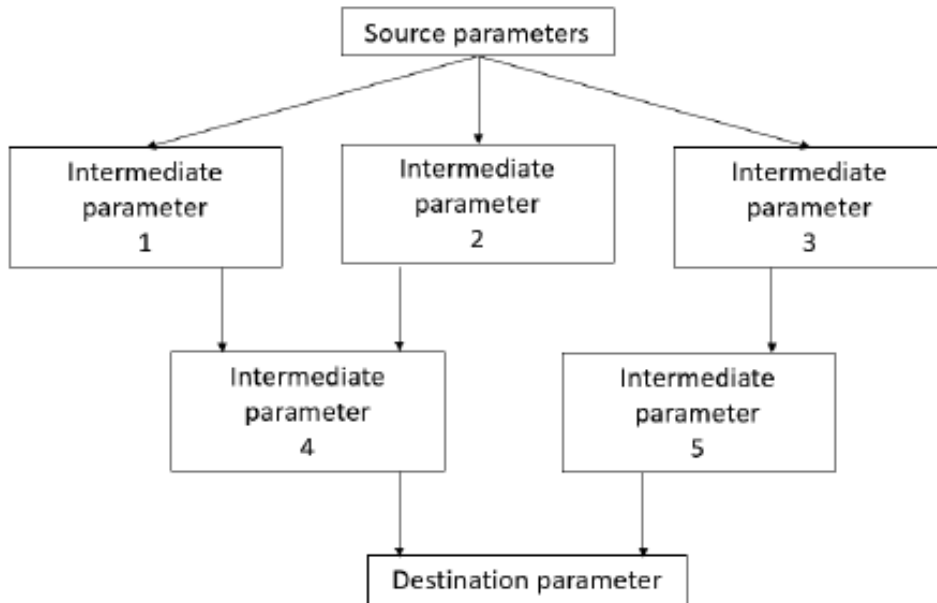


Figure 1.1: Schematic representation of APD's concept, extracted from Hauth (2020)

A significant characteristic of the APD concept is to remain transparent and adaptable. This allows the geotechnical user to remain in control and adapt the information based on experience and visualise how the information is used to arrive at a solution.

1.1.3 State of APD development

Currently, a team of professionals, PhD and MSc students, collaborate on the ambitious project. On the graduation project of Ivanka van Berkom, the graph approach prove to yield consistent outputs, van Berkom 2020. The graphs theory is a mathematical approach that can link entities and show the network graphically. An analogy of operating procedure is the navigator systems used in urban mobility. They show the possible paths to connect two locations at a specific time. In this case, the location would be the parameters to link, the paths the combination of "methods" that are the soil correlations, and the time of each path would represent an evaluation of it, the accuracy. Hence, starting from Cone Penetration Test (source parameters) through different correlations (methods), model parameters for advanced constitutive models can be obtained (final parameters).

In his MSc thesis, Matthias Hauth introduces the reliability in the APD framework, quantifying the accuracy, Hauth 2020. Each correlation uncertainty is propagated through the network. In this way, each parameter obtained from a different path is characterised by its uncertainty. Moreover, a system was defined to cope with the selection of the most

statistically suitable final parameter value. The corresponding validation of the model was successful, and confidence in the framework was built.

1.2 Research Questions and Methods

At the start of this thesis, the APD framework only copes with coarse-grained soils, i.e., sands and gravels. This limitation raises the problem of dealing with fine-grained soils and soils in between coarse and fine-grained.

Therefore, this thesis aims to expand the APD system by implementing fine-grained soils correlations. The expansion is based on the current development of the APD system. Moreover, most soil correlations in literature correspond to pure sandlike behaviour or pure claylike behaviour. Nonetheless, no extensive correlation database exists for the mixed soils of these two categories. Additionally, only normal distribution of the uncertainty over the correlations is considered, whereas many soil correlations' regression has a logarithmic distribution.

The scope of this thesis is to provide fine-grained soil parameters for advanced constitutive models. Therefore soil parameters with other purposes are not treated. Characterisation of fine-grained soils using the Cone Penetration Test (CPT) with pore pressure measurements has many advantages, and it is the only in-situ test used in the APD at the moment. This thesis assumes that the groundwater level is high or accurate pore pressure measurements were taken. Moreover, purely organic soils and their mix are not treated in this study.

CPT classification charts were made and are frequently used in practice. In the APD framework, the classification is essential to allow the program to select correspondent correlations. Internationally accepted charts are mentioned and used in this thesis.

Therefore, the following main research question and sub-questions are intended to be answered:

How can the APD framework be extended to cope with fine-grained soils?

- *Which existing behaviour classification chart is appropriate?*
- *How to include logarithmic-distribution on correlations uncertainties in APD?*
- *What are key-parameters in fine-grained soils that play a dominant role in parameter determination (as RD in coarse-grained soils)?*
- *How can the extended APD system for fine-grained soils be validated?*

From research question and subquestions, the following methods are proposed:

- 1) Literature review and addition of existing correlations in fine-grained soils.
 - *Verify each correlation output and boundaries; check potential circular connections.*
 - *Develop a plan to estimate variability of log-log transformed correlations.*
 - *Identify and implement possible new attributes in APD to allow a better selection of methods.*

- 2) Literature review and identification of key-parameters in fine-grained soils
 - *Determine validity of key-parameters using existing correlations*
 - *If necessary and possible, develop alternative equation from CPT data for the key-parameter*
- 3) Validation of new implementations in the APD system
 - *Verification of method's implementation using APD method unit-test program.*
 - *Compare laboratory test to APD framework results and simulate test with the Plaxis Test Facility.*

1.3 Thesis outline

The Automated Parameter Determination framework is an ambitious project where an enthusiastic group is working. This thesis collaborates along with other developments from the group towards a working program for fine-grained soils. Being a continuation of previous thesis and the group project, a summary of the achievements is given in section 2.4. A literature review of soil characterisation and key parameters in fine-grained soils is presented in 3. Chapter 4 covers the implementation and verification of a selection of correlations together with a variability of the methods' update. In chapter 5 a new approximation for plasticity parameters from CPT data is developed. Finally, a validation of the new methods for fine-grained soils using the Hardening Soil small-strain model and the new approximation for plasticity is presented in chapter 6.

Chapter 2

Automatic Parameter Determination framework achievements

2.1 Introduction

In this chapter, a summary of the achievements is discussed. In section 2.2 the graph theory applied in the APD framework is explained, and in section 2.3 the validation and introduction of reliability.

In her master thesis, van Berkom 2020 developed a generic system for the APD framework. The aim is to obtain final parameters for constitutive models from in situ tests. The graph theory is used to generate different paths for the final parameters. Moreover, the system always remains transparent and flexible, which is considered critical for parameter determination. The verification was successful, using fictitious CPT data as source parameters to obtain final parameters.

The methods that correlate parameters have weights if the user prefers one over the other. However, only experts in soil parametrisation could rely on this strategy, having no statistical framework. In his MSc thesis, Hauth 2020 developed a framework implemented in the APD to statistically select a value for a final parameter with its uncertainty.

2.2 Graph theory in APD framework

Graph theory is a mathematical structure to model pairwise relationships between objects in a network. The network provides the user with a better representation of all the entities, and it is composed of two types of objects, nodes, and edges, van Berkom 2020. The nodes are the graph's entities, while the edges represent the relationship between two nodes, Hauth 2020.

In the APD framework, the word *parameter* characterises the nodes, and the term method the correlations and equations that provide parameter values. The source parameters are the input parameters, i.e., CPT results. The intermediate parameters are calculated through the methods to arrive at the final parameters: the constitutive model parameters. In addition, the relationships of nodes and edges can involve metadata, i.e., properties.

The source, intermediate and final parameters are modelled as nodes. The methods are also modelled as nodes in the APD framework. Since different paths cannot be recognised if the methods are modelled as edges with metadata, no metadata is provided to the edge, van Berkom 2020. The edges of the graph only account for the relationship between the input variables and the output variable of the method Hauth 2020.

A path is defined as a chain of parameter and method nodes to derive a destination parameter. Each path will have a single deterministic value, and it could represent the choice of one engineer. In the APD framework, all the paths are considered and evaluated. A representation of the framework is shown in figure 2.1.

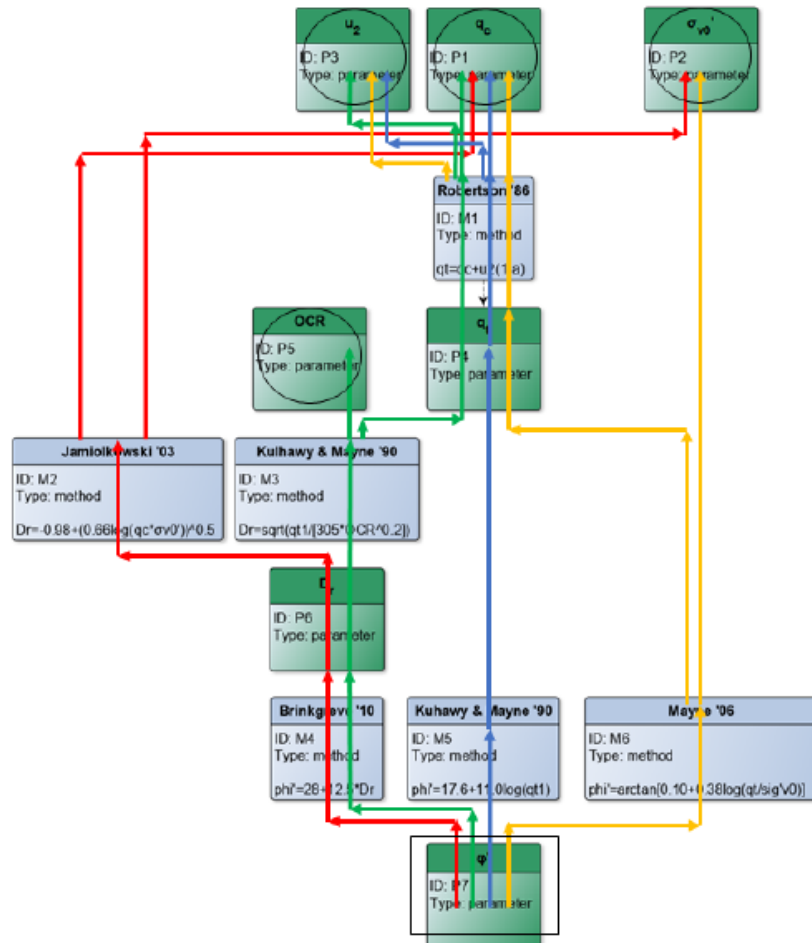


Figure 2.1: Representation of the Graph theory applied in APD: nodes of methods indicated in blue, nodes of parameters shown in green. Source parameters and the destination parameter are indicated by the circles and the square, respectively. In colour, the four paths. Retrieved from van Berkom (2020)

2.2.1 Workflow to generate paths

The functioning of the algorithm to generate paths is described as follows using the representation of figure 2.1:

1. Start reading the final parameter, the destination parameter. In figure 2.1 represented as a green box at the bottom, indicated by a square.

2. Look for methods that can provide the final parameter and call them. The bottom three blue boxes indicate them.
3. A called method, a correlation, may require a single parameter or many ones. They could be the intermediate parameters or the source parameters.
4. Intermediate parameters are required to be calculated. The algorithm finds methods that can provide them and follows step 3.
5. Steps 3 and 4 are repeated until no unknowns are left, ends at the input parameters. This step allows calculating the destination parameter and intermediate parameters as well.
6. The successful paths and parameters values are plotted, represented as the coloured lines in figure 2.1.

2.2.2 External database

All the nodes used in a graph are established in two external databases:

- Parameter database: list of all parameters nodes in the graph. Metadata is associated.
- Method database: list of all methods nodes of the graph. This list includes the correlation equation, input parameters and output parameter and some metadata to filter the correlations to suit the corresponding soil.

The current metadata used in the parameter database include:

- Units of the parameter
- Initial value if applicable
- Standard deviation (sd): total uncertainty of the parameter. The source parameters sd is provided, while for intermediate parameters, it is calculated.
- Lower and upper bound to constrain the computed value, Hauth 2020

The current metadata used in the methods database include:

- Standard deviation on the method that is explained in section 2.3.
- Weight of the method: if there is a user's preference to favour one correlation over others.
- Validity: Soil Behaviour Type (SBT), Soil behaviour type index I_c , $I_{c_{min}}$ and $I_{c_{max}}$ and consolidation (normally consolidated or over-consolidated).

2.3 Statistical framework on APD

In geotechnical engineering, soil characterisation will carry a degree of uncertainty distinguished in inherent soil variability, measurement errors, and transformation uncertainty, Phoon and Kulhawy 1999. Figure 2.2 shows the types of uncertainties covered by the parameter uncertainty and the method uncertainty. The aggregation of them defines the

total uncertainty of the design parameter and in the APD framework is defined in either term of standard deviation σ or terms of coefficient of variation CV :

$$CV_x = \frac{\sigma_x}{\mu_x} \quad (2.1)$$

where σ_x is the standard deviation and μ_x is the mean value.

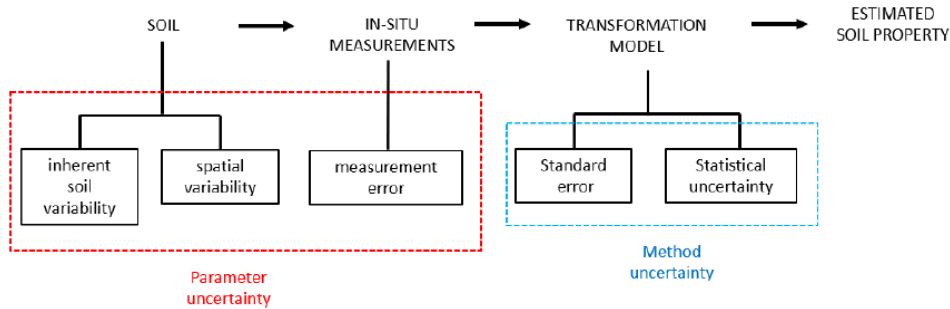


Figure 2.2: Uncertainty in APD framework, retrieved from Hauth (2020).

2.3.1 Parameter's uncertainty

The APD framework uses input parameters and, with a set of intermediate parameters and methods, arrives at a destination parameter. Each parameter is characterised with a mean value $\mu(x_i)$ and a standard deviation $\sigma(x_i)$. It is assumed that the input parameters' uncertainty includes the inherent soil variability and in-situ measurements uncertainty.

2.3.2 Method's uncertainty

Before setting the strategies analysed in propagating the uncertainty, the variability of the transformation models, named the correlations, must be stated.

Most correlations are generally obtained from fitting a curve to test results. Statistically, two errors can be considered when evaluating a correlation, the standard error of the prediction and the fit's standard error. The prediction standard error is used in the APD since it accounts for both the mean trend's uncertainty and the data scatter. Hauth (2020) summarised four possible means to obtain the uncertainty of the correlation:

- The author of the correlation provides the uncertainty parameters.
- Graphical estimation, accounting with the rule that 95% of the data in a normal distribution is comprised of 4σ .
- Calculating the uncertainty if the correlation data is provided.
- Adopting an arbitrary value if none of the above means is possible.

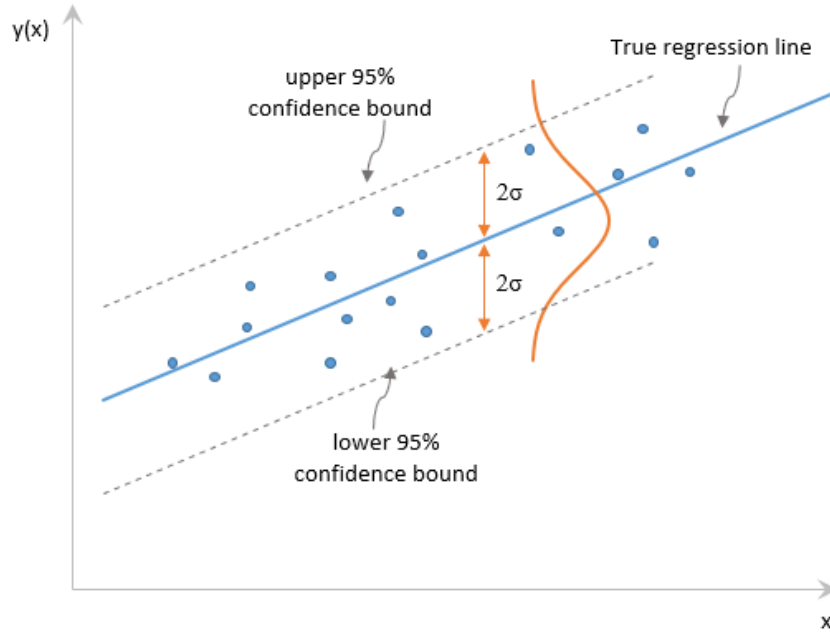


Figure 2.3: Upper and lower 95% bounds for a regression line where σ is the standard error.

The correlation uncertainty also depends on the data points. For the same standard error, a large number of points will tend to higher reliability on the method. A correction is proposed by Hauth (2020) to include this aspect.

2.3.3 Distribution of uncertainty of in-situ measurements

The inherent soil variability and the measurements errors will lead to variability. In practice, the engineers separate soil layers that behave similarly to the problem analysed. This approach considers a mean value representative of the layer and a correspondent uncertainty. In this thesis's scope, the in-situ measurements and their variability are considered provided and will not be part of the analysis.

2.3.4 Propagation of the uncertainty

In the APD framework, the propagation of the uncertainty through the graph was studied to quantify the destination parameter's uncertainty. A First Order Second Moment and Monte-Carlo simulation approaches were evaluated, Hauth 2020.

First Order Second Moment in APD framework

The First Order Second Moment (FOSM) applied to geotechnical correlations was introduced by Phoon and Kulhawy (1999), it relies on the linearisation of the transformation function using Taylor-series expansion Hauth 2020.

A transformation function of a method m is defined as equation 2.2, where y is the output parameter, and x_1, \dots, x_n are the input parameters, Hauth 2020.

$$y = f(x_1, \dots, x_n) \quad (2.2)$$

The total uncertainty of the destination parameter y is decomposed in two terms: the parameter uncertainty $\sigma_{para}^2(y)$ and the method uncertainty $\sigma_{met}^2(y)$. They represent the propagated contribution uncertainty of the input parameters and transformations uncertainty correspondingly.

$$\sigma_{tot}^2(y) = \sigma_{para}^2(y) + \sigma_{met}^2(y) \quad (2.3)$$

The implementation was verified, and the system can provide a mean value with its standard deviation of the parameter for every path. It was tested with geotechnical correlations for a single set of input parameters with its correspondent standard deviations. The parameters were considered to be mutually independent. The results were compared with *CPeT-IT*, a well known CPT interpretation software that estimates soil parameters. The comparison gave good results. However, a normality assumption of the estimated parameter was adopted in the APD program that might not be the most suitable, Hauth 2020. In other words, the APD program's output for a parameter is a mean with its variance, having a normal distribution of the uncertainty.

Monte-Carlo analysis in APD

The Monte-Carlo analysis is a fully stochastic framework. It considers random variables following specific probability density functions. Uncorrelated and normally distributed parameters were run in 2000 simulations, and the same external database used in the FOSM approach was utilised. This database provided the probability density function of the parameters, and the results were compared with the semi-probabilistic FOSM approach, giving good results. Furthermore, the analysis confirmed the non-normality of the path's densities, Hauth 2020.

2.3.5 Model averaging in APD

Since the graph methods show that each path leads to a single value with its variance, a decision must be taken to define the most appropriate and reliable parameter for a soil type from all the generated paths. The estimated parameter $\hat{\theta}$ is considered as the weighted average of the calculated parameters, Hauth 2020:

$$\hat{\theta} = \sum_{i=1}^m w_i \hat{\theta}_i \quad (2.4)$$

where m is the number of paths, the number of estimated parameter values $\hat{\theta}_i$ and w_i is the attributed weight to the path. The weights are naturally normalised.

Rest to define how the weights and the variance is calculated. For the variance, three strategies were considered, Convolution, Propagation and Buckland. The thought best strategy from a geotechnical case is Propagation. It is defined as follows, Hauth 2020:

$$\hat{V}\text{ar}(\hat{\theta}) = \left(\sum_{i=1}^m w_i (\hat{\theta}_i - \hat{\theta}) \right)^2 + \sum_{i=1}^m \sum_{j=1}^m w_i w_j \text{CV}(\hat{\theta}_i, \hat{\theta}_j) \quad (2.5)$$

Four types of weights were also tested: equal weights, inverse Mean Squared Error and Bayesian Model Averaging. However, on the test where geotechnical parameters were estimated, the different weight methods have shown to have little influence, Hauth [2020](#).

2.4 Circular references in fine-grained soils correlations

In the APD system, a circular reference is encountered when a method has an input parameter which is also the destination parameter. This process causes a loop, and the system would crash.

Currently, in the APD framework, the issue is avoided carefully, providing correlations that are checked to do not produce this problem. In the implementation of fine-grained correlations, they will be avoided.

Chapter 3

Literature review of fine grained

3.1 Introduction

Geotechnical engineers need to classify the soil to characterise its behaviour. Apart from its origins, the most known characterisation are physical-based and in situ behaviour-based. The first ones are executed mostly on disturbed samples. These two classifications are explained in sections 3.2 and 3.3. In section 3.5, the most important parameters that lead to many correlations are summarised.

3.2 Physical based characterisation

The physical characterisation used in geotechnics is based on grain size and plasticity, textural properties. The International Organisation for Standardisation (ISO) classifies natural soils into coarse-grained soils, fine-grained soils, and organics soils. Fine-grained soils must have more than 50% of the total quantity of a dry sample retained on a 0.063 mm sieve. The most commonly used worldwide classification in geotechnics, the Unified Soil Classification System (USCS) from ASTM standard, International 2017, vary the sieve dimension to 0.075 mm. The ISO classification, Standardization 2017 and USCS simultaneously sub-classify the fine-grained soils depending on the plasticity. Therefore, the 50% is the primary fraction that gives the soil's name, classified on the particle size and plasticity. The secondary or tertiary fraction is also characterised in both systems, i.e., Silty CLAY. A third group is considered in the physical classifications, the highly organic soils. This last group is not contemplated in this study.

The ISO plasticity classification of fine-grained soils corresponds to clay or silt of low/medium/high/very high plasticity. The plasticity characterisations are done based on the chart from figure 3.1. The variables are the liquid limit w_L , and the plastic limit w_P from what the plasticity index can be calculated $IP = w_L - w_P$. Moreover, the A-line in the chart classifies the soil as clay or silt.

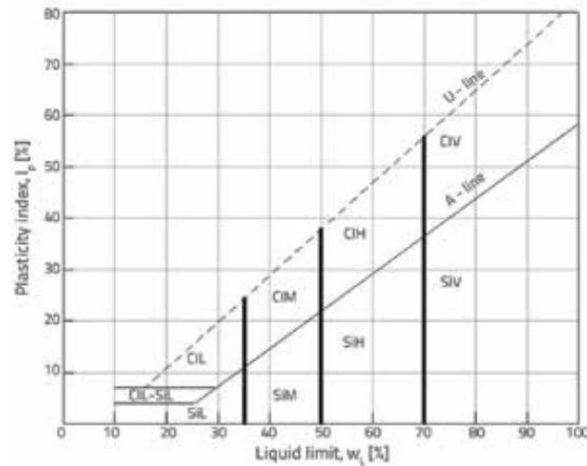


Figure 3.1: Consistency chart according ISO 14688-2:2018

Normally, if the clay fraction on a soil increase, the following can be expected, retrieved from Mitchell and Soga 2005:

- higher the plasticity
- greater shrinkage and swell potential
- lower hydraulic conductivity
- higher compressibility
- higher cohesion
- lower internal friction angle

Therefore, the mineralogy composition is essential for the characterisation of the engineering properties.

3.3 Behaviour based characterisation

The previously defined physical characterisations are derived from remoulded samples, and empirical correlations can have significant uncertainty when using this physical index to predict in situ soil behaviour, Robertson 2016. Since the engineer is interested in the in situ behaviour, a different characterisation is needed.

3.3.1 CPT behaviour based characterisation

The CPT's usefulness is worldwide known since it can give accurate continuous information at a relatively short time since the cone penetrates the soil at a rate of 20 mm per second. When executing a Cone Penetration Test with pore pressure measurements, commonly known as CPTu, an excess of pore pressure can be observed due to the cone's insertion rate and soil characteristics. In this case, the behaviour is called "undrained," and since the consolidation parameter depends on the permeability, soils mostly comprised of fine particles behave undrained. One example of this are clays. On the other hand, coarse-grained soils mostly behave drained under CPT loading rates. It is essential

to mention that the drained or undrained classification corresponds to CPT test rates and could be different for other loading rates.

Following the same reasoning, soils near the limit of fine-grained and coarse-grained can behave partially drained, adding complexity to the choice of correlations. These soils henceforth are called *transitional soils*.

The Critical State Soil Mechanics, CSSM, is widely used and accepted to interpret the in-situ and physical test. It will be briefly introduced, together with the CPT test, used in the APD framework.

Critical State Soil Mechanics, CSSM

The framework offers a rational effective stress coupling on soils' consolidation and compressibility behaviour with a response to shearing, Mayne 2013. The critical state soil mechanics express that soils after large shearing under given effective stress will arrive at a constant void ratio independent of their initial state. There is a unique relation between the normal stress, shear stress, and void ratio at the critical state. For the CSSM, 3 constants are used, the effective friction angle ϕ' , the compression constant C_c or λ and the swelling constant C_s or κ .

The state of the soil is essential to address since it mostly behaves differently at different states, in other words, at different densities related to the critical density. It is a description of physical conditions, as opposed to properties of a material, Been and Jefferies (1985). The state is essential to express the stress path that a soil can follow under different loading cases. For example, loose soils tend to contract under large shear strain and undrained conditions, the pore pressure tends to increase (positive excess pore pressure). In contrast, dense soils tend to dilate, and under undrained loading, the pore pressure tends to decrease (negative excess pore pressure), Robertson 2016. Therefore, the critical state is helpful as a reference to indicate if the soil is loose or dense of the critical state, Mitchell and Soga 2005.

It is essential to mention that the concept is built based on reconstituted soil samples, and factors as cementation are not reproduced. The soil's initial state is commonly addressed in different ways, depending on the soil's characteristics.

On the one hand, the state of coarse-grained soils is expressed in Relative Density (RD) together with stress conditions or state parameter, ψ . The latter is preferred since the normal compression line is not unique for coarse-grained soils, Robertson 2016. On the other hand, to indicate the initial state of fine-grained soils, the Over Consolidation Ratio, OCR , can be used or the preconsolidation stress, σ_p , together with the effective vertical stress, σ'_v and the void ratio, e_0 .

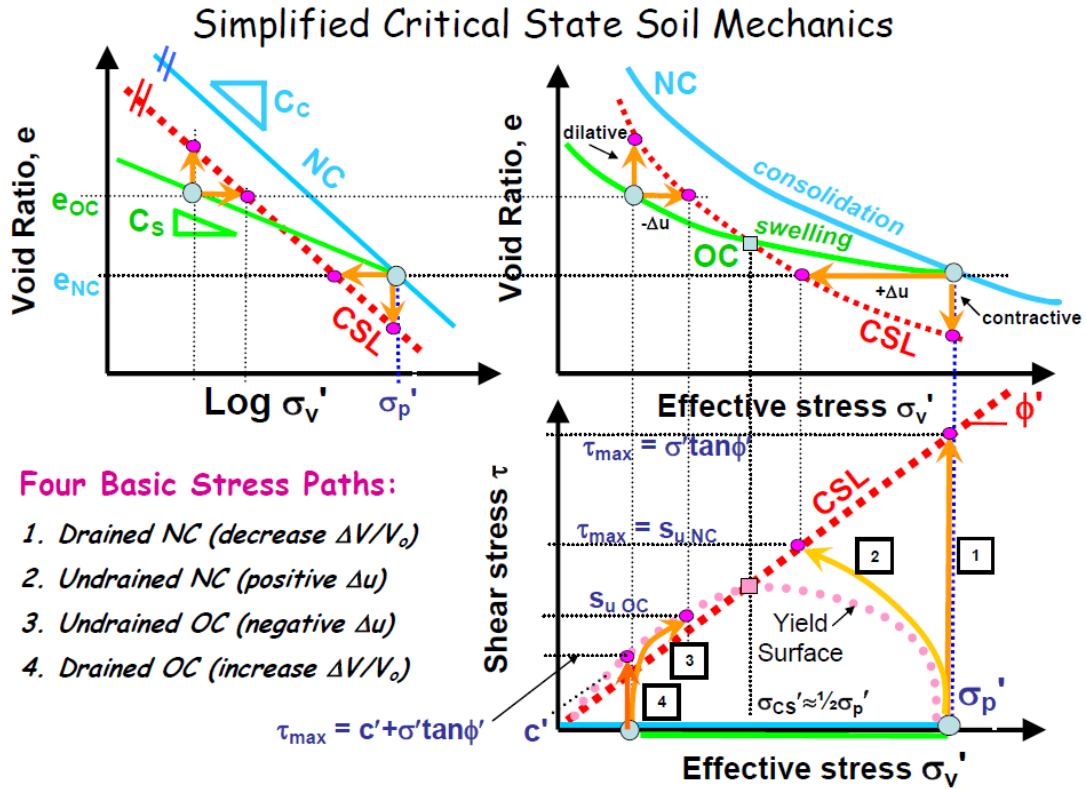


Figure 3.2: Critical state concept, including yield surfaces. Retrieved from Mayne (2007)

Figure 3.2 summarised the basic concepts of the CSSM. Many of the FEM advanced soils models rely on Critical State Soil Mechanics, and their related parameters need to be known for proper modelisation. Therefore, the APD framework should address them.

CPT data

Before the introduction of CPT characterisation charts, the measurements and some definitions need to be addressed.

Developed in the Netherlands, the CPT evolved in time until it became internationally recognised as established, Schnaid 2008. It consists of driving at a constant rate a cone tip of 60 deg into the soil. Different cross-sections are used in the industry, being common the 10 cm^2 one. The first CPT measurements were mechanically transferred by rods, being called mechanical cones. Then, they were substituted by electrical cones, where the measurements are evaluated through load cells. The electrical cone also provides a sleeve friction resistance. Later on, the piezocone or CPTu was introduced, monitoring the pore water pressures during driving. More recently it was introduced the seismic piezocone that measure the shear wave velocity.

The following are the most relevant CPT-related parameters used in APD framework:

- qc : cone penetration resistance
- qt : corrected cone resistance due to unequal end area effects
- fs : sleeve friction

- u_1 : pore pressure measured on the tip
- u_2 : pore pressure measured on the shoulder
- u_0 : in-situ equilibrium water pressure
- $\Delta u = u_2 - u_0$: excess penetration pore pressure (normally u_2 is used)
- $Rf = f_s/q_c$: friction ratio
- $Q_{t1} = (q_t - \sigma_{v0})/\sigma'_{v0}$: normalised cone resistance with stress exponent $n = 1$
- $Q_{tn} = [(q_t - \sigma_{v0})/p_a](p_a/\sigma'_{v0})^n$: where n is the stress exponent that varies with the normalised Soil Behaviour Type $SBTn$
- $F_R = [(f_s/(q_t - \sigma_{v0}))]100\%$: normalised friction ratio
- $B_q = (u_2 - u_0)/(q_t - \sigma_{v0}) = \Delta u/(q_t - \sigma_{v0})$: pore pressure parameter ratio
- V_s : Shear wave velocity
- σ_{v0} and σ'_{v0} : in-situ total and effective vertical stress correspondingly

The CPTu with pore pressure measurements on the cone's shoulder is the most used and gives three measurements: q_c , f_s , and u_2 . The parameters Q_t , F_R and B_q are obtained after normalising q_t , Rf and excess pore pressure respectively ($u_2 - u_0$), Robertson 1990. In this thesis, the data from CPTu is used, and its measurements are considered adequate since while driving CPTu in unsaturated soils, problems in the reading of pore pressure can be presented. The CPT sleeve friction is considered less accurate than the cone resistance, Robertson 2009.

CPT charts

The CPT, developed in the Netherlands, reached popularity for its repeatable measurements, fast execution, and low cost. Different classifications charts were made to describe the in situ soil behaviour or soil type. The first one introduced by Begemann 1965 shows a classification based on the ratio between the cone resistance q_c and the local friction f_s .

The charts provided by Robertson et al. (1986) using Soil Behaviour Type (SBT) and Robertson (1990) based on normalised parameters (SBTn) became popular and widely accepted. They are known as the Robertson 1986 and the Robertson 1990 charts, respectively. The first one had an update, Robertson 2010, to match the classifications of the second, the normalised one. The SBT and SBTn use physical descriptions names to classify the in situ behaviour.

- **Robertson et al. (1986)**: based on the corrected cone penetration resistance, q_t ; friction ratio, R_f and pore pressure ratio, B_q . The soil in-situ mechanical characterisation's name is *Soil Behaviour Type*, SBT and has 12 soil types.
- **Robertson 2010**: based on dimensionless cone resistance, q_c/p_a , where p_a = atmospheric pressure and friction ratio, R_f . The chart is an update of Robertson 1986's chart. The characterisation SBT has been reduced from 12 to 9 to match the Robertson 1990's SBTn zones. The new boundaries of SBT are defined by the *non-normalised Soil Behaviour Type Index*, I_{SBT} .

- **Robertson 1990**: based on normalised cone resistance, Q_{t1} ; normalised friction ratio, F_R and pore pressure ratio, B_q . They are considered more reliable than non normalised charts, Robertson 2009. The soil classification's name is *normalised Soil Behaviour Type*, SBT_n and has 9 soil types. It uses a *normalised Soil Behaviour Type Index*, I_{c1} for this chart.
- **Robertson 2009**: update of the Robertson 1990 SBTn chart normalisation exponent, to normalised Q_{tn} . The *Soil Behaviour Type Index*, I_{cn} uses the updated Q_{tn} .
- **Robertson 2016**: update of the Robertson 1990 Robertson 1990 chart based on $Q_{tn} - F_r$ adding a new characterisation, the *modified normalised Soil Behaviour Type*, $mSBT_n$. The publication also includes a proposed $Q_{tn} - I_G$ chart to identify soils with microstructure and an update of the Schneider et al. (2008) chart based on $Q_{tn} - U_2$. The *modified Soil Behaviour Type Index*, I_B was introduced.

In these classification charts, a soil textural described as Silt could be characterised as sand for its mechanical behaviour type SBT or SBTn. These differences in characterisation could create some confusion in the interpretation. In this line, Robertson (2016) updated the normalised chart and characterised the soil as more sandlike or more claylike behaviour. Besides, contractive or dilative behaviour can be classified.

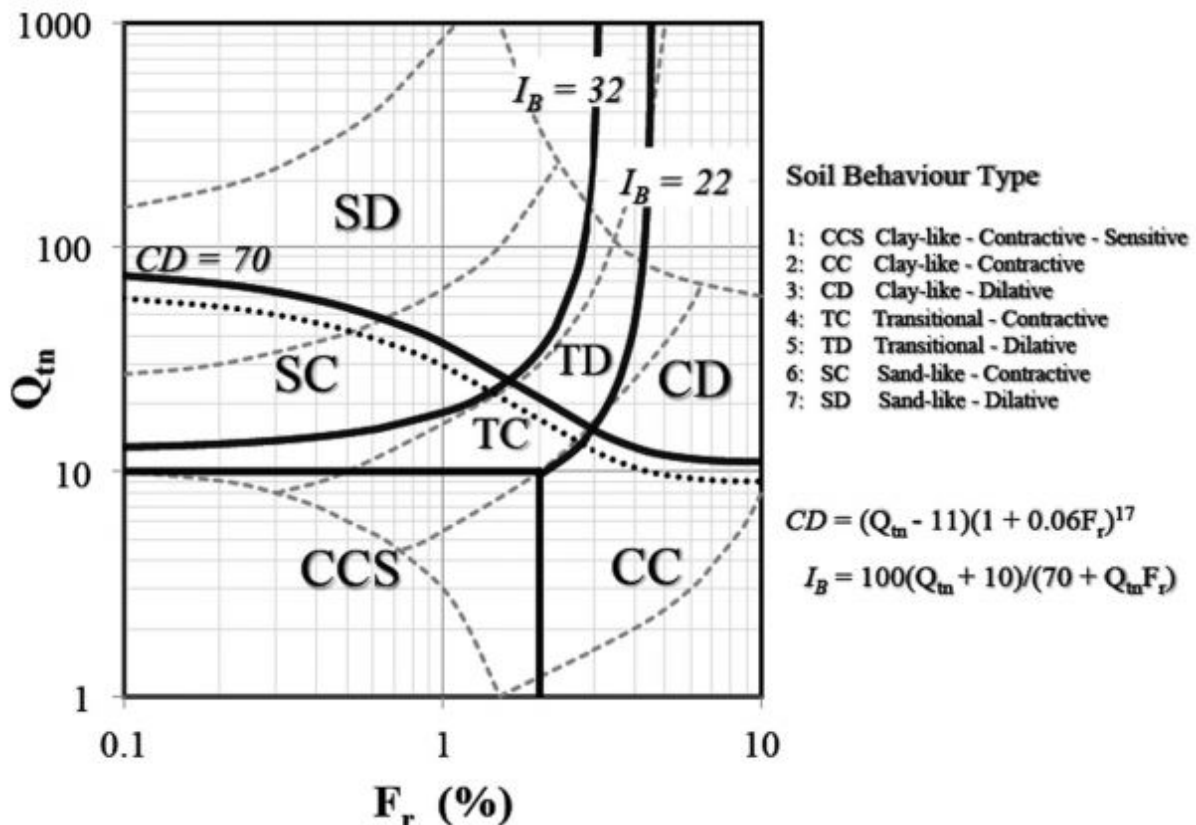


Figure 3.3: 2016 Robertson CPT classification chart - $Q_{tn} - F_r$ update, Robertson 2016

The Robertson 2016 chart is based on the normalised chart Robertson 1990, the most used chart, and comprises nine soil classifications. This update, Robertson 2016, also includes a new index I_B to define three main zones: clay-like behaviour, sand-like behaviour and

transitional. At the same time, other parameters define contractive and dilative zones, the $CD = 70$. In addition, the $F_R = 2$ is considered the limit for sensitive soils, increasing sensitivity on lower values of F_R . The new description category is called SBTm and is shown in figure 3.3.

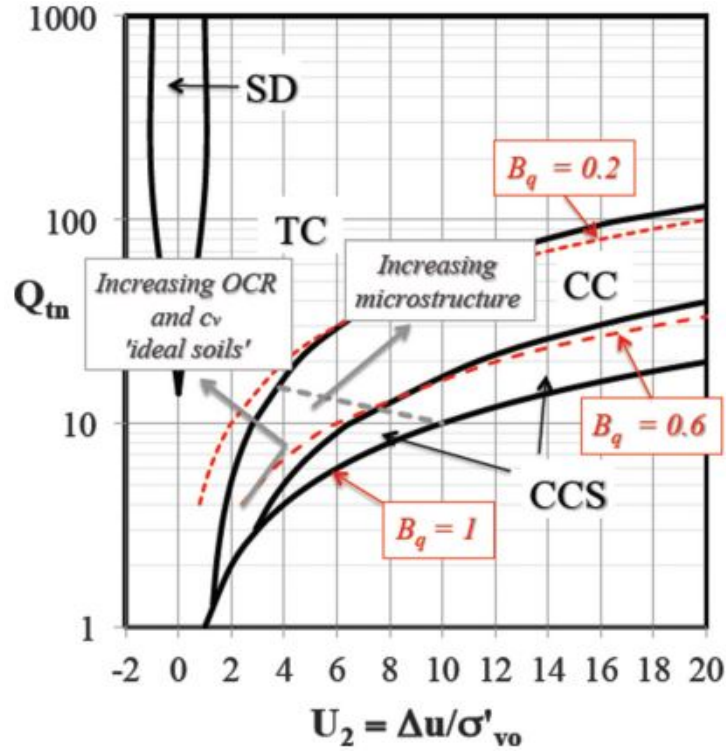


Figure 3.4: 2016 Robertson CPT classification chart - $U_2 - Q_{tn}$, Robertson 2016

A second chart was presented in the update that relates the pore pressure parameter U_2 and normalised cone resistance Q_{tn} , based on Schneider et al. (2008). This chart can provide an extra verification of the characterisation of the modified soil behaviour type SBTm using the excess pore pressure measurements.

3.3.2 Micro-structure identification using SCPT

The decisive advantages of critical state soil mechanics were introduced before. Due to many factors such as geologic processes, environmental factors, physical and chemical processes, the soil can present a structure whose behaviour differs from an "ideal soil", Robertson 2016. The terms ideal soils and structured soils are defined as followed:

- Ideal soils: soils with little or no microstructure, mostly - young and uncemented.
- Structured soils: soils with extensive microstructure, mostly by ageing and cementation.

A structured soil compared to an ideal one has higher yield stress, peak strength, and small-strain stiffness at the same void ratio. This is represented in figure 3.5 where for the same void ratio, a higher volumetric effective stress is needed to pass the yield stress and later, a sudden drop is shown until the critical stress line is reached. This different behaviour from the ideal soils must be identified since a wrong classification can be achieved if not.

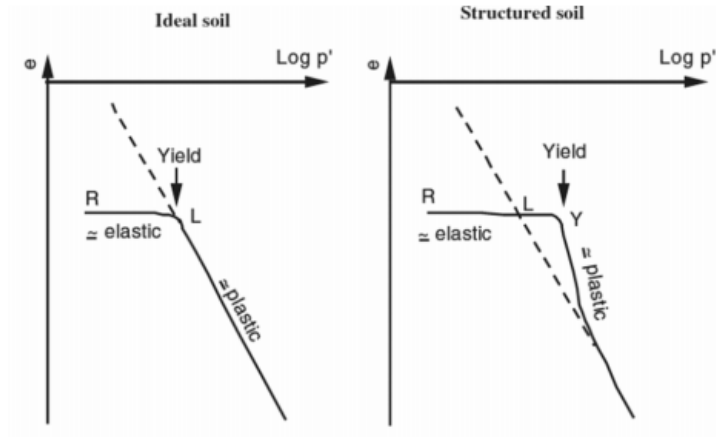


Figure 3.5: Critical state soil mechanics representation on ideal soil and structured soil. Retrieved from Robertson (2016)

Based on the publication of Schnaid (2008), Robertson (2010) and Schneider and Moss (2011), Robertson (2016) introduce a plot that relates the small-strain rigidity index (I_G) to the normalised cone resistance (Q_{tn}) for coarse and fine-grained soils:

$$I_G = G_0/q_n \quad (3.1)$$

$$K_G^* = \frac{G_0}{q_n} (Q_{tn})^{0.75} \quad (3.2)$$

where G_0 is the small-strain stiffness

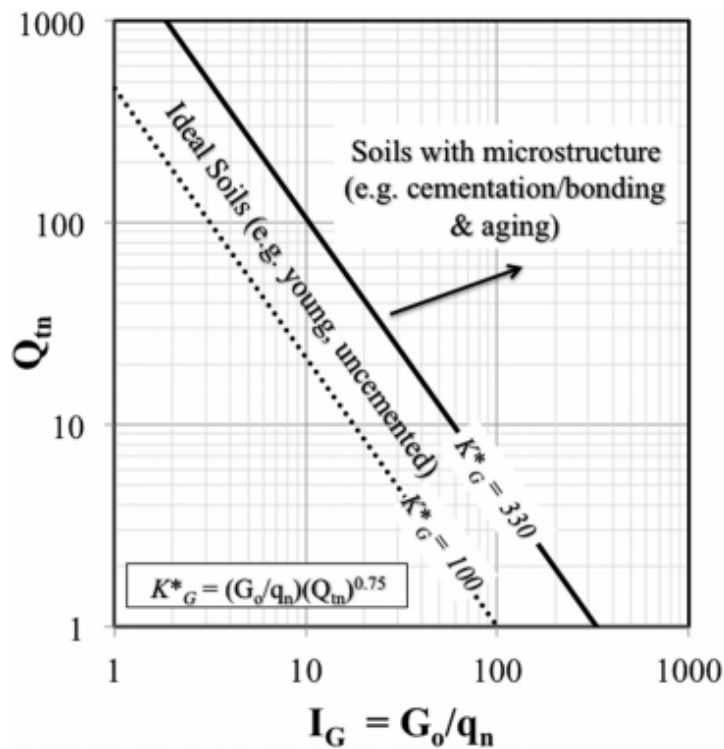


Figure 3.6: Robertson 2016 chart to identify soils with microstructure, Robertson 2016

The author believes that the Robertson 2016's chart, $I_G - Q_{tn}$ could help identify structured soils in the APD framework.

3.4 Key-parameter on fine grained soil engineering properties

Soils' in situ mechanical behaviour depends on void ratio, stress state, mineralogy, cementation, ageing, and over consolidation. The APD framework does not aim to disregard detailed site-specific soil investigation but help mitigate the human factor and have a first advanced FEM model to represent the analysed problem, Brinkgreve et al. 2010.

As the name defines, key parameters are essential since many correlations are related to them; they could estimate other parameters, ideally describing the material behaviour and its state. Due to their importance, the identification and determination of them are vital for the APD framework. Their definition in soil mechanics also depends on the type of analysis. For example, if an ultimate limit state design is pursued, strength parameters like s_u or ϕ' are needed, and in a serviceability state design, the stiffness parameters, Brinkgreve et al. 2010.

An introduction of coarse and fine-grained soils potential parameters is approached in the following sections, and subjective identification of key-parameters is made.

3.4.1 Definition of key-parameter for APD framework on coarse-grained soils

In non-structured coarse-grained soils, the Relative Density (RD) and particle size are the most used properties to correlate other soil parameters. The RD is a measure of the current state of the density in relation to the maximum and minimum. However, the state parameter (ψ) is becoming more popular since it is more meaningful of the state of the soil and relates to the critical state soil mechanics, Robertson 2016. The particle size, shape, mineralogy, and distribution are essential information that can mainly describe constant parameter like ϕ_{cv} . In practice, the RD can be estimated from in situ measurements from correlations and relates well to other parameters that allow getting models' input parameters.

$$Dr = \frac{e_{max} - e}{e_{max} - e_{min}} \cdot 100\% \quad (3.3)$$

Its significant acceptance makes it a key-parameter in the parameter determination of coarse-grained soils. Brinkgreve et al. (2010) develop and validate empirical formulas to determine the model parameters of the Plaxis Hardening Soil model with small-strain stiffness (HSsmall) for sands based on relative density. The previous confirms the usefulness of the RD in the APD framework.

3.4.2 Definition of key-parameter for fine grained soils

In-situ behaviour of fine-grained soils could be considered more complicated to capture than coarse-grained's soils and more site-dependent. The mineralogy is crucial to mechan-

ical behaviour because particle forces are large compared to its volumetric weight, and variability in the mechanical response is linked to the range of clay minerals encountered in nature.

However, the engineering practice shows that a good approximation can be obtained from in situ and basic index tests. Subsequently, additional site investigation can be motivated from first modelling. A review of the most used soil parameter and soil properties is pursued in the following sections. It is concluded that there is no explicit parameter or property in fine-grained soils that can be defined as a key parameter; instead, a combination of them.

Index test

The well known Atterberg limits determine the plastic limit, w_P where the soil ceases to be plastic and become brittle, and liquid limit, w_L where it starts to flow like a liquid. Since they depend on mineralogy, the limits can describe the amount of clay particles in the fine-grained soil. The w_L determination could be done by the Casagrande cup or the fall cone test. The w_P determination is done by the thread rolling plastic limit test. Generalising, clay soil sample at the state of plastic limit has approximately a hundred times the strength that it had at liquid limit state, Wroth 1984. However, the 100-fold ratio is set to be soil-dependent, and a value of 35 seems to be more representative, Vardanega and Haigh 2014. The plasticity index is the water content that separate both states, $I_P = w_L - w_P$. The consistency index, I_c , can describe the soil's state compared to the plastic and liquid limit, $I_c = (w - w_P)/I_P$, being w the water content of the soil and a state parameter. Its complement is the liquidity index, $I_L = (w_L - w)/I_P = 1 - I_c$. Immediately, it can be seen a similarity of I_c or I_L to RD , both can describe the state of the soil, and hence, I_c could be chosen as a *key-parameter* for fine-grained soils.

The critical state soil mechanics, CSSM, describes that the soil sheared at large strains reach a critical state where without further changes in the stress state neither void ratio, the shear distortions continue. The critical state line defines a unique relation between the stress state and the void ratio. Since all soils will reach the critical state at large distortions, this relationship is independent of the initial state and depends only on the nature of the soil's grains, Atkinson 2007. The aforementioned gives way to the possibility of using w_L , w_P and w to determine parameters for CSSM. Schofield and Wroth (1968) relates these index properties to critical state equations, e.g:

$$\lambda \cong 0.92(w_L - 0.09) \quad (3.4)$$

being λ the isotropic compression index. It is clear the importance of index test to model fine grained soils properly. Different frameworks relating CSSM parameters to soil's properties were made, e.g. Favre 1980, Burland 1990, Wood 1990, Wroth 1979, and large empirical correlations for soil's compressibility based on Atterberg limits exist, e.g., Skempton and Jones 1944, Terzaghi et al. 1948, Azzouz et al. 1976 and Sharma and Bora 2015 to name a few. However, a problem is encountered when correlating in situ measurements (i.e. CPT) to I_P , w_L or w_P : the existing correlations have considerable uncertainty. A probabilistic assessment through Bayesian updating methodology was done with the ambition to provide a new characterisation and classification framework. From

the study, a correlation for plasticity index I_P and liquid limit w_L were developed, Cetin and Ozan 2009:

$$I_P = 10^{[2.37+1.33\log(F_R)-\log(q_{t,1,net})]/2.25} \quad (3.5)$$

$$w_L = 10^{[3.79+0.79\log(F_R)-\log(q_{t,1,net})]/2.52} \quad (3.6)$$

Equations 3.5 and 3.6, Cetin and Ozan 2009, uses CPTu measurements normalised friction ratio F_R and normalised corrected cone tip resistance $q_{t,1,net}$ (MPa), different normalisation scheme of $(q_t - \sigma_v)$ than the one used by Robertson 2009.

The standard deviation SD for equation 3.5 and 3.6 is 9.83 and 14.71 respectively, and the actual vs predicted graph is shown in figure 3.7. If the variability of these equations is compared to the range of plasticity index that can define the lower and upper limit between sandlike and claylike behaviour stated by Robertson (2016): $10 < IP < 18$, it cannot be used to characterise the transition soils from coarse-grained to fine-grained soils.

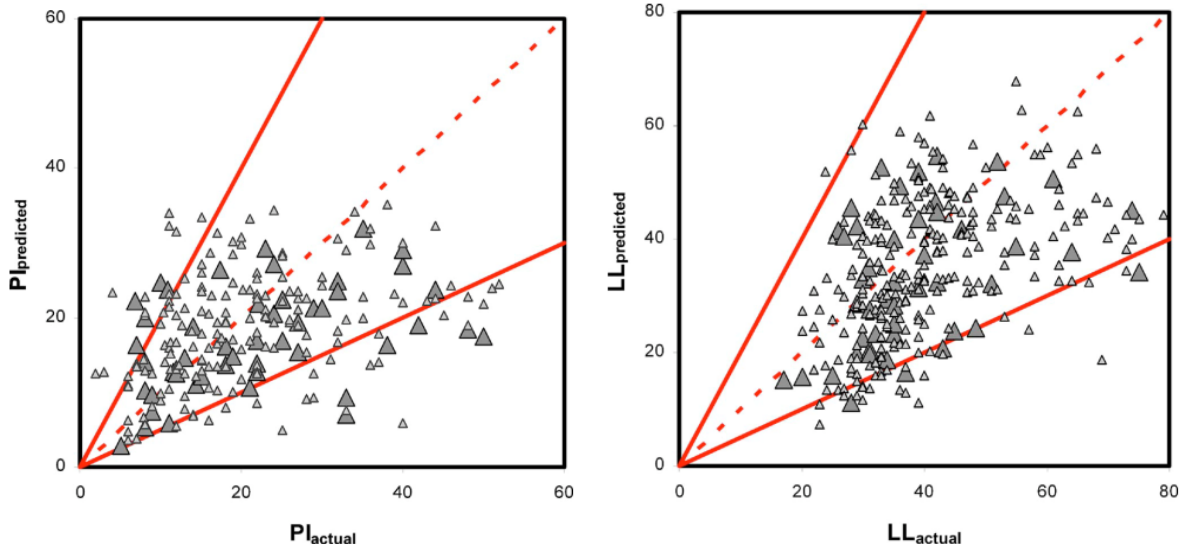


Figure 3.7: Comparison of actual and predicted plasticity index I_P and liquid limit w_L by Cetin and Ozan 2009.

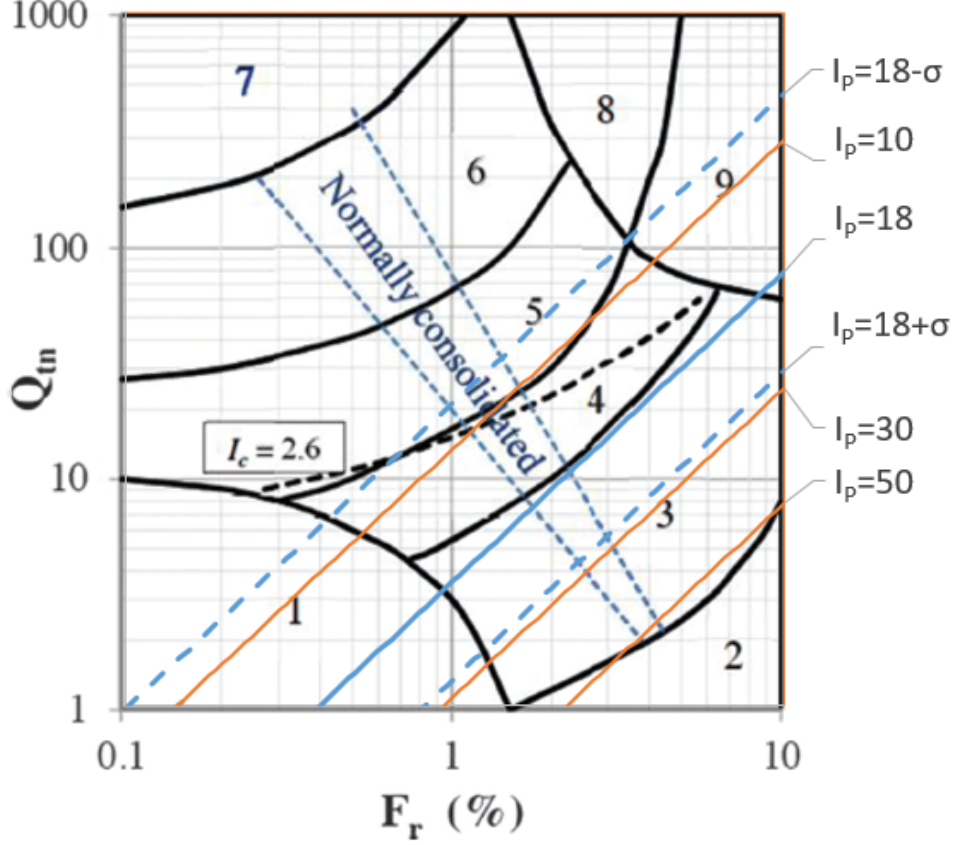


Figure 3.8: Robertson 2016 chart Robertson 2009 together with symbolic representation of plasticity index I_P of Cetin and Ozan 2009, equation 3.5 over different soils. $q_{t,1,net}[MPa] \approx Q_{tn} \cdot p_{atm}[MPa]$ and stress exponent $c = 1$.

In figure 3.8, the equation 3.5 was plotted on the Robertson 1990 chart. The values of $I_P = 10$ for boundary 5 – 4 and $I_P = 18$ for boundary 4 – 3 proposed by Robertson 2016 match the equation 3.5 for normally consolidated soils. It is also plotted the confidence interval of $I_P = 18 \pm SD$ accounting for 68.3% of the data, being SD the standard deviation of the equation 3.5.

To plot equation 3.5 on Robertson chart, the normalised cone tip resistance proposed by Cetin and Ozan 2009 was assumed equal to the Robertson 2009 one, $q_{t,1,net}[MPa] \approx Q_{tn} \cdot p_{atm}[MPa]$. The normalisation factor c proposed by Cetin and Ozan 2009 results similar to Robertson's one, with a general difference of 10% to 15%. Equations 3.5 and 3.6 evaluated with $q_{t,1,net}[MPa] \approx Q_{tn} \cdot p_{atm}[MPa]$ assumption do not change significantly the outputs in fine-grained soils. In figure 3.8 the chosen exponent $c = 1.0$ since the plasticity investigation is done on clayey soils.

$$q_{t,1,net} = \frac{q_t - \sigma_v}{\left(\frac{\sigma'_v}{p_{atm}}\right)^c} \quad 0.25 \leq c \leq 1.0 \quad (3.7)$$

Guglielmelli 2018 evaluates the correlations proposed by Cetin and Ozan 2009 for plasticity index with soils from Groningen, The Netherlands. It is concluded that acceptable results are obtained for sandy Clay Loam and its underestimate for clean clay, silty Clay, and overconsolidated Clay.

Piantedosi et al. 2009 applies specific machine-learning, tree learning and data mining techniques to predict w_L and I_P from CPT data of Chi-Chi, Taiwan. The results seem promising for a first prediction. However, they are based on local data, and further training of the algorithm is needed to predict global data.

Reale et al. 2018 also used machine learning, a feed-forward ANN (Artificial Neural Network) with CPT data to classify fine-grained soils according to European Soil Classification System (ESCS) and Unified Soil Classification System (USCS). Data from Northern Croatia were used to train, test, and validate the ANN model. It was further tested with external CPT data. The ANN model predicts the fine contents, w_L and I_P . The results were compared to equations 3.6 and 3.5 showing substantial improvement in accuracy concluding that CPT data can predict fine contents, w_L and I_P . However, the model needs to be trained with more locations to be used worldwide. An important remark is that equations 3.5 and 3.6 shows low variability with the evaluated data by Reale et al. 2018.

Over-consolidation ratio, OCR and preconsolidation stress, σ_p

Most soils are the result of sedimentation processes where normal consolidation conditions prevail. However, due to physical, environmental, climatological and thermal processes over a considerable period, it becomes overconsolidated. The in-situ soil behaviour will depend on this, and the material's yield stress needs to be addressed. The yield stress σ'_y separates the normally consolidated soils of the overconsolidated ones, assuming plastic response on the normal compression response and pseudo-elastic response on the overconsolidated region, Mayne et al. 2009.

The vertical pre-consolidation stress, σ'_p , is associated with the mechanical unloading of stresses, whereas σ'_y includes additional effects as bonding, fabric and structure. Commonly the preconsolidation stress is used as the yield stress, Mayne et al. 2009. However, in the CSSM, the σ'_p is more appropriate since the framework is based on reconstituted samples. The overconsolidation ratio $OCR = \sigma'_p / \sigma'_v$ can be obtained from σ'_p if the effective vertical stress is known, adding uncertainty if it is not known accurately.

Many correlations exist relating σ'_p or OCR to CPT data. Moreover, many other parameters depend on it, e.g. G_0 , K_0 , which makes it an essential parameter to be determined. Existing charts can indicate if a soil is overconsolidated, and as a reference, the well-known Robertson 1990 chart is shown in figure 3.9, where it shows that OCR increases to the upper right corner.

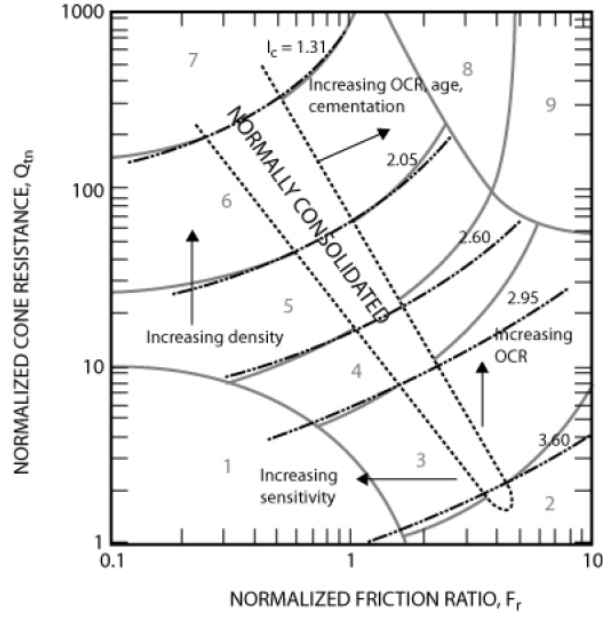


Figure 3.9: Robertson 1990 chart, Robertson 1990, indicating *OCR* trend

Undrained shear strength

The undrained shear strength, s_u , is normally used when the rate of loading or/and the consolidation coefficient c_v do not allow the dissipation of the excess pore pressure leading to unrealistic results if considered drained. The s_u is not a fundamental material property; it is a measured response of soil during undrained loading, which assumes zero volume change, Kulhawy and Mayne 1990. It is one of the most reported values for clays; however, assigning a single value of s_u to a given clay is not possible due to anisotropy, strain rate, the direction of loading and boundary conditions, Mayne and Peuchen 2018. In other words, s_u is different for each test type, e.g. $s_u(VST)$; $s_u(CIUC)$; $s_u(DSS)$.

The undrained shear strength is best represented in normalised form ($S = s_u/\sigma'_v$). The parameter S can be evaluated using CSSM laws or empirical approaches as Stress History and Normalised Soil Engineering Property, SHANSEP, Mayne 2013.

The many existing s_u may produce confusion on the determination of the required value in the modelling. As an example, the following two correlations are retrieved from different methodologies:

$$S = s_u/\sigma'_{v(NC)} = 0.11 + 0.0037 \cdot I_P \quad (I_P\%) \quad (3.8)$$

$$S = s_u/\sigma'_{v(NC)} = \phi'/100 \quad (3.9)$$

Mayne (2013) explains that these two equations are incompatible with one another since they came from different shear modes. Equation 3.8, Skempton 1957, was developed from raw field vane shear data and equation 3.9, Wroth 1984, from triaxial compression test based on CSSM. Both are valid; however, considering that S increases with I_P and ϕ' , a corollary could be that ϕ' increases with I_P . This corollary was shown to be not true by Mayne 2013, and the shear modes and the nature of the samples need to be addressed.

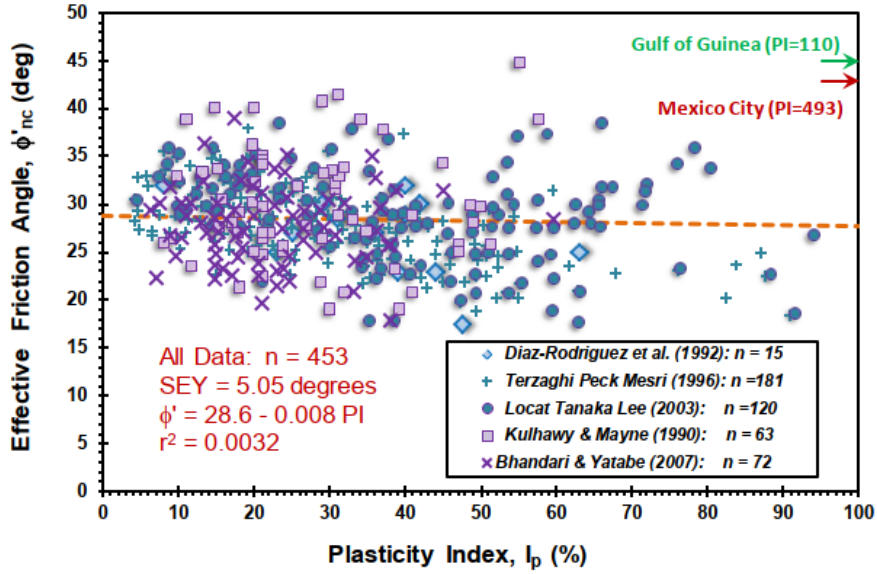


Figure 3.10: Mayne 2013 graph showing no correlation between I_P and ϕ' , contrary to what is seen in many bibliographies.

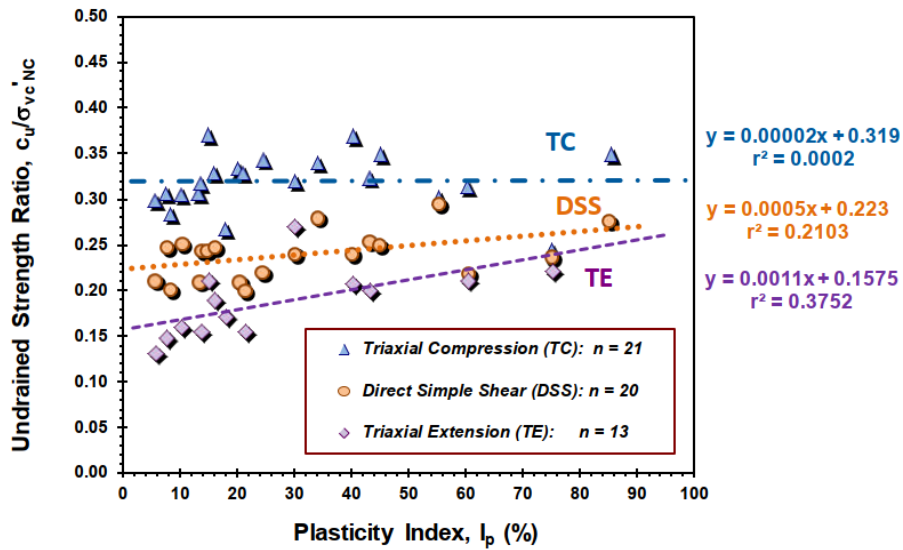


Figure 3.11: Graph retrieved from Mayne 2013 showing undrained strength ratio $S = s_u/\sigma'_{v,NC}$ vs I_P . For triaxial compression, TC , no relation is found. Original publication from Ladd 1991.

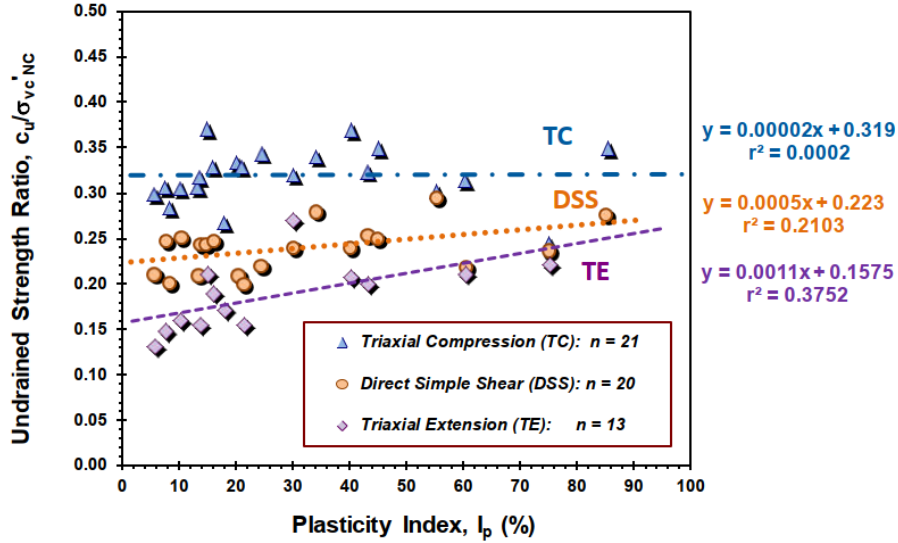


Figure 3.12: Mayne 2013 confirm from independent data the trends of Ladd 1991, figure 3.11, for undrained strength ratio S to plasticity index I_P . For triaxial compression, TC , no relation is found.

In figure 3.10, Mayne 2013 shows from a large database that I_P is not correlated to ϕ' , and suggest to use an average value $\phi' = 28.6^\circ$ with an standard deviation $SD = 5.1^\circ$. This is confirmed in figure 3.11 where the undrained strength ratio S is independent of I_P in triaxial compression mode, Ladd 1991, and confirmed in figure 3.12 with independent data by Mayne 2013, who concludes that "strength ratios from triaxial compression cannot be associated directly with vane shear results, as they are quite different".

Correlations from different shear modes are included in the APD database, aiming to give a sort of average value. First, however, it is essential to understand the modelled scenario's failure mode to determine the input s_u of the original. One example is the NGI-ADP constitutive model, Grimstad et al. (2012), where the undrained shear strength is an input parameter. The NGI-ADP model directly uses the design undrained shear strength profiles in a FEM model and considers anisotropy of s_u . Therefore, in the APD framework, the user needs to define which equations to consider or disregard if a constitutive model like NGI-ADP is used or for a specific shear mode.

3.5 Conclusion on fine-grained soil characterisation on APD framework

Since only one correlation exists to estimate the plasticity index and liquid limit from CPT outputs and have large variability, many accepted correlations for fine-grained soils, mostly related to compressibility characterisation, could result in wrong estimations. Therefore, introducing a second relationship for these parameters could significantly impact the APD final parameters' accuracy.

It is concluded that plasticity characteristics as I_P and w_L , and the "state" parameter I_L are key properties for CSSM parameters and others. Furthermore, the OCR and σ'_p are also key parameters with the undrained shear strength, s_u or undrained shear strength ratio, and S . However, compared to I_P and w_L , for the OCR , σ'_p and s_u there are numerous

correlations in literature. The transparency and flexibility of the APD framework give adaptability to the user deciding which correlations are appropriate to use in a specific problem.

The use of a well known CPT classification chart as the Robertson ones could foster the implementation of the APD in the industry for what they are used. The Robertson 2016 charts and the Robertson 2010 will be used to better describe and apply the correlation correctly within its validity.

Chapter 4

Implementation of correlations for fine grained soils

4.1 Soil correlations introduction

As stated in section 3.1, geotechnical engineers need to characterise the soil to predict its behaviour. They need to approach problems in a practical and reliable strategy, including adopting a behaviour model and the model parameters. However, in most projects, a comprehensive characterisation of the soil could lead to a high cost, Kulhawy and Mayne 1990.

Correlations are widely used in practice to have a first approximation. They mainly consist of test data plotted and compared to a variable. Caution must be taken from its generalisation, and its limitations must be studied. It is reminded that the APD framework does not aim to avoid laboratory test but to have a first impression of the soil behaviour, improving the understanding when they are not available.

4.2 Soil correlations in APD framework

Up to the moment, Cone Penetration Test input data are used. From the values cone resistance q_c and sleeve friction f_s that characterise a soil layer, different parameters are calculated. The inclusion of pore pressure, normally measured at the cone's shoulder and named u , gives a third value for the characterisation.

Correlations found in the literature are added to the database of the program. The uncertainty of the correlation is introduced as the standard deviation, section 2.3. If it is not provided, a graphical approximation can be obtained as described in section 2.3.2. However, it is not stated how to proceed when the variables were log-transformed.

4.2.1 Non normality variability of regression's correlations

Some correlations include large data ranges, and to show it in a graph, many authors apply a log transformation of the axis. In other cases, they use it to do a linear regression on a non-linear trend. Moreover, it is also possible that the spread of the scattering around the trend line, the variability of variable y , change over the range of the measured variable, the

variable x . This unequal variability is called *heteroscedasticity*, and the transformation of the variables can solve it.

The stiffness is stress-dependent in soils, and an exponential variation of correlations' trend can be expected. Thus, the scale's log-transformation is often used to undertake a linear regression. Many of the correlations' graphs that involve the stiffness have applied the scale transformation. The logarithmic transformation is also used to treat heteroscedasticity in these cases. This type of transformation is the only one described since it was the only one observed for this thesis.

The graphical rule that says that 95.45% of the data in a normal distribution comprises 4σ is still valid for log-transformed data; however, differently. An explanation and the recommended procedure is shown below..

Linear regression

When the results of a test are plotted and they are scattered around a straight line, the observations can be described by a model of the type:

$$Y = \beta_0 + \beta_1 x + \epsilon \quad (4.1)$$

The expected value of Y is formed by a mean value function plus a random error term. The linear model is the regression line $y = \beta_0 + \beta_1 x$, composed of the variable x and the coefficients β_0 and β_1 . The random error term is ϵ .

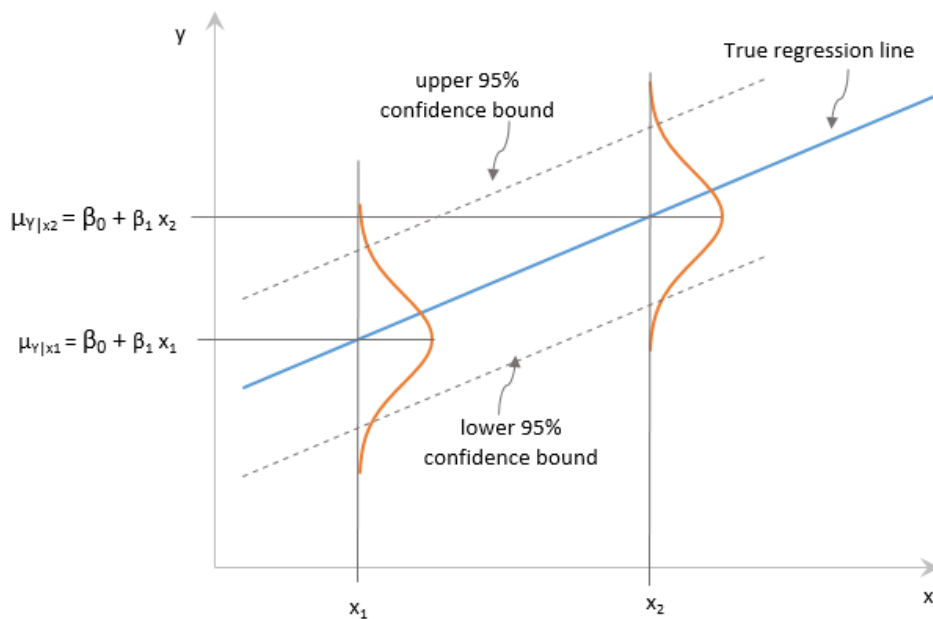


Figure 4.1: Example of a distribution of Y for given values of x

It can be assumed that the error has a normal distribution with mean $\mu = 0$ and variance σ^2 . The variance σ^2 determines the variability of the observations. The upper and lower 95% confidence bound correspondent to an interval of $Y = \mu_{y|x} \pm 2\sigma$ as is shown in figure 4.1.

4.2.2 Logarithmic transformation

It was commented that logarithmic transformations might be applied to the data and in soils that follow an exponential trend or when the variation is not constant over the range of the independent variable. An exponential model has a type of equation, Montgomery and Runger 2014:

$$Y = \beta_0 e^{\beta_1 x} \epsilon \quad (4.2)$$

This function can be transformed to linear using a logarithmic transformation:

$$\ln Y = \ln \beta_0 + \beta_1 x + \ln \epsilon \quad (4.3)$$

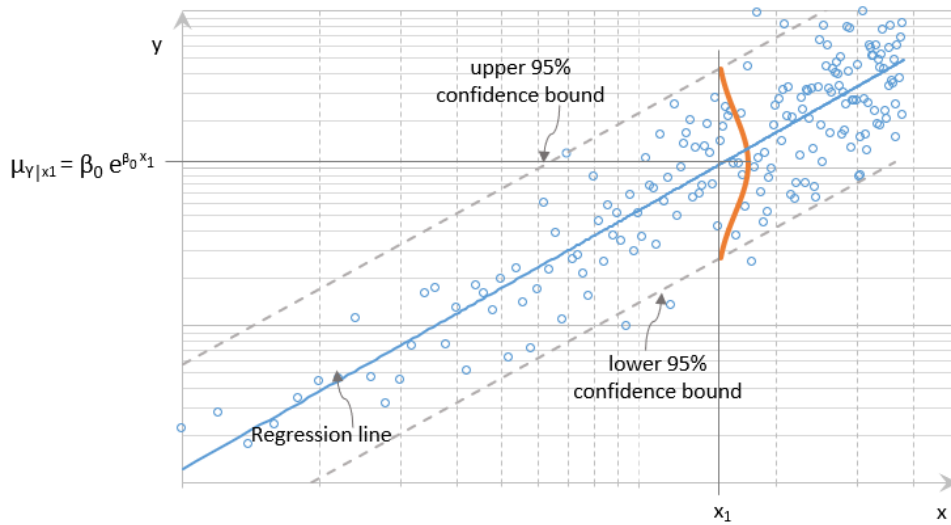


Figure 4.2: Example of linear regression on transformed variables. Note the logarithmic scale of the axis and the normal distribution of $\ln Y$ scattering around the trendline.

The exponential base does not change the relationship's validity. In this case, the logs are applied to both sides of equation 4.2, and it is called a log-log transformation. A semi-log form is possible if the logs are applied to one side of the equation. However, semi-log transformations are not frequently used in soil correlations in the regression process; therefore, they are not considered. Assuming that the transformed variable $\ln(Y)$ is normally distributed with mean ξ and standard deviation θ , the log-normal distributed variable Y has mean and standard deviation as Koopmans et al. 1964:

$$\mu_Y = e^{\xi + \frac{1}{2}\theta^2} \quad (4.4)$$

$$\sigma = e^{\xi + \frac{1}{2}\theta^2} \sqrt{e^{\theta^2} - 1} \quad (4.5)$$

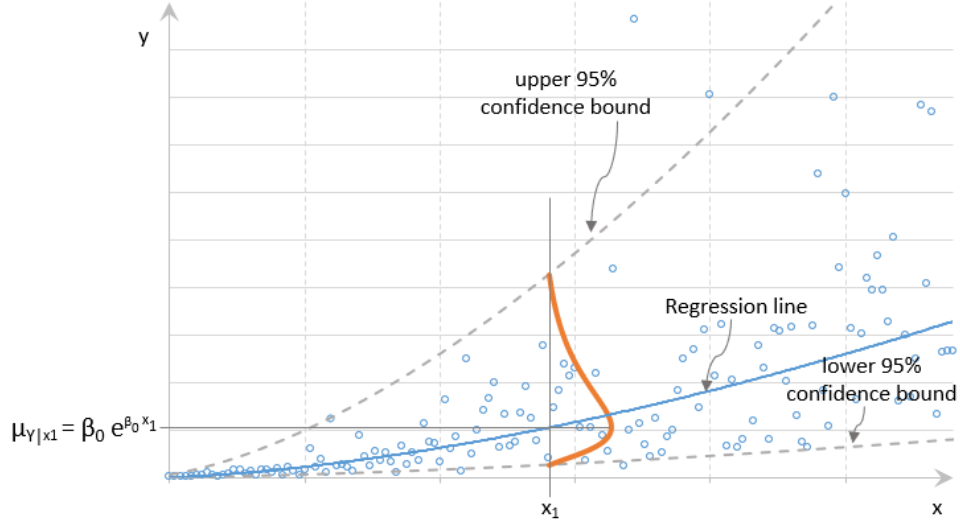


Figure 4.3: Example of an linear regression on transformed variables, as figure 4.2. Note the regular scale of the axis, the log-normal distribution of Y scattering around the trend-line and the heteroscedasticity.

The standard deviation of the normally distributed error $\ln \epsilon$ is sometimes provided under the name of *S.E.Y.*, the standard error of the y-estimator. However, the standard error of the predictor is needed in the method's database of the APD framework, Hauth 2020. For this reason, the required *SD* in the APD varies depending upon the expected value of the correlation, since it is a multiplicative rather than additive factor, Kirkwood 1979, as equation 4.2 shows.

Kirkwood 1979 in these cases recommend using a standard error expressed as a percentage of the mean. Analogous to the coefficient of variation *CV*, on the log-normal distribution, the geometric coefficient of variation was proposed as:

$$GCV_1 = (e^\theta - 1) \cdot 100 \quad (4.6)$$

being e^θ the geometric standard deviation.

However, a different definition and accepted of the geometric coefficient of variation is normally used in practice and can be defined by Koopmans et al. 1964 as:

$$GCV_2 = \sigma / \mu_Y = \sqrt{e^{\theta^2} - 1} \quad (4.7)$$

Log-log transformed correlations in APD

The characterisation of the total uncertainty in the APD considers a normal distribution of the error around the trendline. If strictly a log-normal distribution of the error is considered, the estimation of the final parameter's uncertainty must be changed in the APD statistical framework. Instead, for log-transformed correlations, it is proposed to assume a normal distribution matching the lower boundary.

This is better explained in figure 4.4 where a chosen *CV* assuming normal distribution match the lower 95% confidence bound of the log-normal distributed variable Y .

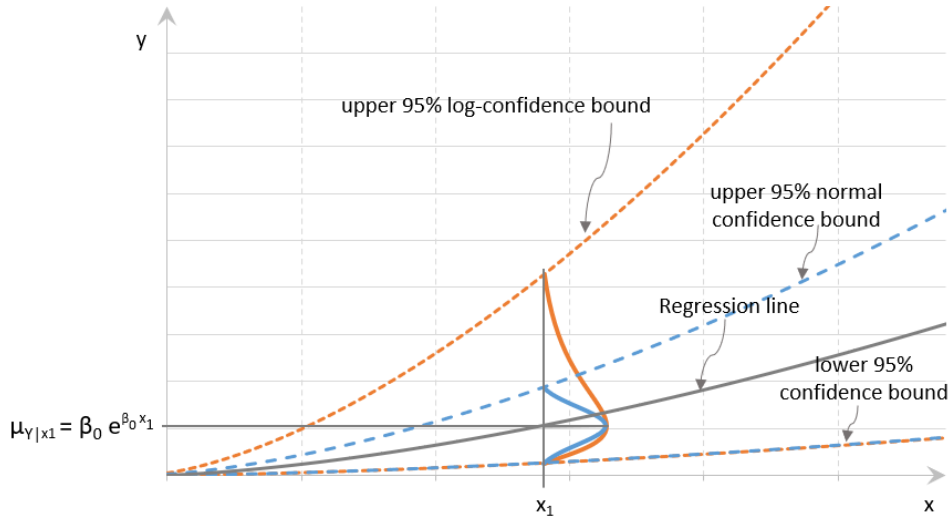


Figure 4.4: Normal distribution of error assumption over log-transformed correlations

Even though the assumption of normality of the error discards the log-normal distribution's upper tail, this is considered acceptable at the APD framework's development stage. The reason lies in the fact that choosing to match the lower boundary in most geotechnical parameters is a conservative approach. For example, the small strain shear modulus, G_0 , is decisive for determining strains in excavations, and we are interested in the smaller values that could give larger displacements. An advantage of using a CV is the flexibility in the case of observing another distribution, e.g. an increasing variability along the $x - axis$ but uniformly distributed in $y - axis$ could be assumed as normally distributed.

Once the CV is estimated for a correlation that matches the lower 95% confidence interval, it can be entered into the APD database. In the following procedure example, decimal logarithm is used since it is the only one encountered in the correlations used in this thesis. If the CV is not provided:

1. If the SD of the log (Y) is provided, find the lower boundary for an x as

$$lower_{95\%} = \frac{Y(x)}{10^{2 \cdot SD(\log Y)}}$$
2. If no data is provided, graphically estimate the lower 95% confidence interval.
3. The $CV = \frac{Y(x) - lower_{95\%}}{2 Y(x)}$

Following the previous steps will result in a CV matching the lower boundary and make possible checking the variability. The equations 4.6 and 4.7 are still valid but will often result in a too conservative lower boundary when using it in a normal distribution assumption.

Example

A correlation from Mayne and Rix (1995) for the shear wave velocity is shown here to exemplify the procedure. The relation of cone penetration tip resistance q_c to estimate the shear wave velocity V_s was studied.

$$V_s = 1.75 \cdot q_c^{0.627} \quad (m/s) \quad (4.8)$$

where q_c is introduced in kPa.

The standard deviation of the transformed variable is provided, $SD(\log V_s) = 0.146$ that is used to estimate a coefficient of variation $CV = 0.24$. Since the standard deviation is provided, step 1) and 3) are followed:

$$Y(1000 \text{ kPa}) = V_s(q_c = 1000 \text{ kPa}) = 133.06 \text{ (m/s)}$$

$$lower_{95\%} = \frac{Y(x)}{10^{2 \cdot SD(\log Y)}} = \frac{133.6}{10^{2 \cdot 0.146}} = 67.927$$

$$CV = \frac{133.06 - 67.927}{2 \cdot 133.06} = 0.24$$

If we assume that the standard deviation was not provided, we can graphically draw a lower boundary as shown in figure 4.5, that accounts for 95% of data. At $q_c = 1000 \text{ kPa}$ the lower boundary would be around 67 m/s , and the step 3) could be taken. The introduction of the variability in the APD database should be as $CV(0.24)$.

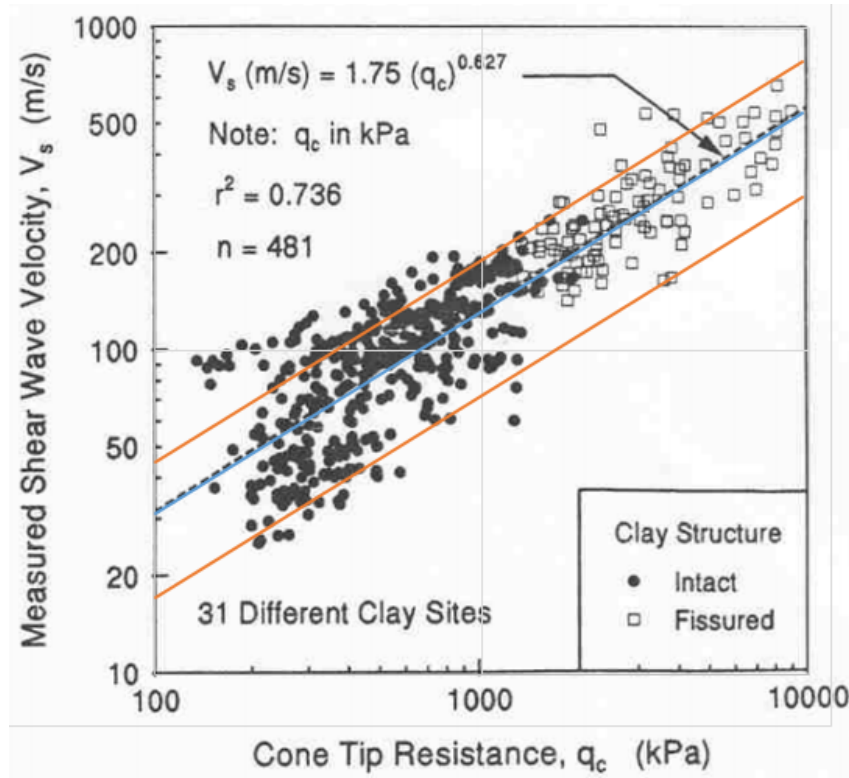


Figure 4.5: Mayne and Rix (1995) relation for V_s from q_c . Estimated bounds for normal distribution of 95% are shown

4.2.3 Implementation of coefficient of variation in APD program variability assessment

Some modifications have been made in the program to identify, read and estimate the standard deviation SD from a provided CV . The idea is to estimate a single standard deviation, SD , for an estimated value of the correlation, $\mu_i = a \cdot x_i$. The program once it has the value of a correlation's output, μ_i and proceeds to calculate the added variability,

it use the CV and multiply it by μ_i , obtaining an approximation of the real SD of the method for x_i input. The proposed way to input the CV using an example of $CV = 0.20$ is $CV(0.20)$.

It is interesting to note that most of the correlations shown in appendix A have a CV around 20 – 30%.

4.3 New filters on correlations

The filters in the APD are the method validity's structure that allows the user to indicate when a method is valid. In other words, it will enable the program to select the methods when certain conditions are met. Along with the already implemented filters for the validity of a correlation, new ones are added. The existing ones are Soil Behaviour Type (SBT), I_c index, and state of consolidation.

The new ones respond to the inclusion of correlations for fine-grained soils. They are the normalised cone resistance (Q_{tn}), pore pressure ratio (B_q), and Sensitivity (S_t). Therefore, it is possible to limit the use of the correlation if the conditions are not met, e.g. the filters $Q_{tn_min}(12)$ and $Q_{tn_max}(20)$ will only allow the correlation to be used if $8 < Q_{tn} < 12$. The same conditions (max & min values) are applied to S_t and B_q .

Caution must be applied when input the filters to the correlations. As an example, if SBT that is based on Robertson 2010 is used together with I_{cn} of Robertson 2009 for a method when the different charts do not match the classification, the method will not be used. Therefore, it is recommended to use the filters that the author of the correlation proposed and never used together with SBT with I_c or I_{cn} .

4.4 Verification of implemented correlations

To test that the new correlations are well implemented, it is decided to use a new tool made by the APD team, the Unit Tests. The list of correlations recompiled are shown in appendix A. No all of them are used necessarily in the APD framework.

4.4.1 Methods Unit Tests

The Methods Unit Test in the APD demands a new database where each method's variables have a value. In addition, the correspondent result of the method evaluated at the assigned values is also included. Since the result is deterministic, the Unit Test tool compares the given outcome with the implemented correlation's output using the provided variables' values. A schematic example of a test for a method is shown in figure 4.6.

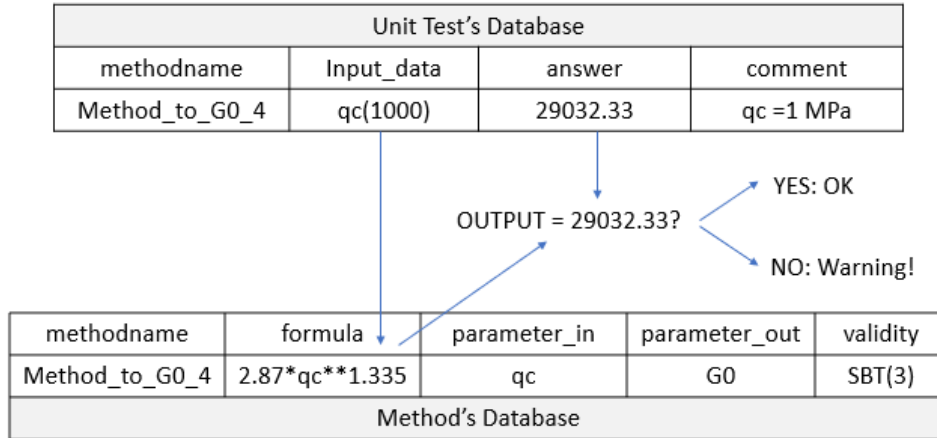


Figure 4.6: Schematic example of Unit test tool operation applied to a method. The complete database of the correlation is not shown.

The APD Unit Test is used to verify the implemented correlations. If the results are good, the process finished without warnings. This means that the outputs of the correlations are the expected ones.

4.5 Conclusions

In this chapter, the variability of the correlations' uncertainty was addressed assuming a multiplicative error, considering normal distribution of it. The aim is to match the lower boundary of the log-transformed data probability density function to estimate the CV later. If the author does not provide the correlation's CV , a procedure is proposed to estimate it in 4.2.2, and the program's adaptations to deal with CV were summarised. Finally, the implementation of the correlations' formulas was tested with the *method unit tests* tool developed by the APD team and prove to be successfully implemented.

Chapter 5

From CPT measurements to clay properties

5.1 Clay properties introduction

It is stated in chapter 3 that the Atterberg Limits, which depends on the particles' mineralogical nature, can be used to estimate intrinsic clay parameters. This means parameters that do not depend on the structure or state, e.g., the slope of the perfect plasticity line, λ . Moreover, since the Atterberg Limits are performed on quasi-saturated samples, the water content w can express the void ratio e of the soil and can be used as a state parameter, compared to the liquid limit, w_L , and plastic limit, w_P . Therefore, the parameters w_P and w_L could be considered soil "properties" since they do not depend on the soil's state.

The APD framework aims to give a first characterisation of the in-situ soil behaviour by means of advanced constitutive model's parameters. In the APD framework, a problem is encountered when estimating critical state soils mechanics constants: most of the correlations use Atterberg Limits, and there is a unique equation in literature to correlate it to CPTu data. Moreover, many fine-grained soil parameters use w_L or the plasticity index, I_P , to have a better estimation, for which having a second estimation of them is highly interesting.

This chapter proposes a second correlation for w_L and I_P . Any proposition that involves a single set of correlations will result in a homogenisation of the results, e.g. a single correlation of liquid limit - plasticity index will result in a broad generalisation of the plasticity index. However, the procedure aims to provide a second value of w_L and I_P .

Moreover, correlations for stiffness model parameters of the Hardening Soil with small stiffness model (HSsmall) and the Soft Soil model parameters are summarised to complete the APD database.

5.2 The objective: Hardening Soil model's parameters

As an objective, it is proposed to provide model parameters for the Hardening Soil with small-strain stiffness model and the Soft Soil model through the APD framework. A brief

description of the model parameters is introduced in this section to exhibit which ones are crucial to the APD framework.

Since most of the Soft Soil model's parameters are relative or included in the Hardening Soil models, it is decided to focus on the second, which is used in the validation in chapter 6.

5.2.1 The Hardening Soil model with small-strain stiffness, (HSsmall)

The Hardening Soil model, HS, is an advanced model that allows the simulation of soft soils and stiff soils, Schanz et al. 1999. This versatile model contains compression hardening and shear hardening and elastic material behaviour during unloading and reloading. The hardening Soil model with small-strain stiffness, HSsmall, includes small strain stiffness and its non-linear dependency on strain amplitude, PLAXIS Material Model 2020.

Model parameters, PLAXIS Material Model 2020:

Parameters	Description
c	(Effective) cohesion
ϕ	(Effective) angle of internal friction
ψ	Angle of dilatancy
σ_t	Tension cut-off and tensile strength

Table 5.1: Failure parameters as in Mohr-Coulomb model, PLAXIS Material Model 2020

Parameters	Description
m	Power for stress-level dependency of stiffness
E_{50}^{ref}	Secant stiffness from triaxial test at reference pressure
E_{oed}^{ref}	Tangent stiffness from oedometer test at p^{ref}
E_{ur}^{ref}	Reference stiffness in unloading / reloading
ν_{ur}	Poisson's ratio for unloading-reloading
G_0^{ref}	Reference shear modulus at very small strains $\epsilon < 10^{-6}$
$\gamma_{0.7}$	Threshold shear strain at which $G_s = 0.722G_0$

Table 5.2: Basic parameters for soil stiffness, PLAXIS Material Model 2020.

Parameters	Description
C_c	Compression index
C_s	Swelling index or reloading index
e_{init}	Initial void ratio

Table 5.3: Alternative parameters for soil stiffness basic parameters, PLAXIS Material Model 2020.

Table 5.3 provides an alternative for the stiffness parameters when soft soils are considered. The Compression index C_c is used to estimate E_{oed}^{ref} and E_{50}^{ref} together with the initial void ratio and reference pressure p^{ref} . The Swelling index C_s can be used to estimate E_{ur}^{ref} .

$$E_{oed}^{ref} = \frac{p^{ref}}{\lambda^*} \quad \lambda^* = \frac{\lambda}{1 + e_0} \quad (5.1)$$

5.2.2 Soft Soil model

The soft soils comprise the near-normally consolidated clays, clayey silts and peat with a high degree of compressibility compared to normally consolidated sands. As features, it has a logarithmic compression behaviour, distinguish between primary loading and unloading-reloading, memorise the pre-consolidation stress and has a Mohr-Coulomb failure behaviour. The Soft Soil model is partially based on Cam-Clay theory, and one of the main differences is that the Soft Soil uses volumetric strain rather than void ratio, PLAXIS Material Model 2020.

Model parameters, PLAXIS Material Model 2020:

Parameters	Description
λ^*	Modified compression index
κ^*	Modified swelling index
c	Effective cohesion
ϕ	Friction angle
ψ	Dilatancy angle
σ_t	Tensile strength

Table 5.4: Basic parameters, PLAXIS Material Model 2020

5.2.3 Identification of current model parameter determination problem for fine-grained soils

It has been seen that the HSsmall parameter E_{oed}^{ref} , could be estimated from the compression index C_c and swelling index C_s . In the Soft Soil this consideration is also valid. It is important to notice that equation 5.1 is valid only for small load steps, since the void ratio is variable. Most of the current correlations to estimate C_c and C_s lie on the plasticity index, I_P , liquidity index, I_L , water content, w , void ratio, e_0 or liquid limit, w_L , Skempton and Jones 1944, Terzaghi et al. 1948, Azzouz et al. 1976, Wroth 1979, Favre 1980, Nagaraj and Jayadeva 1983, Wood 1990, and Sharma and Bora 2015 to name a few. Moreover, many of the HSsmall or Soft Soil model parameters characterisation for fine-grained soils depends on them for a better prediction. As an example, equation 5.2 uses the I_P to estimate the preconsolidation stress, σ_p , from CPT data, Chen and Mayne 1996, and equation 5.3 also uses the I_P to estimate the undrained shear strength factor $N_{\Delta u}$ for sensitive clays ($S_t < 15$), Karlsrud et al. 2005.

$$\sigma'_p = pa \cdot 0.86 \cdot [(q_t - \sigma_v)/pa]^{0.93} \cdot I_P^{-0.28} \quad (5.2)$$

$$N_{\Delta u} = 6.9 - 4.0 \log(OCR) + 0.07(I_P) \quad I_P \text{ in } \% \quad (5.3)$$

It could be concluded that C_c , C_s or λ and κ are essential parameters for the HSsmall and Soft Soil models. Moreover, since I_P and w_L can be used to estimate them and other parameters in fine-grained soils, at least a first-estimation value is needed for a good characterisation in the APD framework.

$$C_c = \text{Compression index} = -\delta e / \delta \sigma'_v \quad \text{on compression} \quad (5.4)$$

$$C_s = \text{Swelling index} = -\delta e / \delta \sigma'_v \quad \text{on swelling} \quad (5.5)$$

In section 3.4.2, the existing correlation from CPT data to I_P and w_L resulting from a Bayesian update methodology, Cetin and Ozan 2009, was shown to have a large variability. In section 5.4 it is proposed a new method aiming to explore a different approach for I_P and w_L for clayey soils in the APD framework. It is not easy to believe that from CPT data, a better correlation than the proposed by Cetin and Ozan 2009 can result. However, due to the importance of those parameters in the APD framework, it is worth trying differently for clayey samples.

5.3 Existing clay constants correlations and frameworks

A review of different authors' work is presented in this section. All of them are based on statistical data of remoulded clay samples tests. Therefore, they do not account for microstructure.

5.3.1 Liquidity Index - effective stress frameworks

Schofield & Wroth

The Critical State Soil Mechanics, CSSM, was introduced by Roscoe et al. 1958, and then on the classic textbook for geotechnical engineering, Schofield and Wroth 1968. The textbook shows that index properties, under some assumptions, help to characterise the soil under the critical state concept. The dependency of clay's behaviour under normally consolidated paths to the index properties, e.g., I_P , w_L , was largely studied, Skempton and Jones 1944, Schofield and Wroth 1968, Favre 1972 and Burland 1990, to name a few.

Schofield and Wroth 1968 demonstrates that the isotropic compression index can be calculated from measured water contents, stating that *"the loss of water content that corresponds to a certain proportional increase in strength is a measure of plastic compressibility of the soil"*. The "strength" of clays with indentation test equipment at different states were also studied, resulting in an approximate relationship of strength at w_L and w_P states of 100 times, and compared to field vane test data. Considering that the indentation test strength ratio is an indirect measure of the increase of effective spherical pressure, the figure 5.1 was presented. It was also assumed that the limits p_{w_L} and p_{w_P} are fixed values, being the effective spherical pressure at the liquid limit and plastic limit correspondingly.

The assumption of a single equation $I_L - \ln p$ is based on the extrapolation of the compressibility curves, finding that all of them could be considered to converge in a single point at $p_\omega = 1500 \text{ lb/in}^2 \approx 10.3 \text{ MPa}$.

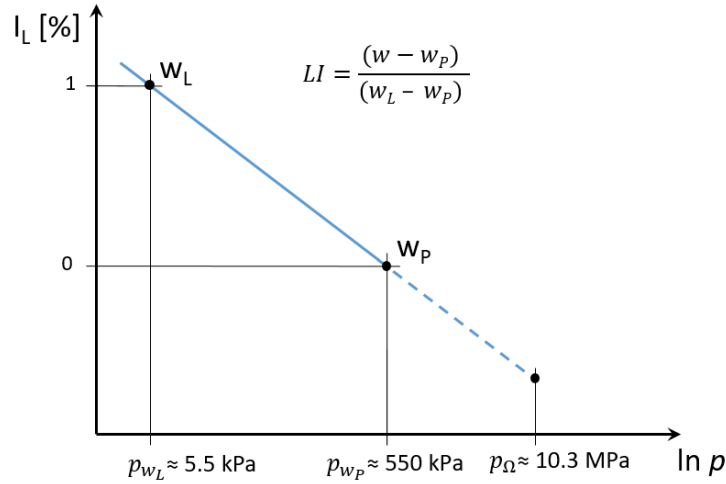


Figure 5.1: Idealized Critical State Line related to Liquidity Index LI , Schofield and Wroth 1968.

The following set of equations were developed, Schofield and Wroth 1968:

$$\lambda \approx 0.585I_P \quad (5.6)$$

$$\lambda \approx 0.92(w_P - 0.09) \quad (5.7)$$

$$\lambda \approx 0.36(w_L - 0.09) \quad (5.8)$$

where I_P , w_P and w_L are expressed in percentages.

Later on, Wroth 1979 simplify the effective spherical stress p to the effective vertical stress in one dimensional compression σ'_v , shown in equation 5.9 where σ'_v is measured in kN/m^2 . The limits w_L and w_P coincide to the vertical stresses of 6.3 kPa and 630 kPa correspondingly. These values were validated by Sharma and Bora 2015. The remoulded undrained shear strength, s_u was related to I_L , where vane shear test was used

$$I_L = 1 - \frac{\log(\sigma'_v/6.3)}{\log 100} \quad (5.9)$$

$$s_{ur} = 1.7R^{1-I_L} \quad (5.10)$$

where R is the strength ratio $s_{ur(w_P)}/s_{ur(w_L)}$ set as 100, corresponding to $s_{ur(w_L)} = 1.7 \text{ kPa}$ and $s_{ur(w_P)} = 170 \text{ kPa}$.

Wood 1990

Wood 1990 summarised and expanded the work of Schofield and Wroth 1968 on the critical state soil mechanics. Following similar paths, arrives to characteristic values of s_u and σ'_v at w_L :

$$\begin{aligned} s_{u(w_L)} &= 2 \text{ kPa} \\ p'_{(w_L)} &\approx 4 \text{ kPa} \\ \sigma'_{v(w_L)} &\approx 8 \text{ kPa} \end{aligned} \quad (5.11)$$

$$I_L = 1 - \frac{\log(\sigma'_v/8)}{\log 100} \quad (5.12)$$

These values result from a procedure where critical state soil parameters as λ , κ , and ϕ are taken from average values. It is also summarised an approach that was first suggested by Wroth 1979 to estimate the *OCR* variation from the $\sigma'_v - I_L$ plane when the possibility of obtaining unaltered samples is complex, e.g., offshore sites.

In figure 5.2, curves for different Cam clay model parameter $\Lambda = (\lambda - \kappa)/\lambda$ are drawn. Wood 1990 summarised that for values in the range of $\phi' = 20^\circ$ to 25° and $\Lambda = 0.6$ to 0.8 a ratio $\sigma'_v/s_u = 4$ is found and was used to estimate the vertical effective stress at liquid limit, $\sigma'_{v(w_L)} = 4 \cdot s_{u(w_L)} = 8 \text{ kPa}$. Favre 1980 also arrives to this assumption.

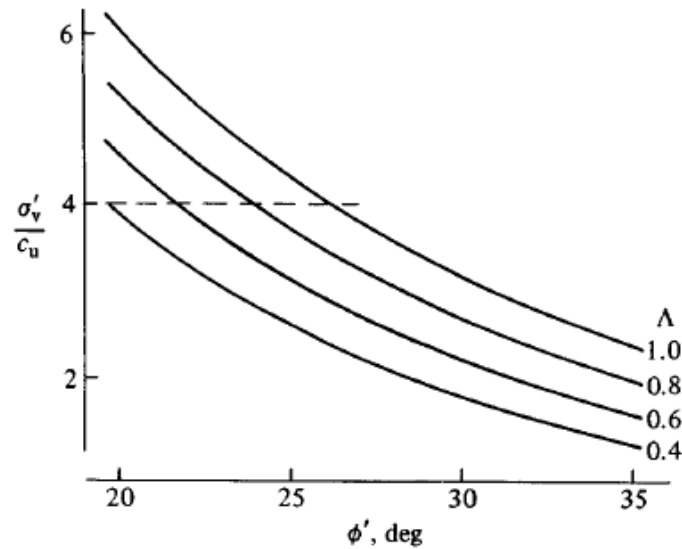


Figure 5.2: Ratio of vertical effective stress in one-dimensional normal compression, and undrained strength at same specific volume as function of $\Lambda = \frac{\lambda - \kappa}{\lambda}$ and friction angle ϕ' , from Wood 1990.

Biarez & Favre model

Favre 1972 and Favre 1980 also studied the importance of the clay "properties" to describe its mechanical behaviour. They found that the w_L and w_P approximately correspond to the oedometer loading of 6.5 and 1000 kPa, respectively, and the following relations were

made, Favre and Hattab 2008:

$$\begin{aligned} w_{sat} &= w_L \text{ for } \sigma'_v \sim 6.5 \text{ kPa} \\ w_{sat} &= w_P \text{ for } \sigma'_v \sim 1000 \text{ kPa} \end{aligned} \quad (5.13)$$

Besides, Favre 1972 describe the liquid limit, w_L , as an essential factor that rules the consolidation compressibility and also links it to the plasticity index, I_P in the following general equation:

$$I_P = 0.73(w_L - 13) \quad (5.14)$$

$$C_c = 0.009(w_L - 13) \quad (5.15)$$

$$C_c = \frac{I_P}{81} \quad (5.16)$$

Equations 5.15 and 5.16 considers a specific unit weight of solids $\gamma_s/\gamma_w = 2.7$ to obtain the compressibility index C_c . Equation 5.15 shows a close similarity to the popular empirical equations of Skempton and Jones 1944: $C_c = 0.007(w_L - 10)$ and to Terzaghi et al. 1948: $C_c = 0.009(w_L - 10)$. Moreover, the liquidity index, I_L can be expressed as a function of the vertical effective stress σ'_v , Favre and Hattab 2008:

$$I_L = 0.46(3 - \log \sigma'_v) \quad \sigma'_v(\text{kPa}) \quad (5.17)$$

Considering the approximations of equation 5.13, equation 5.17 was developed and shows that the arrangement of the grains appears to be directly linked to the consolidation process through the mineralogical properties, Favre and Hattab 2008.

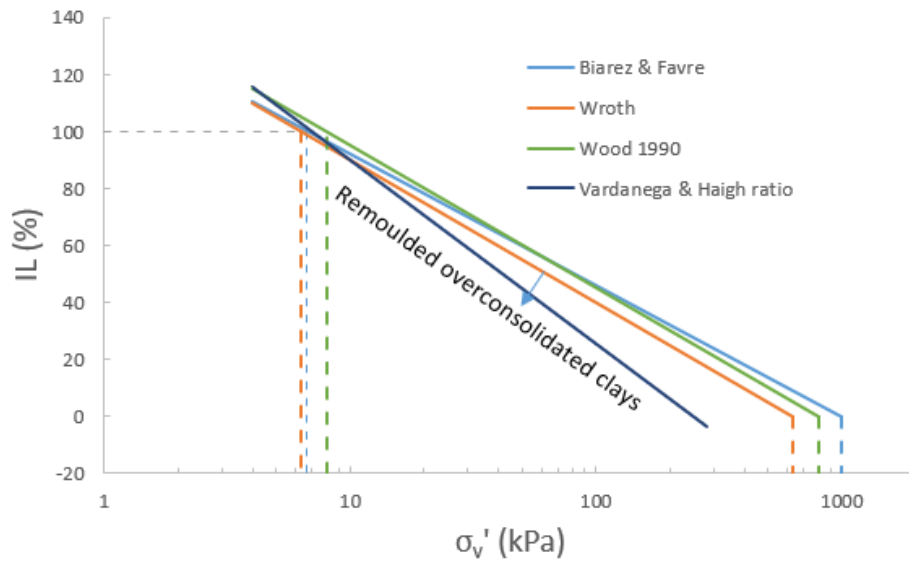


Figure 5.3: Favre 1972 and Wroth 1979, Wood 1990 Normally Consolidated Remoulded Simplified line on the $(I_L - \sigma'_v)$ plane. Wood 1990 equation is also plotted with Vardanega and Haigh 2014 proposed ratio, $R = 35$.

Figure 5.3 shows the plane of the Biarez & Favre Normally Consolidated Remoulded Simplified (NCRS), by equation 5.13. It is also shown the relationship made by Wroth 1979 and Wood 1990, to compare the frameworks. A normally consolidated remoulded clay would be located on the NCRS line and an overconsolidated one below the NCRS line. In this framework, the material's over-consolidation only depends on the clay loading history, OCR , Favre and Hattab 2008.

Burland's model

Burland's model, Burland 1990, follows a similar work as the Favre and Hattab 2008, the description of the oedometer compressibility of remoulded clay sediments to be used as a basic frame to describe natural clays. However, Burland's model expresses the results in the $(e - \log \sigma'_v)$ space. It is considered that the intrinsic compressibility index C_c^* is deducted from the difference in e_{*100} and e_{*1000} , the voids ratios corresponding to the consolidation stress of 100 and 1000 kPa. The normalised void index, I_v , was introduced analogy to I_L and from experimental data, an equation relating I_v and σ'_v is shown in equation 5.20 and represented in figure 5.4 the Burland's Intrinsic Compression Line, ICL.

$$C_c^* = e_{*100} - e_{*1000} \quad (5.18)$$

$$I_v = \frac{e - e_{*100}}{C_c^*} \quad (5.19)$$

$$I_v = 2.45 - 1.285 \log \sigma'_v + 0.015(\log \sigma'_v)^3 \quad (5.20)$$

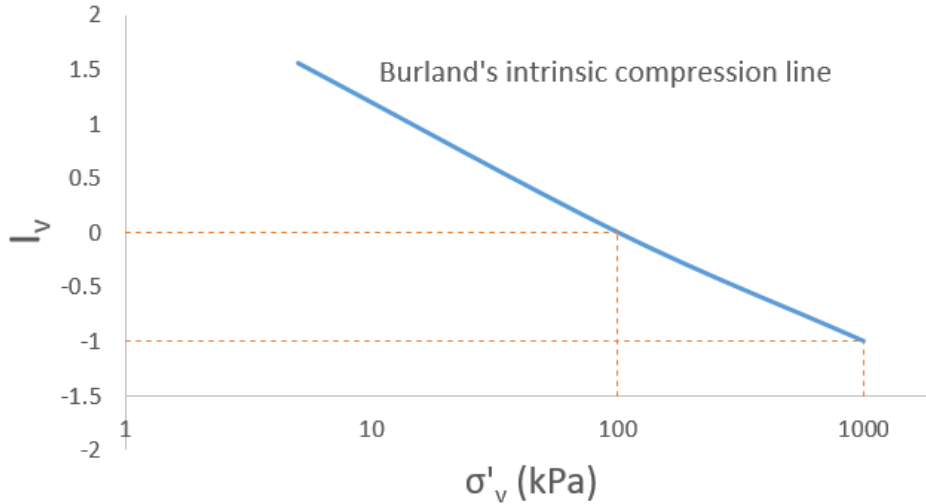


Figure 5.4: Burland's Intrinsic compression Line on the $I_v - \sigma'_v$ plane, Burland 1990

In Burland's framework, the void ratio at the liquid limit, e_L could be the unique property in this case to represent the mechanical behaviour of the clay:

$$C_c^* = e_{*100} - e_{*1000} = 0.256e_L - 0.04 \quad (5.21)$$

Burland's model describes the compressibility of remoulded reconstituted clays based on two voids ratio at fixed σ'_v while the Biarez & Favre with two "clay properties", w_L and w_P or e_L and e_P . Favre and Hattab 2008 compares the Burland's model, Burland 1990 to the Biarez & Favre one, Favre 1972, and assumed $e_P = e^*_{1000}$ to allow the comparison in the same space. Favre and Hattab 2008 concludes that Burland's ICL is more representative for a large range of w_L where the Biarez & Favre is not for high values of w_L . However, the variables w_L and w_P are well known with plenty of correlations, while the variables e^*_{1000} and e^*_{100} are not. Burland's framework cannot be simplified to a single line in a $I_L - \sigma'_v$ without taking an assumption, as it was done in Favre and Hattab 2008 taking $e_P = e^*_{1000}$. For this reason, it is decided not to use this framework.

5.3.2 The undrained shear strength at plastic and liquid limits

Wood 1990, commented on the assumption explored by Schofield & Wroth that all critical state lines converge in a single point at p_ω , addressing that might be a too bold generalisation. Therefore, Wood 1990 proposed that this point depends on the ratio of undrained shear strength at plastic limit and liquid limit, $R = s_{uP}/s_{uL}$. Previously, Schofield and Wroth 1968 establish $R = 100$ and Wood 1990 correlates the ratio R to the clay mineralogy, being approximately 30 for kaolinitic soils and 100 for montmorillonitic soils. However, the value of R being a mineralogy function was not observed by Vardanega and Haigh 2014.

Vardanega and Haigh 2014 study 641 data on 101 samples from 12 countries of fall cone test determining a relationship linking undrained shear strength to liquidity index. It is shown that the ratio $R = 100$ in the linear relationship $I_L - \log s_u$ over predict the soil strength and that a factor of 35 is more realistic and accounts for the large variability. The following relationship was found, valid for $0.2 < I_L < 1.1$

$$s_{ur} = s_{ur(w_L)} 35^{(1-I_L)} \quad (5.22)$$

There is a general agreement on the shearing strength of fined grained soils at liquid limits lying in between $1.7 - 2.0 \text{ kPa}$, Schofield and Wroth 1968, Wroth 1979, Whyte 1982, Vardanega and Haigh 2014 to name a few, having variations depending on the determination method. The standard test to define w_L are based on a fixed strength in the fall cone test or fixed specific strength in the percussion test. However, according to Vardanega and Haigh 2014, there is no fixed strength value at the plastic limit, and w_P is a measure of soil brittleness. Haigh et al. 2014 summarised different data showing a large range of strength at the plastic limit, being measured with different methods. Moreover, the thread rolling plastic limit is the standardised test, and its determination could have large variability, Whyte 1982, thus impacting the correlations' accuracy.

Equation 5.23 shows a proposal for a new definition of plastic limit and plasticity index to relate it to an increase of 100 times the strength at the liquid limit, Haigh et al. 2014.

$$I_{P100} = w_L - w_{P100} \quad (5.23)$$

In table 5.5 a brief summary of equations relating to remoulded undrained shear strength,

liquidity index and effective vertical stress is shown. Shimobe and Spagnoli 2020 summarised a large number of equations correlating remoulded and intact shear strength to liquidity index and evaluated them with 500 data showing that the correlation proposed by Shimobe and Spagnoli 2019 have a good fit for remoulded samples.

5.3.3 Plasticity index - liquid limit relationships

Different authors studied the relationship of plasticity index I_P to liquid limit w_L . The relationship depends on how these limits are defined or measured, e.g. w_L with cup or cone methods and w_P with rolling test or 100 times the w_L strength, $w_{P_{100}}$. Moreover, they are subjected to high variability since w_P could have a significant operator dependency, Whyte 1982.

Sivapullaiah and Sridharan 1985 evaluate the w_L of soil mixtures with the Casagrande cup and the cone method giving a relationship for both methods. Later, Spagnoli 2012 also evaluates the Casagrande cup that is used in DIN standard with the British standard fall cone test, both methods for pure clay and proposed the following relationship:

$$w_{L(\text{cone}(BS \text{ standard}))} = 0.99w_{L(\text{cup}(DIN \text{ standard}))} \quad (5.24)$$

The well-known Atterberg plasticity chart, $w_L - I_P$ have the Casagrande A-line, $I_P = 0.73(w_L - 20)$ that separates silts from clays. Different authors with the aim of use a unique relation developed similar equations, e.g. Nagaraj and Jayadeva 1983, Favre 1980, Baroni and Almeida 2017 to name a few.

Favre 1972 defines an equation similar to the A-line and generalised it for mineral clays. Okkels 2018 propose an extension of the Casagrande A-line when w_L exceeds 120%. Sivapullaiah and Sridharan 1985 studied the relation using soil mixtures of bentonite, kaolinite, sand and silts. Baroni and Almeida 2017 develop an equation for very soft organic clays of Rio de Janeiro, Brazil.

Polidori 2003 studied pure kaolinite clay minerals and montmorillonite with fine silica sand mixtures and proposed correlations based on the percentage of Clay Fraction, % CF. However, Spagnoli et al. 2018 did not found a significant correlation between w_L clay fraction for smectite and kaolinite clays, and proposed correlations $w_L - I_P$ for both clay minerals concluding that the clay mineralogy controls the Atterberg limits and that the clay mineralogy is required to estimate I_P from w_L correctly.

Schofield and Wroth 1968 using the assumptions of unique void ratio at large pressure, fixed strength, and effective volumetric stress at w_L reach an equation that depends on the ratio of strength R . In the same path, Sharma and Sridharan 2018 assumed strength at w_L and $w_{P_{100}}$ of 1.7 and 170 kPa respectively and reach to an equation that is experimentally validated. Nagaraj and Jayadeva 1983 also used similar considerations arriving at another equation validated empirically.

Author	$\sigma'_v(w_L)$	$\sigma'_v(w_P)$	$s_u(w_L)$	$s_u(w_P)$	$I_L - s_{ur}$ (kPa)	$I_L - s_{ur}$ (kPa)	Comments
Wroth 1979	6.3	630	1.7	170	$s_{ur} = 1.7x10^2(1-IL)$	$I_L = 1 - \frac{\log(\sigma'_v/6.3)}{\log 100}$	$R = 100, s_{ur}(VST)$ $1.7 \approx (0.7 + 2.65)/2$ $0.5 < I_L < 2.5$ $1.5 < I_L < 6$
Leroueil et al. 1983					$s_{ur} = 1/(I_L - 0.21)^2$		$R = 30$ kaolinitic;
Locat and Demers 1988			1.46		$s_{ur} = (1.167/IL)^{2.44}$		100 montmorillonitic
Wood 1990	8	800	2	200	$s_{ur} = s_u(w_L)R^{(1-IL)}$		$s_u = \sigma'_v/4$
Favre 1972	6.5	1000	~ 1.625	~ 250	$s_u(w_L)35^{(1-IL)}$	$s_{ur}I_L = 0.46(3 - \log \sigma'_v)$	$0.20 < I_L < 1.1$
Vardanega and Haigh 2014			1.7				w_{P100} is considered
Sharma and Sridharan 2018			1.7	170	$\log(s_u/1.7) = -4.9 \log(w/w_L)$		
Shimobe and Spagnoli 2019			1.95	74.28	$s_{ur} = 98 \cdot \exp[\ln\{\frac{0.4755}{(I_L+0.5012(1-IL))}\}/0.19]$		s_{ur} from LVT, UC, TC test. I_L from cup and cone
Shimobe and Spagnoli 2020					$s_{ur} = \frac{1.4}{((1-R_p)I_L + R_p)^{4.5}}$		$R_p = I_P/w_L; 0.1 < R_p < 0.9$

Table 5.5: Brief summary of frameworks to estimate I_L from σ'_v (kPa) or s_{ur} (kPa).

Author	$IP =$	w_L min	w_L max	Comments
Casagrande A-line	$0.73(w_L - 20)$	20	120	Kaolinite-quartz mixtures.
Seed et al. 1964	$0.98(w_L - 27.5)$			
Schofield and Wroth 1968	$0.615(w_L - 9)$			Natural clays, heterogeneous mineralogy.
Favre 1972	$0.73(w_L - 13)$			
Nagaraj and Jayadeva 1983	$0.74(w_L - 8)$			Bottom boundary for fine-grained soils of East of Canada
Leroueil et al. 1983	$0.73w_L - 15$	20	90	
Leroueil et al. 1983	$0.86w_L - 13$	15	90	Top boundary for fine-grained soils of East of Canada
Sivapullaiah and Sridharan 1985	$0.9767w_L - 37.95$			w_L Casagrande. Soil mixtures
Polidori 2003	$0.96w_L - 23$	28.5		
Polidori 2003	$0.96w_L - 37$			Inorganic, 50% CF
Spagnoli et al. 2018 & Al 2017	$0.97w_L - 37.6$		680	Inorganic, 100% CF.
Spagnoli et al. 2018	$5.94e^{(0.023w_L)}$		85	Smectitic clays. Casagrande Cup
Baroni and Almeida 2017	$0.70w_L - 4.29$	50		Kaolinite clays. Casagrande Cup.
Sharma and Sridharan 2018	$0.63(w_L - 1.03)$	33	82	Very soft organic clays
Sharma and Sridharan 2018	$0.6w_L$	33	82	w_{P100} considered
Okkels 2018	$0.82(w_L - 31)$	120	350	Organic soils

Table 5.6: Summary of some liquid limit w_L to plasticity index I_P correlations.

Extensive correlations are found in literature, mostly for local data. Some of them are summarised in table 5.6 and figure 5.7. A mean of the non-zero values is shown, and it plots slightly above and almost parallel to the Casagrande A-line. A large variability is observed, resulting from the different sources considered; some correspond to pure clay minerals mixed with sand or silt and others from natural clays that include a wider particle distribution. The w_L determined by the cup method is converted to cone w_L by Sivapullaiah and Sridharan 1985 with their conversion proposition. The ones proposed by Spagnoli et al. 2018 are converted with Spagnoli 2012 proposition. The linear regression of the mean shown in figure 5.7 has the following equation:

$$I_P = 0.72x - 11.25 = 0.72(w_L - 15.5) \quad (5.25)$$

The standard deviation of I_P along w_L increases following an approximately linear equation $sd(I_P) = 0.076w_L + 1.7$. This standard deviation does not include the variability of the correlations itself, for what SD of equation 5.25 would increase 5 to 15 units approximately. The variability around these correlations strongly suggests that experience on the analysed site would increase the accuracy.

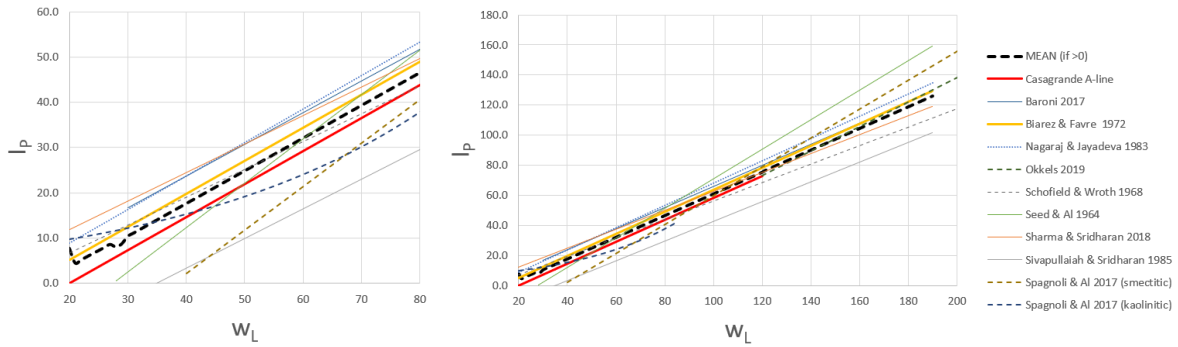


Figure 5.5: Liquid limit w_L Plasticity index I_L relationships. Left graph shows a close-view for low plasticity soils.

5.3.4 Compressibility correlations

Numerous attempts were made to correlate compressibility with index properties. Kulhawy and Mayne 1990 reported that over 70 different correlations were published. A few of them are described in this section to show them in figure 5.6 and observe a general trend.

Azzouz et al. 1976 evaluated soil compressibility through a regression analysis of more than 700 consolidation test and summarised the existing empirical correlations. Three-quarters of the data were obtained from Greece and its environs, the rest from different US parts. The dependent variables $C_c = \text{compression index}$ and $C_r = \text{compression ratio} = C_c/(1 + e_0)$, were compared to the following independent variables: e_0 , w_n , w_L and its combination. Azzouz et al. 1976 concludes from the linear regression analysis that 80% and 74% of the variation in C_c and C_r respectively, are explained with the model that involves the void ratio. The inclusion of w_L on a multiple linear regression did not increase the accuracy markedly.

Sharma and Bora 2015 studied seventeen inorganic remoulded clay samples from low to high plasticity, concluding that C_c is an exclusive function plasticity index, I_P and specific

gravity, G_s , being the following equation identical with Wroth and Wood 1978 if G_s is assumed as 2.7 and I_P is considered as the change of water content producing a 100-fold change in strength, $I_{P,100}$:

$$\begin{aligned} C_c &= G_s \cdot I_P/200 & I_P \text{ in } \% \\ C_c &= I_P/74 & \text{if } G_s = 2.7 \text{ and } I_P \text{ in } \% \end{aligned} \quad (5.26)$$

Sridharan and Nagaraj 2000 concludes that the compressibility is more closely related to the shrinkage index, $I_S = w_L - w_S$, than to I_P or w_L . However, since correlations based on I_P and w_L will help in the proposed framework and are still useful, the last ones are used in this proposition. In table 5.8 some of the correlations found in literature are summarised and plotted in 5.6.

Author	$C_c =$	Comments
Skempton and Jones 1944	$0.007(w_L - 10)$	Remoulded clays. Retrieved from Schofield and Wroth 1968. No boundaries found, adopted $w_L < 150$
Terzaghi and Peck 1967	$0.009(w_L - 10)$	Normally consolidated clays. from Azzouz et al. 1976
Schofield and Wroth 1968	$0.013I_P$	λ conversion
Azzouz et al. 1976	$0.83(w_L - 0.09)$	No boundaries, adopted $w_L < 100$
Wroth and Wood 1978	$0.006(w_L - 9)$	All clays $w_L < 100$
	$1/2I_P G_s$	If $G_s = 2.7 \Rightarrow C_c = I_P/74$ Remoulded, normally consolidated clays. From Kulhawy and Mayne 1990: $I_P < 100$.
Mayne 1980	$(w_L - 13)/109$	$w_L < 165$
Mayne 1980	$(I_P + 12)/172$	$I_P < 90$
Biarez and Favre 1976	$0.009(w_L - 13)$	$G_s = 2.7$
Sridharan and Nagaraj 2000	$0.014(I_P + 3.6)$	All clays, $9 < I_P < 38$
	$0.008(w_L - 12)$	All clays, $37 < w_L < 74$
Tiwari and Ajmera 2012	$0.0075w_L$	Activity <1 $10 < w_L < 470$
	$0.012w_L$	Activity >1 $10 < w_L < 470$
	$0.014I_P$	$I_P < 450$
Baroni and Almeida 2017	$0.0125w_L$	Organic clays - Rio de Janeiro $30 < w_L < 610$

Table 5.7: Summary of some liquid limit w_L to compression index C_c correlations.

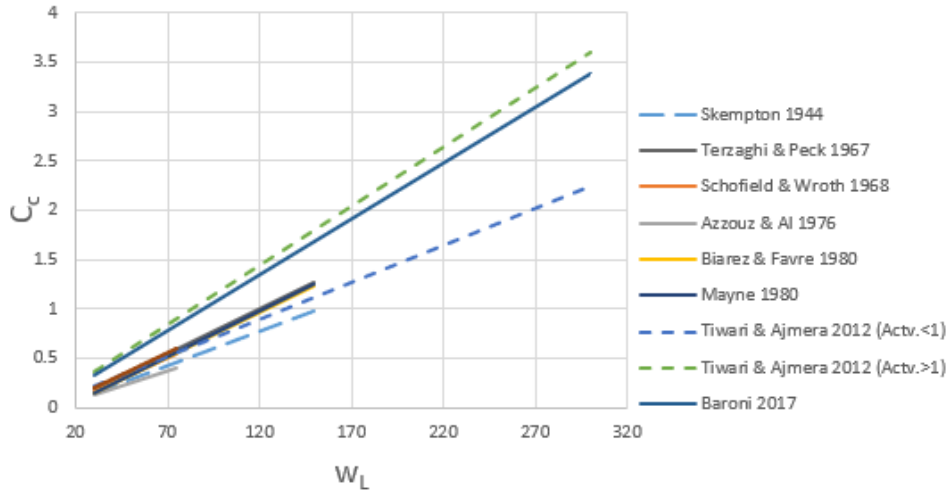


Figure 5.6: Correlations for compression index (C_c) and liquid limit (w_L)

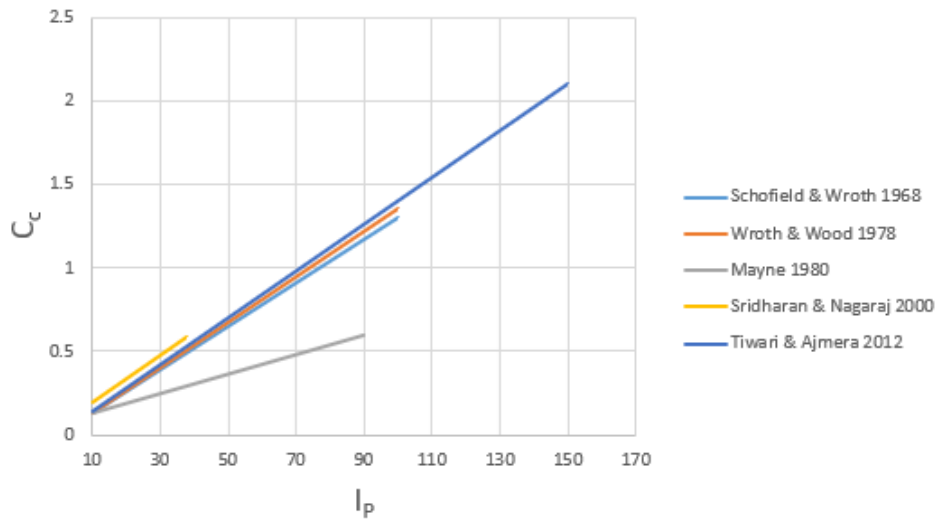


Figure 5.7: Correlations for compression index (C_c) and plasticity index (I_P)

5.4 Proposition of clay parameters estimation from CPT data

The following proposition approach aims to explore a different estimation of the liquid limit, w_L , and plasticity index, I_P , from CPT data for clayey soils in the APD framework. These clay properties or parameters can characterise compressibility, likewise useful for many models' parameters.

Starting from the liquidity index, I_L , w_L can be obtained using an estimation of saturated volumetric weight, a value for the relation $G_s = \gamma_{solids}/\gamma_{water}$ and a relation $I_P(w_L)$. Two methods are explored to get the state variable I_L . Once obtained, the following procedure is similar for both methods as described below.

From liquidity index to liquid limit

From CPT or CPTu data, different correlations exist to estimate the unit weight of the

soil. Therefore, under complete saturation, the void ratio can be calculated if G_s is assumed:

$$e_0 = \frac{\gamma_{sat} - G_s \gamma_w}{\gamma_w - \gamma_{sat}} \quad (5.27)$$

$$w_0 = 100\% \frac{e_0}{G_s} \quad (5.28)$$

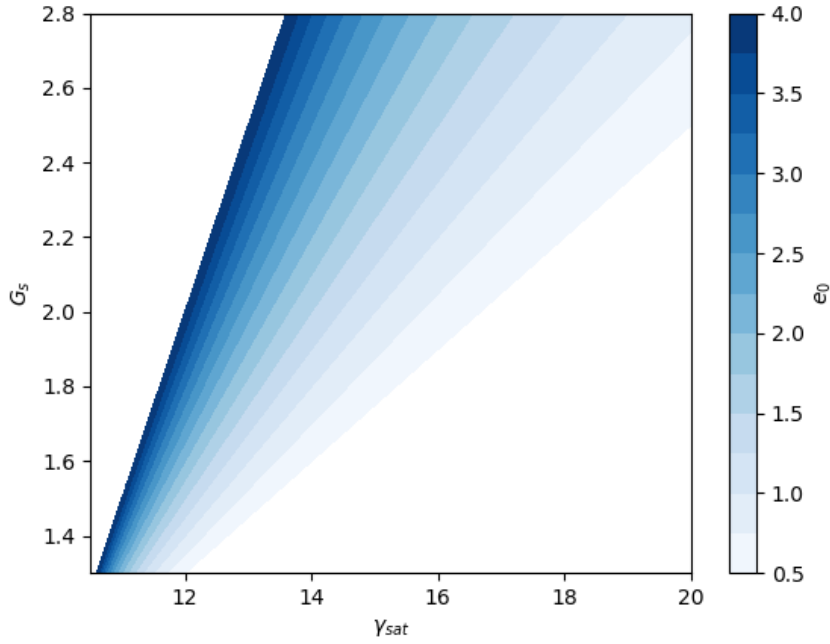


Figure 5.8: Variation of e_0 based on G_s adoption.

In figure 5.8 is observed the sensitivity of e_0 to an assumption of G_s . The lower the γ_{sat} it is, the more sensitive it is.

Liquidity index is defined as:

$$I_L = \frac{w_0 - w_P}{I_P} = 1 - \frac{w_L - w_0}{I_P} \quad (5.29)$$

Most of the $I_P - w_L$ correlations are in the form of:

$$I_P = a(w_L - b) \quad (5.30)$$

Rearranging I_L definition:

$$w_L = \frac{-ab + I_L ab + w_0}{1 - a + I_L a} \quad (5.31)$$

With equation 5.31, the I_P can be calculated with one of the existing correlations. This allows the use of the many equations to estimate compressibility constants. An assumption of G_s in equation 5.27

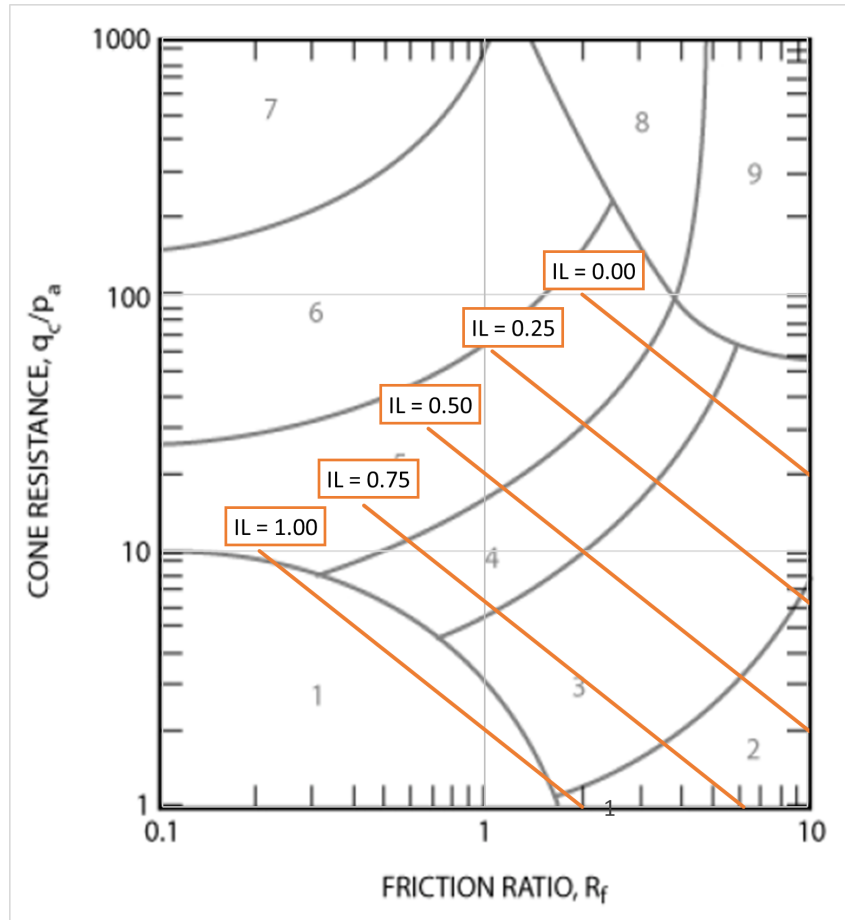


Figure 5.9: Liquidity Index, I_L , resulted of equation 5.32 on non normalised chart of Robertson 2010

Method I

The first method consists of estimating, with the preconsolidation stress, the I_L at preconsolidation stress, $I_{L,p}$. This allows using equation 5.31 if the water content at the preconsolidation state is found, $w_{0,p}$. To find $w_{0,p}$, an iterative procedure is needed, estimating the swelling from the difference in states at preconsolidation and the current state. If $C_s \approx C_c/4$ as Biarez and Favre 1976 proposed, after a couple of iterations an approximate value of w_L , I_P and C_c can be obtained. This is explained in figure 5.10.

However, this method has many drawbacks. It assumes that all clayey soils with equal preconsolidation stress will have equal I_P and w_L , which does not seem reasonable if a single $I_P(w_L)$ equation is used. Moreover, it relies on estimating OCR , the iterative process, and $C_s(C_c)$ relation. This first method is not tested since no extensive data was available and the belief that it already includes large variability in the assumptions.

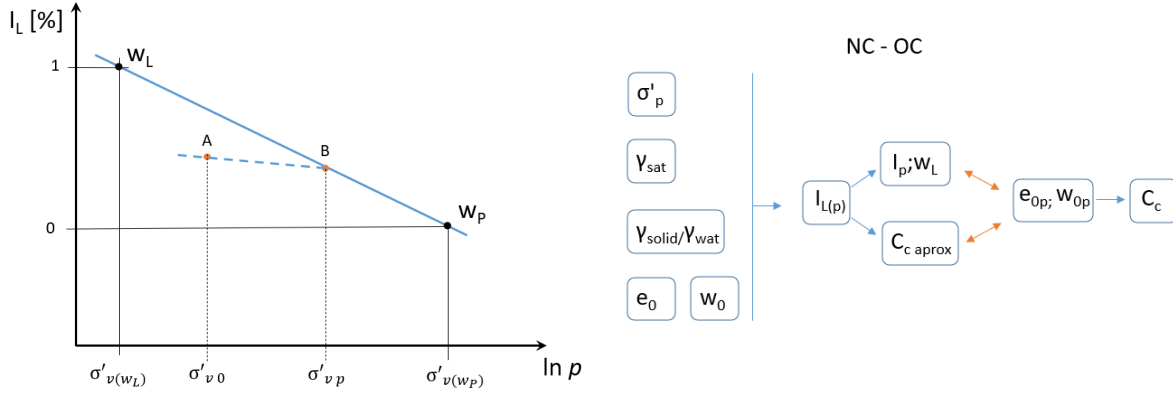


Figure 5.10: First proposed framework to approximate I_L from vertical effective stress and OCR, to obtain w_L ; I_P and C_c . It is not further studied for large number of assumptions.

Method II

The second method takes a different approach to estimate I_L , to later use equations 5.27 - 5.31. The remoulded undrained shear strength, s_{ur} , was shown to be related to the liquid limit, and equations were built with the assumption of a relation of strength between plastic state and liquid state, $R = s_{ur;w_P}/s_{ur;w_L}$, as shown in section 5.3.2.

On the one hand, the remoulded undrained shear strength can be assumed to be equal to the sleeve resistance f_s , Robertson and Cabal 2014, Mayne 2014. On the other hand, Low et al. 2010 do not recommend using f_s for the estimation of s_{ur} due to considerable uncertainties in measurements of CPTu sleeve friction. However, it is decided to proceed with the assumption $s_{ur} = f_s$, and compare it with the existing correlations for I_P and w_L .

To estimate I_L from $f_s = s_{ur}$, Wood 1990 equation is used, having $s_{u;w_L} = 2 \text{ kPa}$ and $s_{u;w_P} = 200 \text{ kPa}$ giving $R = 100$:

$$I_L = 1 - \log(f_s/2)/\log(100) \quad (5.32)$$

To estimate the liquid limit, equation 5.14 of Biarez and Favre 1976 is used, having coefficients of equation 5.30 $a = 0.73$ and $b = 13$. Replacing them in equation 5.31 gives:

$$w_L = \frac{-0.73 \cdot 13 + I_L \cdot 0.73 \cdot 13 + w_0}{1 - 0.73 + I_L \cdot 0.73} \quad (5.33)$$

The plasticity index can be calculated once w_L is obtained using equation 5.14, to open a large number of equations for C_c , e.g. equations of table 5.8. The volumetric weight used in equation 5.27 is calculated using Robertson 2010 equation:

$$\frac{\gamma}{\gamma_w} = 0.27[\log(\frac{f_s}{q_t})] + 0.36[\log(\frac{q_t}{p_a})] + 1.236 \quad (5.34)$$

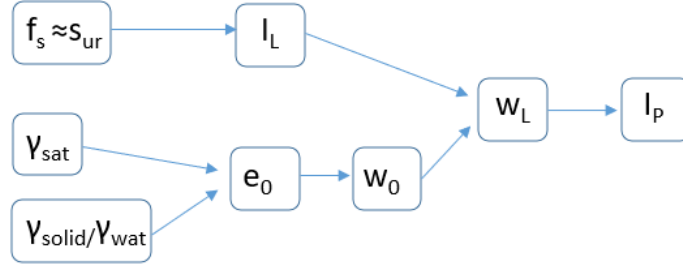


Figure 5.11: Proposed framework to approximate I_L from sleeve resistance f_s , saturated volumetric weight γ_{sat} and $G_s = \gamma_{solids}/\gamma_{water}$.

5.5 Validation of proposed estimation of plasticity indexes

The proposed method to obtain the plasticity index I_P and liquid limit w_L are tested with literature. As shown in section 3.4.2, Cetin and Ozan 2009 estimate through Bayesian update a set of correlations from CPT data q_t and f_s to I_P and w_L . The provided data is used to verify the proposal and shown in appendix B. Only clayey samples are used from the original data.

Firstly, the equation 5.32 for the liquidity index is plotted above the non normalised Robertson 2010 chart, Robertson 2010. This can be considered as a first step in validation since the correlation for liquid limit, equation 5.33 depends on the liquidity index. Secondly, the literature data is compared to the resulted liquid limit.

Liquidity Index validation

The result of equation 5.32 is shown in figure 5.12. Since no data linking CPT data to liquidity index was found, a subjective analysis of the results is made. The figure 5.12 shows that the liquidity index, I_L , is 0.0 when the Soil Behaviour Type, SBT, is classified as a very stiff fine-grained soil, corresponding with a water content equal to the plastic limit:

$$I_L = 0.0 \implies w_0 = w_P$$

When $0.75 < I_L < 0.50$, it plots on the normally consolidated soil trends and when $I_L = 1.0$, it is plotted close to the limits of sensitive soils. The increase of sleeve friction results in a decrease of I_L , being a reasonable trend compared to the Robertson 2010 chart.

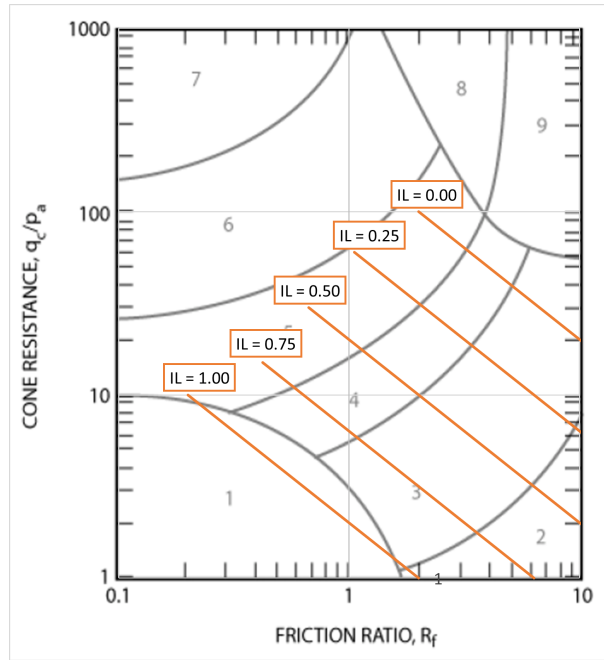


Figure 5.12: Liquidity Index, I_L , resulted of equation 5.32 on non normalised chart of Robertson 2010

Natural Water content validation

The resulting values of the natural water content w_0 , using the Robertson equation to calculate the soil unit weight, equation 5.34, are lower than the measured values of liquid limit provided by Cetin and Ozan 2009, as show figure 5.13 (left). Having the water content larger than the liquid limit is a non-real situation. In this case, it is decided to add 2 kN/m^3 to the equation B.1 in order to simulate a non-complete saturation in the correlation. In the rightmost part of figure 5.13 the corrected water content is shown.

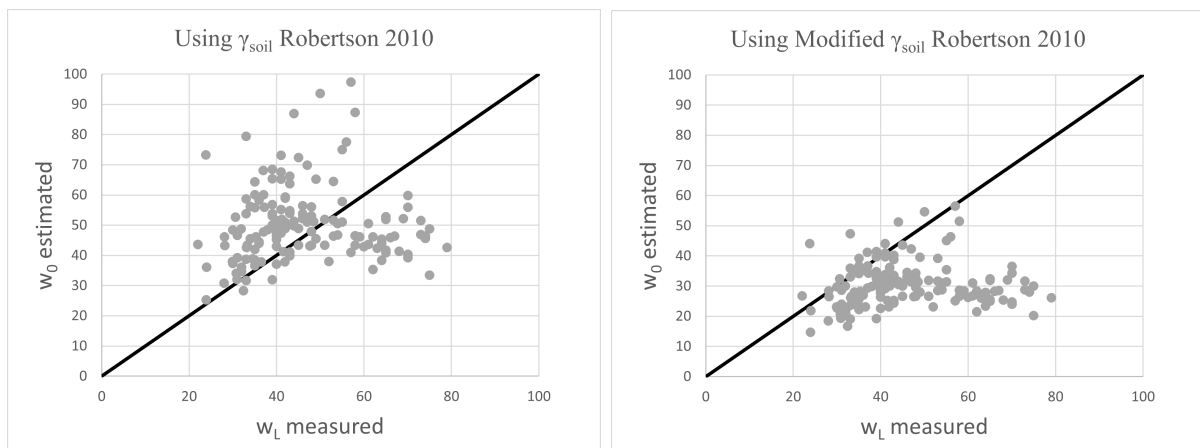


Figure 5.13: Comparison of measured liquid limit and estimated water content. On the left, using equation 5.34. On the right, equation 5.34 is modified adding 2 kN/m^3 . Both cases assumed $G_s = 2.65$.

Liquid Limit validation

Firstly, the sensitivity of w_L to the assumed G_s is studied, and secondly, using a fixed value of G_s , the output values are compared to a database.

In figure 5.14 two scenarios are considered to show the influence of G_s in the liquid limit determination proposition. When the organic matter increases, the specific weight of the solids decreases. Therefore, the w_L estimation decrease while G_s decreases for the same CPT parameters. The higher q_c , the larger influence of G_s , and for the range of G_s in between 2.65 – 2.75, not large sensitivity is observed. In conclusion, for mineral soils, the sensitivity of G_s is not of considerable importance, while it is for clays with increasing organic content.

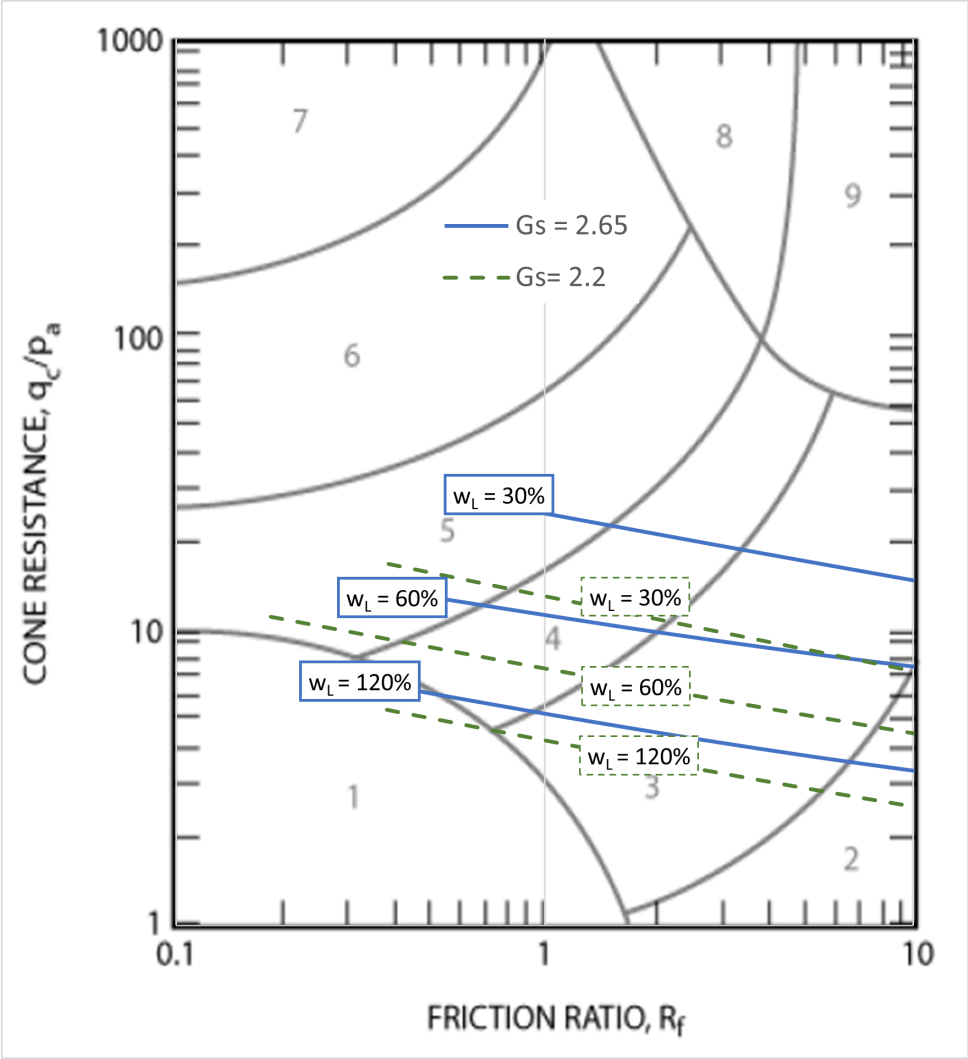


Figure 5.14: Sensitivity of liquid limit w_L to the specific weight of the solids G_s . Two scenarios are considered, the first with $G_s = 2.65$ on straight line and the second, on dashed line, $G_s = 2.20$

The resulted I_P and w_L from the proposed method are plotted above the graph provided by Cetin and Ozan 2009, figure 5.15 and 5.16. It is also plotted the result of equations proposed by Cetin and Ozan 2009 for I_P and w_L , using as normalisation exponent $c = 1$ to calculate $q_{t,1,net}$, as shown in section 3.4.2 and the modified equation for γ_{sat} . The back-calculated data do not show large sensitivity to the modified γ , while the proposed equation is highly sensitive to γ .

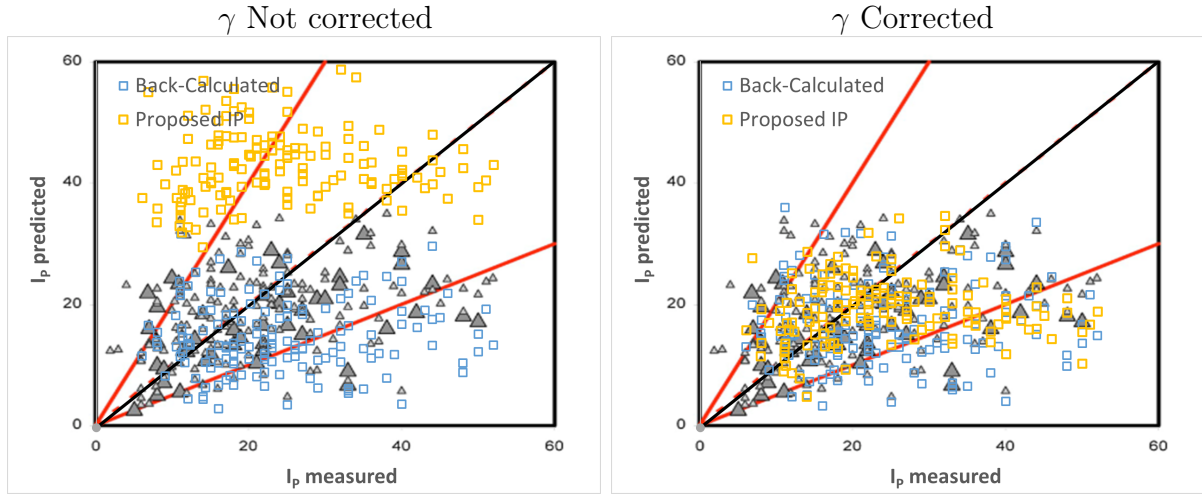


Figure 5.15: Comparison of predicted plasticity index $I_{P\ predicted}$ to the actual value of I_P , $I_{P\ actual}$, Plotted above Cetin and Ozan 2009 graph, grey triangles. On blue is shown the back-calculated result of Cetin and Ozan 2009 equations with the provided data. Only clayey samples are used for the prediction.

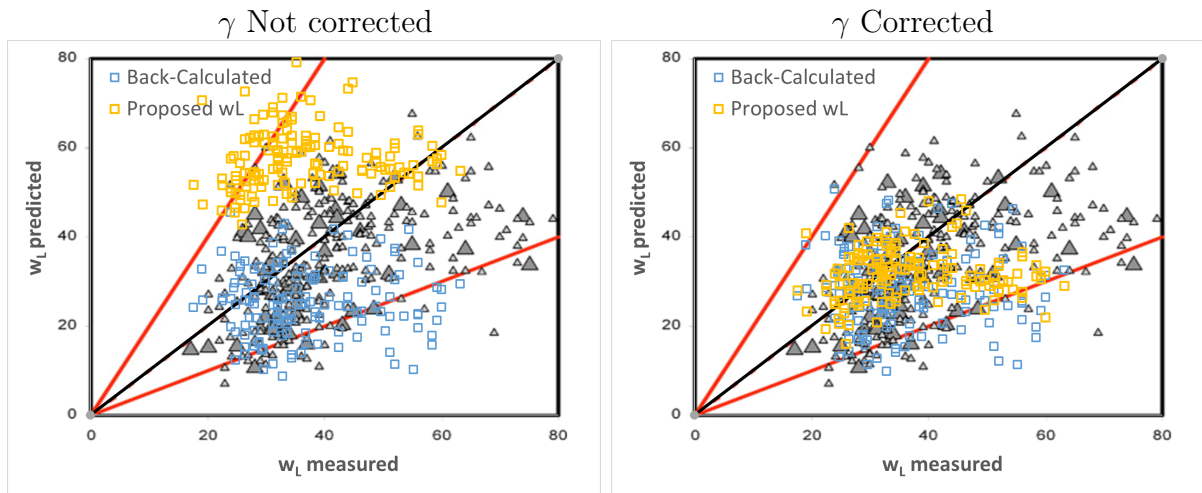


Figure 5.16: Comparison of predicted liquid limit $w_{L\ predicted}$ to actual value of w_L , $w_{L\ measured}$. Plotted above Cetin and Ozan 2009 graph, grey triangles. On blue is shown the back-calculated result of Cetin and Ozan 2009 equations with the provided data. Only clayey samples were used for the prediction.

The results of the correlations do not change significantly if other than Favre 1980 and Wood 1990 correlations are used. In figure 5.15, the predicted plasticity index I_P was plotted above the graph provided by Cetin and Ozan 2009. A similar graph is figure 5.16 for liquid limit w_L . The Residual Standard Deviation, S_{res} is calculated, defined as:

$$Residual = Y_{measured} - Y_{estimated}$$

$$S_{res} = \sqrt{\frac{\sum(Residual)^2}{n - 2}} \quad (5.35)$$

The resulted S_{res} expressed in % of back-calculated (B-C) data of Cetin and Ozan 2009 and the proposed correlations is:

	w_L B-C	w_L proposed	I_P B-C	I_P proposed
S_{res}	20.06	15.7	14.49	12.79

Table 5.8: Residual Standard Deviation for the back-calculated data using the published equations by Cetin and Ozan 2009 (B-C), and the proposed correlation (proposed)

The I_P prediction seems less accurate than w_L , and the reason might be attributed to an extra step in the calculation, the $I_P(w_L)$ correlation. Even if the correction factor of 2 kN/m^3 to the γ is changed to 1 kN/m^3 , the proposed correlations have lower residual standard deviation than the back-calculated data. To avoid a total dependency of the sleeve friction value, f_s , an undrained shear strength, s_u , could be calculated and averaged with f_s to obtain I_L . However, the addition of an estimated s_u to obtain an average f_s is not considered in this report since extra empiricism is needed to adopt local-variable cone factors.

The author believes that w_L estimation can be used in the APD framework to have a second value, using a modified γ_{soil} to obtain reasonable void ratios. An average of both might be a good solution. Moreover, the proposed equation can be customised to local correlations, adding flexibility to the database.

5.6 Additional option to estimate elasticity parameters for fine-grained soils

In the previous sections, index parameters were used to get the compressibility index, C_c , a parameter that can be an input value of the HSsmall and Soft Soil models, replacing E_{oed}^{ref} if the void ratio is known. From existing literature it is shown an alternative equation for E_{oed}^{ref} , a normalisation scheme to reference stress pressure, a recommendation for E_{50}^{ref} and E_{ur}^{ref} .

5.6.1 Constrained modulus from CPT data

The constrained modulus is usually called M or E_{oed} , and in the APD database, it is called CPT_M . The $1 - D$ constrained modulus is defined as:

$$M = \delta\sigma_v / \delta\epsilon = 2.3(1 + e_0)\sigma'_{v0} / C_c \quad (5.36)$$

being e_0 the in situ void ratio, σ'_{v0} the in-situ vertical effective stress, C_c the compressibility index and $2.3 = \ln 10$ a conversion factor from natural to decimal logarithm. Robertson 2009 proposed an equation for coarse and fine-grained soils, equation 5.37. Robertson and Cabal 2014 comment that the estimations can be improved with additional information as plasticity index or water content. From CPT data, the constrained modulus can be estimated as:

$$M = \alpha_M(q_t - \sigma_{v0}) \quad (5.37)$$

When $I_c > 2.2$ fine-grained soils:

$$\begin{aligned} \alpha_M &= Q_t & \text{when } Q_t < 14 \\ \alpha_M &= 14 & \text{when } Q_t > 14 \end{aligned} \quad (5.38)$$

When $I_c < 2.2$ coarse-grained soils:

$$\alpha_M = 0.0188[10^{0.55I_c+1.68}] \quad (5.39)$$

The HSsmall has as input parameter E_{oed}^{ref} , defined as the tangent stiffness at a vertical stress of $-\sigma'_1 = \frac{\sigma'_3}{K_0^{nc}=p^{ref}}$, PLAXIS Material Model 2020, and represented in figure 5.17.

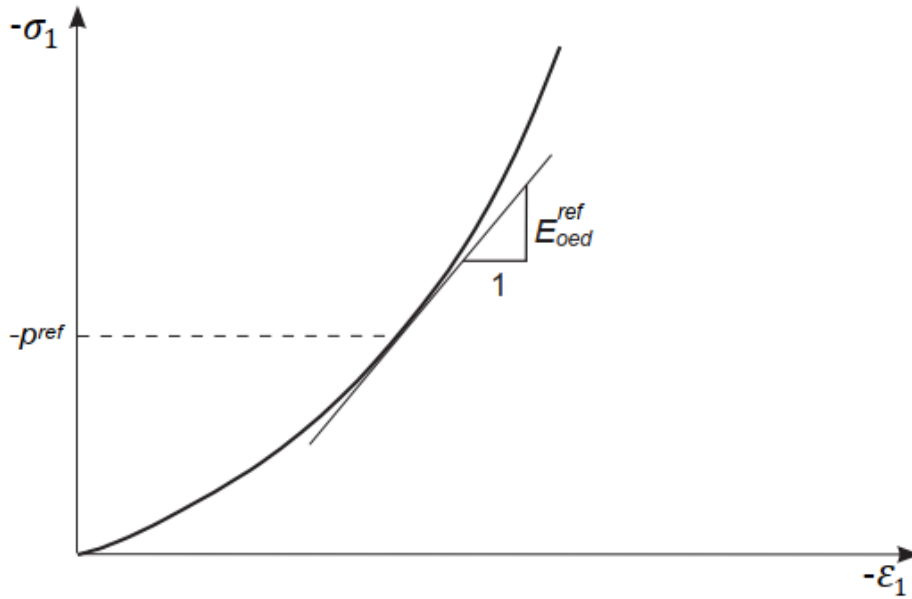


Figure 5.17: Definition of $1-D$ constrained modulus at reference stress E_{oed}^{ref} in oedometer test result. Retrieved from PLAXIS Material Model 2020.

The oedometer stiffness at reference stress level, E_{oed}^{ref} can be converted to tangent stiffness modulus, E_{oed} (also called M), by the following equation used by PLAXIS software for HSsmall:

$$E_{oed} = E_{oed}^{ref} \left(\frac{c \cos \phi - \frac{\sigma'_3}{K_0^{nc}} \sin \phi}{c \cos \phi + p^{ref} \sin \phi} \right)^m \quad (5.40)$$

were ϕ' is the effective friction angle, $K_0^{nc} = \sigma'_h/\sigma'_v$ the ratio of horizontal to vertical effective stress, p^{ref} the reference pressure, taken normally as 100 kPa and m a power for stress-level dependency of stiffness.

The assumption $-\sigma'_1 = \frac{\sigma'_3}{K_0^{nc}} = p^{ref}$ is taken as PLAXIS Material Model 2020 defines, being σ'_1 the largest compressive principal stress in a triaxial test. For soft soils if the power m is taken as 1.0 a logarithmic compression behaviour is simulated, PLAXIS Material Model

2020. Taking in account this and if $\sigma'_1 = \sigma'_v$, equation 5.40 for soft soils, rearranged for E_{oed}^{ref} , results:

$$E_{oed}^{ref} = E_{oed} \left(\frac{c \cot \phi + p^{ref}}{c \cot \phi + \sigma'_v} \right) \quad (5.41)$$

Equation 5.41 allow to use the constrained modulus at a reference stress level of $p^{ref} = 100 \text{ kPa}$. This add a second source of values for the parameter E_{oed}^{ref} , to compare with the resulting from C_c .

5.6.2 Secant stiffness

The CUR 2003 recommends to use the secant stiffness in standard drained triaxial test, E_{50}^{ref} can be assumed to be half the one dimensional constrained modulus E_{oed}^{ref} for normally consolidated clays and equal for overconsolidated soils:

$$\begin{aligned} E_{50}^{ref} &\approx 2 E_{oed}^{ref} \text{ for clays with } OCR = 1 \\ E_{50}^{ref} &\approx E_{oed}^{ref} \text{ for clays with } OCR > 1 \end{aligned} \quad (5.42)$$

Equation 5.42 is an estimation and larger values than 2 can be encountered, e.g. 4 to 11 by Fu et al. 2020. For Dutch soils, the ratio is in between 1 and 3.

5.6.3 Unload-reload stiffness

The unloading reloading stiffness can be obtained from the following chart, Benz et al. 2009a after Alpan 1970:

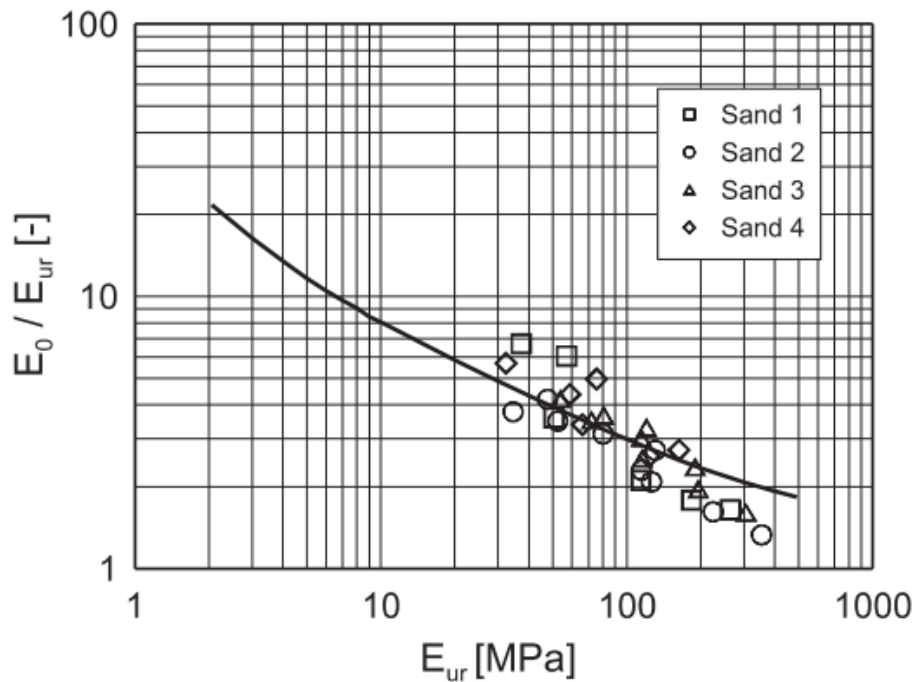


Figure 5.18: Relationship for small strain stiffness E_0 and secant stiffness E_{50} , extracted from Benz et al. 2009a.

The E_{ur}^{ref} modulus can be obtained from loading-reloading loops. However, there are no many correlations for this model parameter. Therefore, the author suggests obtaining the shear modulus at small strain, G_0 , from the many reported correlations and correlate it to the E_{ur}^{ref} using the Alpan chart of figure 5.18. This would avoid a single value for the ratio E_0/E_{ur} for fine-grained soils if from figure 5.18 a linear relation with plasticity index I_P can be introduced. In figure 5.18 in the division of cohesive to granular soils a $I_P = 10$ corresponding to $E_0/E_{ur} = 3$ can be taken, and similar with $I_P = 80$ corresponding to $E_0/E_{ur} = 20$, yielding the following equation:

$$E_{ur}^{ref} = \frac{G_0^{ref} 2(1 + \nu)}{0.243 I_P + 0.57} \quad (5.43)$$

A different form can be obtained if instead $I_P = 80$ a value of 120% is taken, matching the maximum value of Casagrande chart. In the norm CUR 2003, the following recommendations are noted for consolidated clays:

$$\begin{aligned} E_{ur}^{ref} &\approx 8E_{50}^{ref} \\ &\geq 5E_{50}^{ref} \end{aligned} \quad (5.44)$$

For overconsolidated clays:

$$E_{ur}^{ref} \approx 4E_{50}^{ref} \quad (5.45)$$

However, it is noted that for dutch soils in practice, $E_{ur}^{ref} \approx 4E_{50}^{ref}$ is taken in most of cases. The CUR recommendations are used in the validation.

5.6.4 Shear modulus

The shear modulus at small strains, G_0 , is calculated with some direct correlations from CPT data and shear wave velocity, V_s . This parameter is estimated at an in-situ stress level. From PLAXIS Material Model 2020 it can be normalised to a reference stress level as:

$$G_0^{ref} = \frac{G_0}{\left(\frac{c \cos \phi - \sigma'_3 \sin \phi}{c \cos \phi + p^{ref} \sin \phi} \right)^m} \quad (5.46)$$

were $m = 1.0$ for soft soils. In the validation, the K_0 used to estimate σ'_3 for the normalisation of G_0 is coming from correlations valid for overconsolidated soil too, since $K_{0;NC}$ values yielded inconsistent large G_0^{ref} .

The stiffness reduction for fine-grained soils are related to plasticity index, I_P , as reduction modulus reduction at a reference shear strain $\gamma_{0.7}$ can be calculated from the following equation for fine-grained soils reported by Benz et al. 2009b:

$$\gamma_{0.7} = (\gamma_{0.7})_{ref} + 5x10^{-6} I_P (OCR)^{0.3} \quad (5.47)$$

where $(\gamma_{0.7})_{ref}$ is the reference shear strain for $I_P = 0$ and can be taken as $1x10^{-4}$.

5.7 Conclusion on parametrisation of clayey soils

This chapter introduced a problem of lacking correlations to obtain compressibility characteristics of clayey soils to be used in the Hardening Soil Small and Soft Soil models. The compressibility parameters can be approximated from plasticity characteristics: the plastic index, I_P , and liquid limit, w_L . In section 3.4.2 it is concluded that I_P and I_L are among the key parameters for fine-grained soils, which is confirmed in this chapter.

Different existing frameworks are shown in this chapter to estimate the liquidity index I_L from effective vertical stress, σ'_v , and remoulded undrained shear strength, s_{ur} . Assuming $\gamma_{solids}/\gamma_{water}$ ratio and obtaining γ_{sat} from existing CPT correlations, a simplified method is introduced to get a liquid limit, w_L and plasticity index, I_P from I_L . Two methods were chosen to estimate I_L from CPT measurements, one from σ'_v and the other from sleeve resistance $f_s = s_{ur}$. The first one using σ'_v is discarded, and the second using f_s is compared to the existing correlations provided by Cetin and Ozan 2009.

The results show that the estimation of specific unit weight with conventional equations leads to large water contents, and corrections were needed. An increase of 2 kN/m^3 to the natural volumetric weight of Robertson and Cabal 2014 equation is recommended to use in order to estimate w_0 and e_0 . It also shows similar variability to the existing correlation for I_P estimation. For the analysis of w_L , the results are acceptable, in line with the largely variable existing correlation. The proposed method yield higher values of w_L than Cetin and Ozan 2009 equations, and an average might be the best option. The advantage of the presented method is the possibility of customise it. Therefore, the new estimations of w_L and I_P can be included in the APD framework. Once w_L and I_P are determined, C_c can be obtained from the existing empirical correlations, giving a place to some model parameters for the Hardening Soil Small and Soft Soil models.

Chapter 6

Validation of extended APD implementations database

6.1 Introduction

A clay layer of the south of The Netherlands is analysed and compared to oedometer and undrained triaxial data to have a first validation of the APD framework. This first validation needs to be complemented with a more extensive database to avoid biased conclusions.

The APD framework currently works with CPTu data and includes a stratification program that provides a succession of layers classified by Soil Behaviour Type, SBT; having the possibility of merging continuous layers provided a minimum layer thickness. The correspondent layers to the oedometer and triaxial sample depths are chosen, and the tests are simulated with the Plaxis Soil Test facility.

6.2 The soil data

The CPT data correspond to a levee in the south of The Netherlands. The chosen clay layer is a Calais deposit, resulted from the Holocene marine transgression. This deposit is commonly covered by the Holland peat, which is buried beneath the Dunkirk deposits. Due to the deposition environment, the Calais deposits frequently are laminated with silt or sand layers. The younger Calais deposit is chosen to validate the APD output results, which is less silty.

The available data is composed of anisotropically consolidated undrained triaxial, CAU, and Oedometer tests. The CAU triaxial are consolidated to in situ effective stress state, paired to an oedometer test. The CPTu is located next to each correspondent borehole, having five CPTu-borehole pairs where the denominated deposit Calais A is studied.

The CPTu data correspond to an electric Fugro cone of 10004 mm^2 with a pore pressure sensor.

6.2.1 Physical description

The 5 samples classified as Calais A, have a physical classification as "CLAY, moderately silty, weakly humus, peat remnants, grey". The saturated specific weight and water content are provided, and with the reported assumed specific solid weight ($G_s = 2.65$), the void ratio is calculated. The values are shown in table 6.1.

Sample no.	1	2	3	4	5
$\gamma_{sat} [kN/m^3]$	16.10	16.10	13.30	14.50	16.50
$w_0 [\%]$	72.60	64.50	112.50	86.30	34.37
$e_0 [-]$	1.92	1.71	2.98	2.29	1.57

Table 6.1: Laboratory results of samples on physical characterisation.

The resulted layer CPTu values are plotted in the Robertson 2010 and Robertson 2016 charts. The local values might be slightly different from the representative layer values, which account for a larger thickness. All samples fall in the $SBT = 3$ zone in the non-normalised Robertson 2010 plot, and most of them in the claylike contractive classification in the normalised Robertson 2016 chart. Regarding the rightmost plot of 6.2, where the excess pore pressure parameter U_2 is used, it shows that only sample 5 has a proper undrained behaviour, while the rest do not generate sizeable excess pore pressure. The silt fraction or peat remnants could explain the partially drained behaviour, resulting of greater permeability or compressibility.

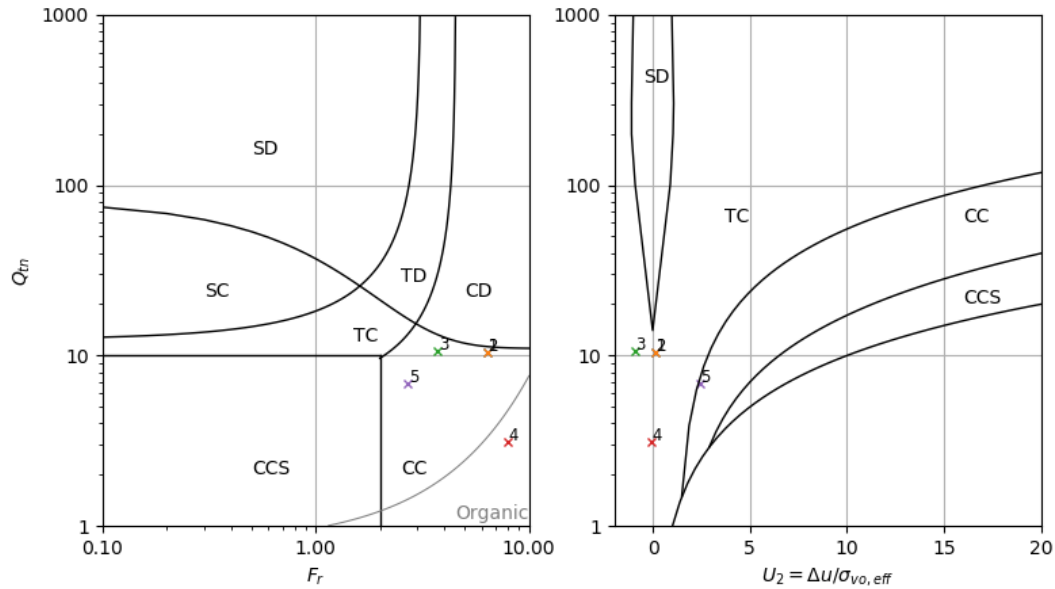


Figure 6.1: Classification of Calais A clay layer on Robertson 2016 chart. Representative values of CPTu data of the correspondent layer to the sample are used.

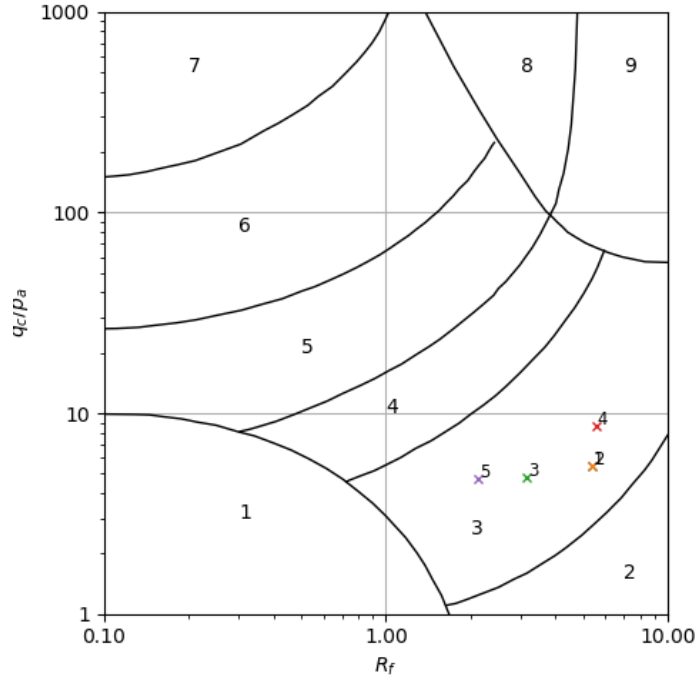


Figure 6.2: Classification of Calais A clay layer on Robertson 2010 chart. Representative values of CPTu data of the correspondent layer to the sample are used.

6.3 Methodology of validation

The APD framework currently includes a stratification algorithm that allows the automatic stratification using the Robertson CPT chart 2010 and 2016. The validation of the algorithm is not part of this thesis. However, the representative values are checked before continuing with the methodology.

A representative layer that includes the CAU and oedometer samples' depth is chosen from the stratification algorithm. This adds variability since the dimensions of the samples are many times smaller than the selected layer. A minimum layer of 20 cm is set up in the stratification algorithm, exciding the zone of influence in soft soils reported by Ahmadi and Robertson 2011, equal to two times the cone diameter.

In the same program, the mean value of the model parameters is transferred to Plaxis 2D software, where the test facility is used for correspondent Calais A stratified layer to compare to the laboratory data. In the oedometer, the simulation includes a first phase of loading to the first reported load increment, a second up to the reported preconsolidation stress, a third one to the maximum load before unloading, fourth and fifth is the unloading-reloading phase and the last one until the maximum stress in the test. The averaged value of preconsolidation stress is taken between the reported linear method and Koppejan one.

For the triaxial, the reported K_0 and consolidation stresses are used in the simulation. In all cases, the Hardening Soil with small strain stiffness (HS small) is used.

6.4 Validation

Firstly, the measured water content is compared with the two liquid limit predictions, the one proposed by Cetin and Ozan 2009 introduced in chapter 3, and the presented in chapter 5. This first step can give an idea of the validity of the liquid limit estimation on this specific clay. Secondly, the Plaxis Test Facility simulation of the oedometer test and undrained triaxial is shown compared to laboratory data. Lastly, a verification of the shear modulus is done.

The simulations are set to the same load steps, preconsolidation stress, and cell pressure of the laboratory data. In the case of the oedometer, the first load step strains are reset to zero.

6.4.1 Liquid limit

The measured water content of the samples is compared with the estimated liquid limit, predictions based on the existing correlation presented by Cetin and Ozan 2009 and the proposed in this report in chapter 5. Usually, the liquid limit should be larger than the water content. On the contrary, the soil would be in a "liquid state." In figure 6.3, the existing correlation, the proposed one, and the average of them are represented. For all the cases, the results of the merged layer by the current stratification program are used.

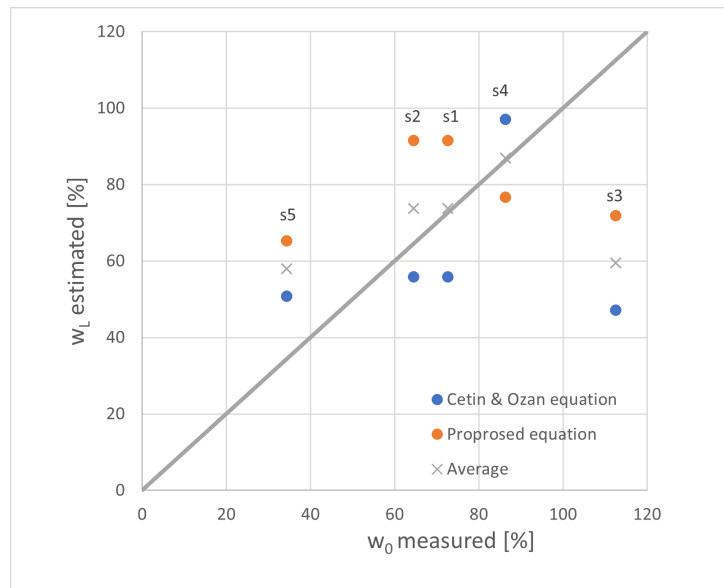


Figure 6.3: Measured water content compared with the existing correlation of Cetin and Ozan 2009, with proposed correlation presented in chapter 5, and the average of the two.

The figure 6.3 shows that the average w_L of both correlations falls in most of the cases above of the water content w_0 . It is also demonstrated that the proposed correlation in this report yields larger w_L compared to Cetin and Ozan 2009 in most of the cases, when using the $G_s = 2.65$ assumption. If a smaller value of G_s is adopted to consider organic content, the liquid limit estimation would decrease. Sample number 3 has a significant water content that could be attributed to peat remnants and it also shows large compressibility in the laboratory oedometer test.

6.4.2 Oedometer test

The oedometer test data is plot together with the simulated test using APD data in figure 6.4. In figure 6.5, the reloading parameter RR and compression parameter RR are compared to the laboratory report data.

Below the preconsolidation stress σ_p :

$$\frac{\Delta h}{h_0} = RR \log\left(\frac{\sigma'}{\sigma_0}\right) \quad \text{for } \sigma_0 < \sigma' < \sigma_p \quad (6.1)$$

For the virgin compression:

$$\frac{\Delta h}{h_0} = CR \log\left(\frac{\sigma'}{\sigma_0}\right) \quad \text{for } \sigma_0 < \sigma' < \sigma_p \quad (6.2)$$

In the appendix C, each sample simulation is shown for better interpretation. It is also included a simulation concerning data from a small layer (30-50 cm) around the sample depth, compared to the merged layer. The previous comparison permits removing the merged layer's variability to directly compare the CPT data at the sample dept.

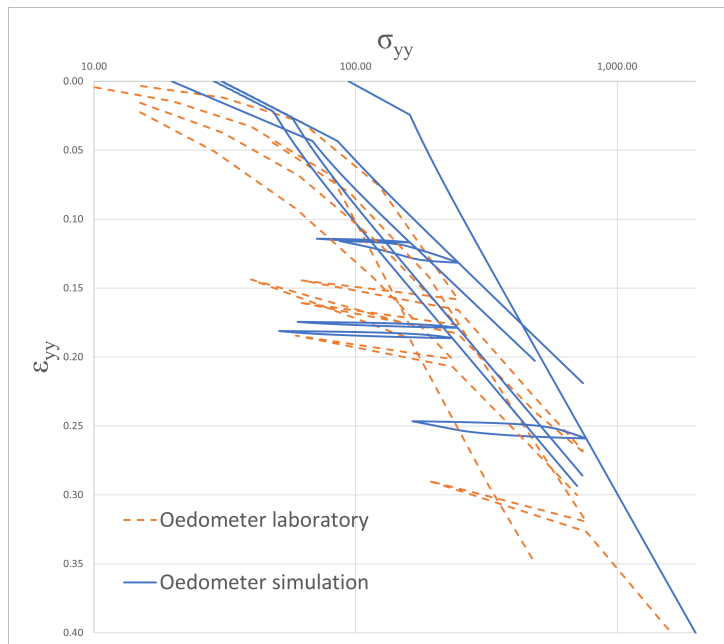


Figure 6.4: Oedometer laboratory data of Calais A clay together with simulated test using APD data.

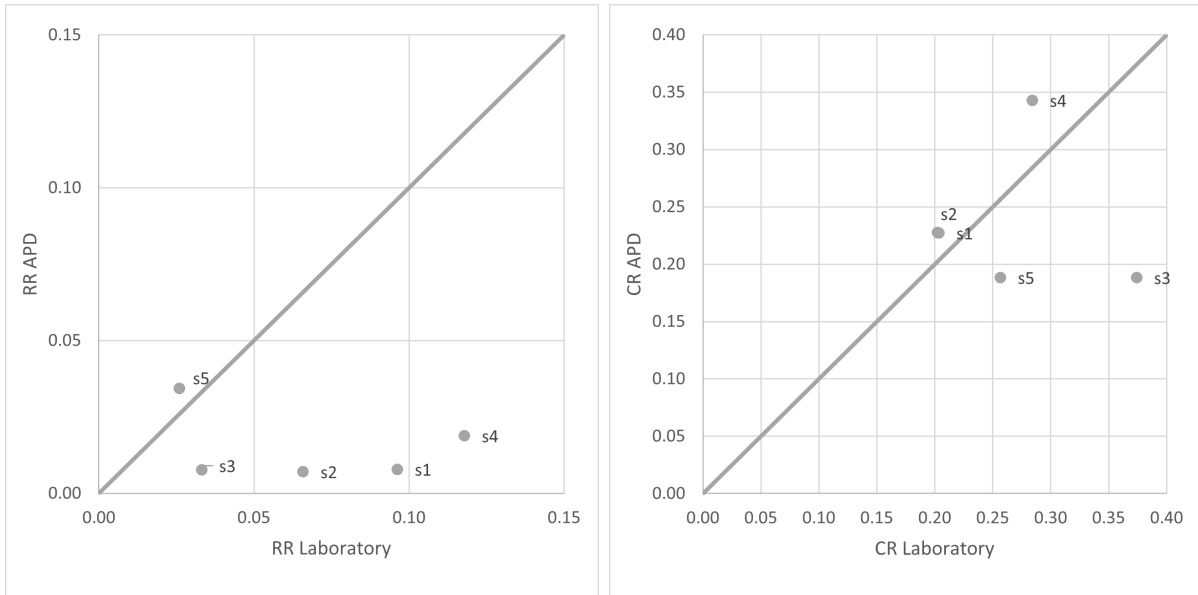


Figure 6.5: Oedometer laboratory data of Calais A clay together with simulated test using APD data.

6.4.3 CAU triaxial test

Anisotropically Consolidated Undrained, CAU, triaxial tests were executed on Calais A samples. The tests are compared to simulations using the same consolidation stress and K_0 ratio. All tests are consolidated at an in-situ stress state. Similar to the oedometer simulation, the resulted layer from the stratification program, which includes the sample depth, is used for the simulation. The appendix C presents a second simulation with a customised soil layer at the sample depth to remove the layer's variability.

The friction angle for the studied layer is underestimated. From the reported test, a friction angle of normally consolidated samples results in $\phi \approx 38^\circ$ and being higher for some samples, while the result from the correlations is $\phi \approx 27^\circ$. Due to the low estimation of the friction angle, discussed in section 6.5, a friction angle of $\phi = 38^\circ$ is set to appreciate better the whole set of variables in the test simulation.

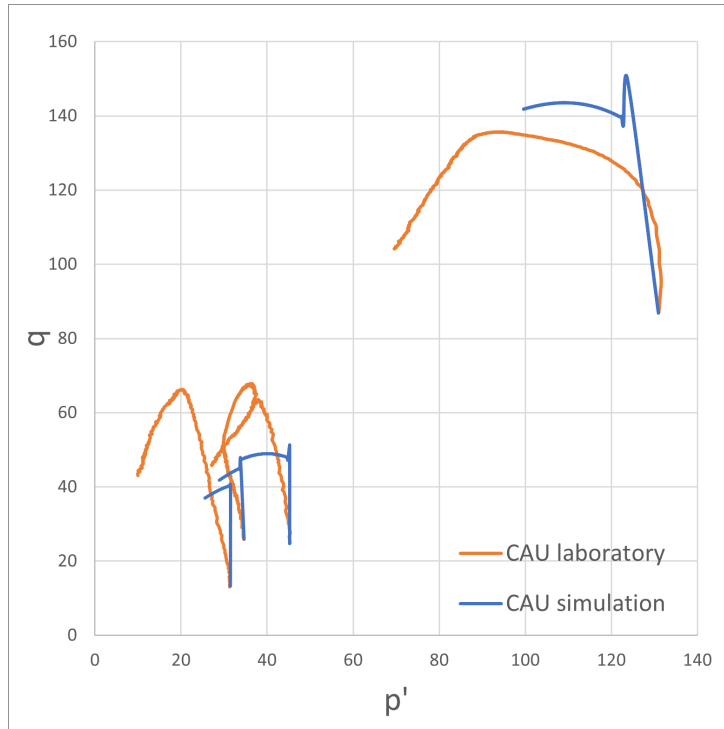


Figure 6.6: $q - p'$ plot of CAU data of Calais A clay together with a simulated test using APD data. The friction angle ϕ' is set to 38° due to the low-estimation of existing correlations.

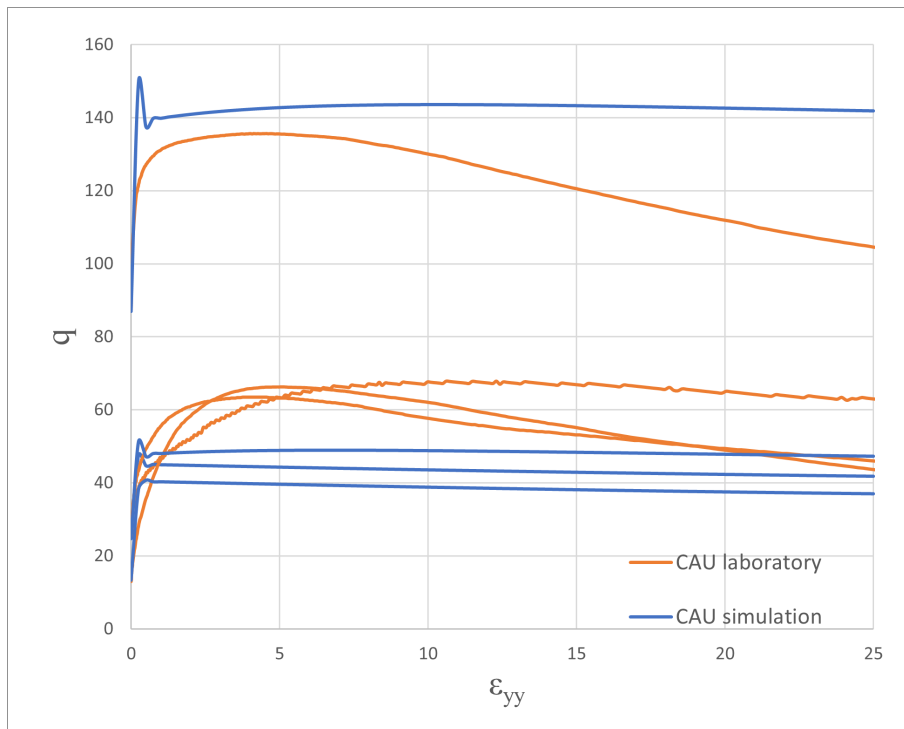


Figure 6.7: $\varepsilon_{yy} - q$ plot of CAU data of Calais A clay together with a simulated test using APD data. The friction angle ϕ' is set to 38° due to the low-estimation of existing correlations.

An undrained shear strength, s_u , is given by the APD methods, for what the S ratio, $S = s_u/\sigma'_v$ can be calculated and compared to the laboratory CAU test s_u . The results

are plotted in figure 6.8 labelled as *S ratio APD*. It is also shown the s_u resulted from the maximum deviator stress in the simulated test, labelled as *S ratio Soil Test*. It is reminded that the CAU test simulation is done using a $\phi = 38^\circ$ for all samples since the current correlations under-predict it in this case as discussed in section 6.5.

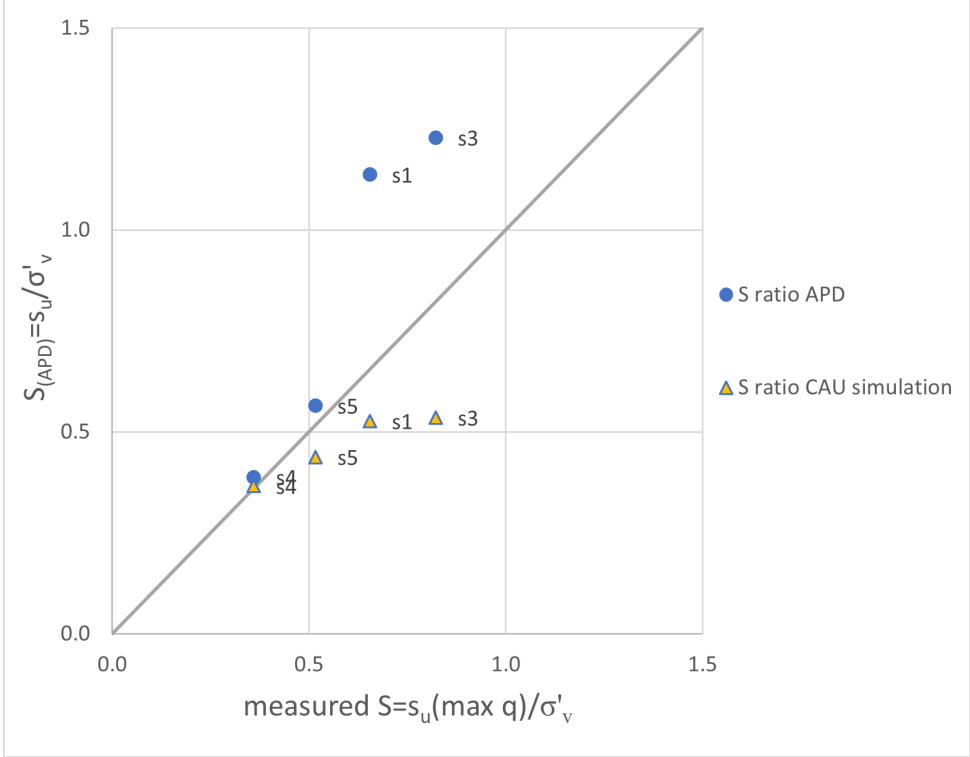


Figure 6.8: S ratio, $S = s_u / \sigma'_v$ from CAU test compared to the provided parameter by APD methods and the simulated CAU test using adopted $\phi = 38^\circ$

6.4.4 Shear modulus at small strains

Having no laboratory/in-situ measurements of the shear wave nor the shear modulus G_0 , the normalised modulus could be compared to figure 6.9, using the provided void ratio from laboratory data. It is important to mention that no correlation based on void ratio was used to arrive to G_0 , what possibilities this comparison.

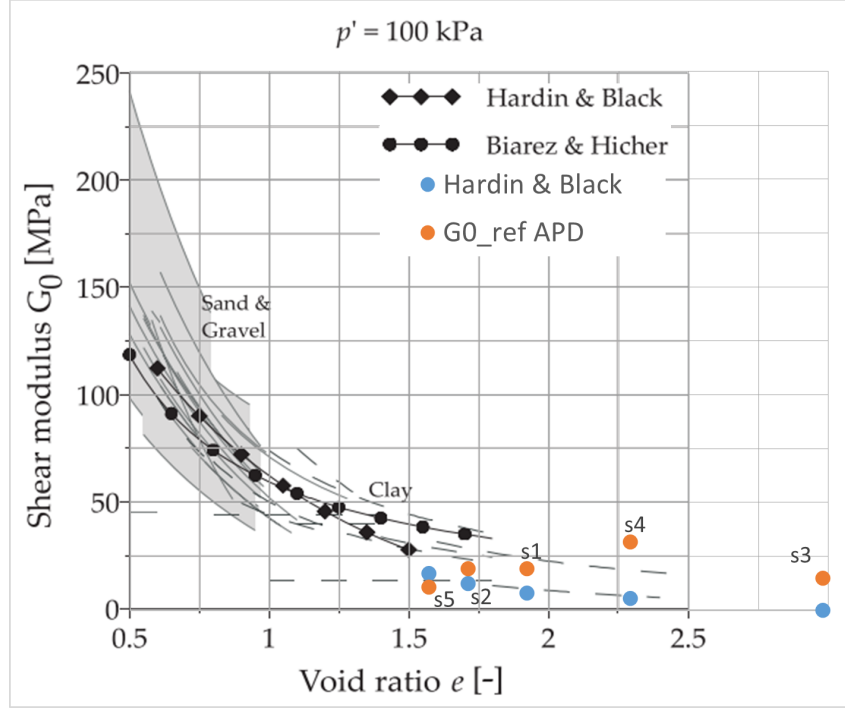


Figure 6.9: Shear modulus G_0^{ref} from APD framework compared to the correlation of Hardin and Drnevich 1972, based on measured void ratio, plotted above graph provided by Benz 2007. The horizontal axis is enlarged to cope with sample number 3.

The equation used in figure 6.9 of Hardin and Drnevich 1972 is:

$$G_0 [MPa] = 33 \frac{(2.97 - e)^2}{1 + e} \left(\frac{p}{p_{ref}} \right)^{0.5} \quad (6.3)$$

were e is the void ratio, p is the mean effective stress and $p_{ref} = 100$ is the reference pressure. The laboratory reports a $G_s = 2.65$. However, it is an assumed value, and it can be lower. If a lower value is taken to deal with the organic content of the Calais A deposit, a smaller void ratio would be obtained, increasing G_0 values using equation 6.3.

6.5 Discussion of validation

Oedometer and CAU triaxial test were simulated using the Hardening Soil model with small stiffness. The oedometer simulation yielded good results for a first validation. Considering the stiffness around the in-situ stress state, the parallelism of graphs increase. The oedometer plot shows sample disturbance in some tests when the plot is far from a bi-linear one. The importance of a good estimation of E_{oed}^{ref} is considerable since other model parameters depends on it, e.g. E_{50}^{ref} .

In the case of the CAU test, the maximum shear strength was not well simulated, being the detected leading cause of the elevated friction angle, reported in the test as $35 < \phi < 90$. The significant silt/sand content and the organic particles could explain the significant friction angle. For this reason, an adopted value of $\phi = 38^\circ$ is used in the CAU simulation. The initial stiffness is well estimated, slightly overestimated, while the direction of the

paths is similar. The undrained strength is best estimated when using the APD output parameter s_u , giving acceptable results.

The low friction angle estimation results from clay correlations, and these samples are not physically classified as pure clays, which is the most common situation in nature. Many correlations to get the friction angle based on plasticity index, I_P , are found in literature, were the one presented by Kulhawy and Mayne 1990 was the only used:

$$\phi_{cv} = \arcsin 0.8 - 0.094 \ln I_P \quad (6.4)$$

being ϕ_{cv} the friction angle at a critical void ratio, what could be taken as peak friction angle for uncemented, insensitive cohesive soils. In the publication, the authors describe a large variability in the correlation. The correlation expresses a decrease of the friction angle when the plasticity increase, a trend that other authors report, e.g., Sorensen and Okkels 2013. However, as was stated in section 3.4.2, the same year Mayne 2013 describes that there is no relation between the plasticity and the friction angle. Mayne 2013 recommends not to use this kind of correlation and instead, assuming a mean value of $\phi = 28.6$ deg with a standard deviation of $SD = 5.1$ deg. In the APD database used in the simulation of this report, the average value of Mayne's recommendation and equation 6.4 are used, resulting in $25.3 \text{ deg} < \phi_{cv} < 28 \text{ deg}$ for the Calais A simulated.

The five samples' layers have a Robertson 2010 soil behaviour classification has a clear $SBT = 3$, and in the Robertson 2016 chart as a clay contractive, CC , with one sample falling in the organic soil area. The laboratory water content of these samples was in the order of $59\% < w_0$ what gives an idea of the minimum possible liquid limit. If the Casagrande A-line is used as a reference, a minimum $I_P = 28.5\%$ is obtained considering $w_{L,min} = w_0 = 59\%$, and nor the equation 6.4 neither the ones published by Sorensen and Okkels 2013 would achieve a $\phi > 35$ deg.

6.6 Conclusion on validation

The proposed equation for the liquid limit w_L based on the liquidity index I_L yields larger values compared to the existing one of Cetin and Ozan 2009. The average value of the current correlations for liquid limit, that modifies the average value of compressibility parameters using the APD database, plots above the water content for most of the cases. Considering the large influence of the w_L on the E_{eod}^{ref} and the results obtained in the oedometer simulations, the average result is acceptable for the APD framework's purpose.

It was stated that the friction angle for soils not physically characterised as pure clays is a major difficulty. However, this low prediction for mixed soils could be detected with the estimated undrained shear strength, s_u , compared to a test simulation. In the case of one-dimensional stiffness, good results were obtained for a first estimation.

The APD framework's potential to give a first impression of a project and anticipate geotechnical soil investigations can be confirmed. Further work should be done on transition soils, the ones in between coarse-grained and fine-grained since few correlations exist for these soils.

Chapter 7

Conclusions and Recommendations

7.1 Conclusions

The present report is involved in the APD project, where a group of professionals collaborate in its development. The project result is the APD framework, which aims to determine advanced model parameters from in situ tests based on the graph method. Quite some improvements were achieved at the moment of writing these lines, from the concept of APD elaborated by van Berkom 2020, followed by a quality assessment developed by Hauth 2020 and different, but no minor tasks, realised by the rest of the enthusiastic group such as an own CPT stratigraphy program and automating of the process for each layer. The main objective of this thesis was to answer the following main research question: "*How can be the APD framework be extended and validated to cope with fine-grained soils?*". Answering this question came up with many sub-questions that are answered below:

- *Which existing behaviour classification chart is appropriate?*
Robertson's charts are chosen to be used in the APD framework as the most used in engineering practice. Since each chart has its advantages and disadvantages, the non-normalised Robertson 2010 chart, Robertson 2010, together with the normalised Robertson 2016, Robertson 2016 are used in the APD framework.
- *How to include a logarithmic-distribution variation on correlations uncertainties in APD?*
Mostly all correlations that have a logarithmic distribution of the scattering around the trendline result from log-log or log transformation. Typically, geotechnical engineers are more interested in the lower distribution of the parameters. Therefore an assumption of normality matching the lower bound of the 95% of the distribution is assumed. Finally, a step guide with an example is elaborated to facilitate its use.
- *What are key parameters in fine-grained soils that play a dominant role in parameter determination (as R_D in coarse-grained soils)? Are there existing correlations to appropriately define them?*
In fine-grained soils, it was observed the importance of the w_L and I_P . The equivalent to R_D for coarse-grained soils would be the liquidity index I_L . However, the significance of the OCR and undrained shear strength is not minor and should also be considered as key parameters.

A second equation for w_L is developed in this thesis, aiming to better estimate when averaging with the unique equation existing in the literature. The developed correlation is validated and exposes a low estimation of γ_{sat} of the Robertson 2010 equation. A correction for γ is proposed, and once implemented, an acceptable result is obtained.

- *How can the extended APD system for fine-grained soils be validated?*

A comparison of laboratory tests with simulations using the output results of APD is done for a first validation of the APD results. Since the validation data used correspond to a specific site, supplementary validation should be executed. The chosen data corresponds to a levee in the south of The Netherlands, where the oedometer and triaxial test were executed, and CPTu data were available next to the boreholes. The results concluded that the compression constants showed in the oedometer simulation are good. In the case of the triaxial, good stiffness is acquired but the friction angle ϕ' is not well predicted. The underprediction of ϕ' comes with a dilemma of the acceptability of correlations based on the plasticity index for ϕ' .

7.2 Recommendations

The APD system had experienced large improvements from its proof of concept by van Berkom 2020. However, the system still needs improvements to be openly used. In the following bullet points, the personal recommendations are summarised:

- The system has the incorporation of fine-grained soils correlations. Firstly, the denomination of fine-grained soils could be changed to clay-like soils, which would be completed by sand-like soils, transition soils and organic ones. This classification introduced by Robertson 2016 would suit better the APD framework classification that is based on in-situ measurements when filtering the suitable methods since most correlations are made for clay-like soils and sand-like soils.
- Only clay-like or fine-grained soils together with sand-like or coarse-grained soils are included in the APD database. Because most of the correlations are done for these two groups of soils, and there is a lack of transitional soils correlations, an interpolation of them could be studied. It could be possible to use the IB index provided by Robertson 2016 to interpolate between clay-like and sand-like soils. The organic soil correlations also need to be included, and if no correlation exists for them, at least approximations could be used.
- For the validation, the Hardening Soil model with small stiffness was used. In the case of the triaxial test, the undrained shear strength was under-predicted, a result of an under prediction of the friction angle. New correlations should be elaborated based on CPT classification and not in physical classification, especially for soils with organic content that do not increase the excess pore pressure.

Bibliography

- Ahmadi, M. and Robertson, P. (2011). “Thin-layer effects on the CPT qc measurement”. In: *Canadian Geotechnical Journal* 42, pp. 1302–1317.
- Alpan, I. (1970). “The geotechnical properties of soils”. In: *Earth Science Reviews* 6.1, pp. 5–49.
- Atkinson, J. (2007). *The Mechanics of Soils and Foundations*. 2nd ed. London: CRC Press.
- Azzouz, A. S., Krizek, R. J., and Corotis, R. B. (1976). “Regression Analysis of Soil Compressibility”. In: *Soils and Foundations* 16.2, pp. 19–29.
- Baroni, M. and Almeida, M. d. S. S. (2017). “Compressibility and stress history of very soft organic clays”. In: *Proceedings of the Institution of Civil Engineers - Geotechnical Engineering* 170.2, pp. 148–160.
- Been, K. and Jefferies, M. G. (1985). “A state parameter for sands”. In: *Geotechnique* 35.2, pp. 99–112.
- Begemann, H. K. S. (1965). “The friction Jacket Cone as an Aid in Determining the Soil Profile”. In: *6th International Conference on Soil Mechanics and Foundation Engineering*. Montreal.
- Benz, T. (2007). “Small-Strain Stiffness of Soils and its Numerical Consequences”. PhD thesis. Pfaffenwaldring 35, 70569 Stuttgart, Germany: Universität Stuttgart.
- Benz, T., Schwab, R., and Vermeer, P. (2009a). “Small-strain stiffness in geotechnical analyses”. In: *Bautechnik* 86.S1, pp. 16–27.
- (2009b). “Small-strain stiffness in geotechnical analyses”. In: *Bautechnik* 86.S1, pp. 16–27.
- Biarez, J. and Favre, J. L. (1976). “Correlations de parametres en mecanique des sols”. In: *Ecole Central des arts et manufactures*.
- Brinkgreve, R. B. J., Engin, E., and Engin, H. K. (2010). “Validation of empirical formulas to derive model parameters for sands”. In: *Numerical methods in geotechnical engineering, (NUMGE 2010)*. Ed. by T. Benz and S. Nordal. London: CRC Press, pp. 137–142.
- Brinkgreve, R. (2019). “Automated model and parameter selection”. In: *Geostrata 23: Computational geotechnics*, pp. 39–45.
- Burland, J. B. (1990). “On the compressibility and shear strength of natural clays”. In: *Géotechnique* 40.3, pp. 329–378.
- Cetin, K. O. and Ozan, C. (2009). “CPT-Based Probabilistic Soil Characterization and Classification”. In: *Journal of Geotechnical and Geoenvironmental Engineering* 135.1, pp. 84–107.
- Chen, B. S. Y. and Mayne, P. W. (1996). “Statistical relationships between piezocone measurements and stress history of clays”. In: *Canadian Geotechnical Journal* 33, pp. 488–498.
- CUR (2003). *Rapport 2003-7 Bepaling geotechnische parameters*.

- D'Ignazio, M. et al. (2019). "Estimation of preconsolidation stress of clays from piezocone by means of high-quality calibration data". In: *AIMS Geosciences* 5, pp. 104–116.
- International, A. (2017). *Standard Practice for Classification of Soils for Engineering Purposes (Unified Soil Classification System)*. West Conshohocken, PA,
- Favre, J. (1980). *Milieu continu et milieu discontinu: mesure statistique indirecte des paramètres rhéologiques et approche probabiliste de la sécurité*.
- Favre, J. L. (1972). *Table ronde sur les corrélations de paramètres en mécanique des sols*. Ed. by J. Biarez, pp. 1–51.
- Favre, J. L. and Hattab, M. (2008). "Analysis of the 'Biarez–Favre' and 'Burland' models for the compressibility of remoulded clays". In: *Comptes Rendus Geoscience* 340.1, pp. 20–27.
- Fu, Y. et al. (2020). "Parameter Analysis on Hardening Soil Model of Soft Soil for Foundation Pits Based on Shear Rates in Shenzhen Bay, China". In: *Hindawi, Advances in Materials Science and Engineering* 2020.
- Grimstad, G., Andresen, L., and Jostad, H. (2012). "NGI-ADP: Anisotropic shear strength model for clay". In: *International Journal for Numerical and Analytical Methods in Geomechanics* 36, pp. 483–497.
- Guglielmelli, C. (2018). "Soil interpretation in Groningen, Verification and improvement of CPT-base correlations". MA thesis. Delft University of Technology.
- Haigh, S. et al. (2014). "The plastic limit of clays". In: *Géotechnique* 64.7, pp. 584–586.
- Hardin, B. O. and Drnevich, V. P. (1972). "Shear Modulus and Damping in Soils: Design Equations and Curves". In: *Journal of the Soil Mechanics and Foundations Division* 98.7, pp. 667–692.
- Hauth, M. (2020). "Quality assessment of a graph-based approach for a multi-methods determination of geotechnical model parameters". MA thesis. Delft University of Technology.
- Hicks, M. A., Pisano, F., and Peuchen, J., eds. (2018). *Proceedings of the 4th International Symposium on Cone Penetration Testing (CPT'18)* (Delft, The Netherlands). London: CRC Press.
- Jamiolkowski, M., Lancellotta, R., and Lo Presti, D. C. F. (1995). "Remarks on the stiffness at small strains of six Italian clays". In: *Proceedings of the First International Conference on Pre-failure Deformation Characteristics of Geomaterials* (Sapporo, Japan). Ed. by S. Shibuya, T. Mitachi, and S. Miura. Rotterdam: A.A. Balkema, pp. 197–216.
- Karlsrud, K. et al. (2005). "CPTU correlations for clays". In: *Proceedings of the 16th International Conference on Soil Mechanics and Geotechnical Engineering* (Osaka, Japan). Vol. 2. Rotterdam: Millpress Science Publishers, pp. 693–702.
- Kirkwood, T. B. L. (1979). "Geometric Means and Measures of Dispersion". In: *Biometrics* 35.4, pp. 908–909.
- Koopmans, L. H., Owen, D. B., and Rosenblatt, J. I. (1964). "Confidence Intervals for the Coefficient of Variation for the Normal and Log Normal Distributions". In: *Biometrika* 51.1/2, pp. 25–32.
- Kulhawy, F. H. and Mayne, P. W. (1990). "Manual on Estimating Soil Properties for Foundation Design". In: *Electric Power Research Institute, California*.
- Ladd, C. C. (1991). "Stability Evaluation during Staged Construction". In: *Journal of Geotechnical Engineering* 117.4, pp. 540–615.
- Leroueil, S., Tavenas, F., and Bihan, J.-P. L. (1983). "Propriétés caractéristiques des argiles de l'est du Canada". In: *Canadian Geotechnical Journal* 20.4, pp. 681–705.

- Levesque, C., Locat, J., and Leroueil, S. (2007). “Characterisation of postglacial sediments of the Saguenay Fjord, Quebec, Canada”. In: *Characterisation and Engineering Properties of Natural Soils* 3, pp. 2645–2677.
- Locat, J. and Demers, D. (1988). “Viscosity, yield stress, remolded strength, and liquidity index relationships for sensitive clays”. In: *Canadian Geotechnical Journal* 25.4, pp. 799–806.
- Low, H. et al. (2010). “Estimation of intact and remoulded undrained shear strengths from penetration tests in soft clays”. In: *Géotechnique* 60.11, pp. 843–859.
- Mayne, P. W. (1980). “CPT-Based Probabilistic Soil Characterization and Classification”. In: *Journal of Geotechnical and Geoenvironmental Engineering* 135.1, pp. 84–107.
- (1991). “Determination of OCR in Clays by Piezocone Tests Using Cavity Expansion and Critical State Concepts”. In: *Soils and Foundations* 31.2, pp. 65–76.
 - (2007). “In-situ test calibrations for evaluating soil parameters”. In: *Proceedings of the Second International Workshop on Characterisation and Engineering Properties of Natural Soils* (Singapore). Ed. by T. S. Tan et al. Vol. 3, pp. 1601–1652.
 - (2013). “Updating our geotechnical curricula via a balanced approach of in-situ, laboratory, and geophysical testing of soil”. In: *61st Annual Geotechnical Engineering Conference*.
 - (2014). “Interpretation of geotechnical parameters from seismic piezocone tests”. In: *3rd International Symposium on Cone Penetration Testing (CPT14)* (Las Vegas). Ed. by P. K. Robertson and K. I. Cabal. Vol. 102. ISSMGE Technical Committee TC 102, pp. 47–73.
 - (2016). “Evaluating effective stress parameters and undrained shear strengths of soft-firm clays from CPT and DMT”. In: *Australian Geomechanics Journal* 4, pp. 27–55.
 - (2017). “Stress History of Soils from Cone Penetration Tests”. In: *Soils and Rocks* 40, pp. 203–216.
- Mayne, P. W. and Agaiby, S. (2018). “Evaluating undrained rigidity index of clays from piezocone data - CPT18 Delft”. In: *Proceedings of the 4th International Symposium on Cone Penetration Testing (CPT’18)* (Delft, The Netherlands). Ed. by M. A. Hicks, F. Pisano, and J. Peuchen. London: CRC Press, pp. 65–71.
- Mayne, P. W. and Peuchen, J. (2018). “Evaluation of CPTu Nkt cone factor for undrained strength in clays - CPT18 Delft”. In: *Proceedings of the 4th International Symposium on Cone Penetration Testing (CPT’18)* (Delft, The Netherlands). Ed. by M. A. Hicks, F. Pisano, and J. Peuchen. London: CRC Press, pp. 423–429.
- Mayne, P. W. and Rix, G. J. (1993). “ $G_{max} - q_c$ Relationship for Clays”. In: *Geotechnical Testing Journal, GTJODJ* 16, No.1, pp. 54–60.
- (1995). “Correlations between shear wave velocity and cone tip resistance in natural clays”. In: *Soils and Foundations* 35.2, pp. 107–110.
- Mayne, P. W. et al. (2009). “State-of-the-art paper (SOA-1): geomaterial behavior and testing”. In: *17th International Conference on Soil Mechanics and Geotechnical Engineering* (ICSMGE, Alexandria, Egypt). Vol. 4. Rotterdam: Millpress/IOS Press.
- Mitchell, J. and Soga, K. (2005). *Soil Mechanics*. 3rd ed. Hoboken, New Jersey: John Wiley & Sons Inc.
- Montgomery, D. and Runger, G. (2014). *Applied statistics and probability for engineers*. 3rd ed. John Wiley & Sons, Inc.
- Nagaraj, T. S. and Jayadeva, M. S. (1983). “Critical Reappraisal of Plasticity Index of Soils”. In: *Journal of Geotechnical Engineering* 109.7, pp. 994–1000.

- Okkels, N. (2018). “Modern guidelines for classification of fine soils”. In: *XVII European Conference on Soil Mechanics and Geotechnical Engineering*. Ed. by S. E. Haraldur Sigursteinsson and B. Bessason. Reykjavík, Iceland: Icelandic Geotechnical Society, IGS.
- Phoon, K.-K. and Kulhawy, F. H. (1999). “Characterization of geotechnical variability”. In: *Canadian Geotechnical Journal* 36.4, pp. 612–624.
- Piantedosi, M. C. et al. (2009). “Predicting Soil Liquid Limit and Plasticity Index”. In: *Proceedings of the 17th International Conference on Soil Mechanics and Geotechnical Engineering*. Ed. by M. Hamza, M. Shahien, and Y. El-Mossallamy. IOS Press., pp. 1020–1023.
- PLAXIS Material Model (2020). *PLAXIS 2D Connect Edition V20 - Material Models Manual*. Bentley Systems.
- Polidori, E. (2003). “Proposal for a new plasticity chart”. In: *Géotechnique* 53.4, pp. 397–406.
- Reale, C. et al. (2018). “Automatic classification of fine-grained soils using CPT measurements and Artificial Neural Networks”. In: *Advanced Engineering Informatics* 36, pp. 207–215.
- Robertson, P. K. (1990). “Soil classification using the cone penetration test”. In: *Canadian Geotechnical Journal* 27, pp. 151–158.
- (2009). “Interpretation of Cone Penetration Test - a unified approach”. In: *Canadian Geotechnical Journal* 46, pp. 1337–1335.
- (2010). “CPT-based Soil Behaviour Type (SBT) Classification System – an update”. In: *Canadian Geotechnical Journal* 53.
- (2016). “Cone penetration test (CPT)-based soil behaviour type (SBT) Classification System – an update”. In: *Canadian Geotechnical Journal* 53.
- Robertson, P. K. and Cabal, K. (2014). *Guide to Cone Penetration Testing for Geotechnical Engineering*. 6th ed. Signal Hill, California: Gregg Drilling & Testing, Inc.
- Robertson, P. K. et al. (1986). “Use of Piezometer Cone Data”. In: *Use of In-situ Testing in Geotechnical Engineering* (In Situ '86, Blacksburg, Virginia, United States). Ed. by S. P. Clemence. New York, NY: American Society of Civil Engineers.
- Roscoe, K. H., Schofield, A. N., and Wroth, C. P. (1958). “On The Yielding of Soils”. In: *Géotechnique* 8.1, pp. 22–53.
- Schanz, T., Vermeer, P. A., and Bonnier, P. G. (1999). “The hardening soil model: Formulation and verification”. In: *Beyond 2000 in Computational Geotechnics*. Ed. by R. B. J. Brinkgreve. Ten Years of Plaxis International. Rotterdam: Balkema, pp. 281–290.
- Schnaid, F. (2005). “Geo-characterisation and properties of natural soils by in-situ tests”. In: *Proceedings of the 16th International Conference in Soil Mechanics and Geotechnical Engineering*. Ed. by O. Committee. Vol. 38. Millpress Science Publisher/IOS Press, pp. 23–24.
- (2008). “In Situ Testing in Geomechanics: The Main Tests”. In: Taylor & Francis.
- Schneider, J. and Moss, R. E. S. (2011). “Linking cyclic stress and cyclic strain based methods for assessment of cyclic liquefaction triggering in sands”. In: *Géotechnique Letters* 1, pp. 31–36.
- Schneider, J. et al. (2008). “Analysis of Factors Influencing Soil Classification Using Normalized Piezocone Tip Resistance and Pore Pressure Parameters”. In: *Journal of Geotechnical and Geoenvironmental Engineering* 134.11, pp. 1569–1586.
- Schofield, A. and Wroth, P. (1968). *Critical State Soil Mechanics*. New York: McGraw-Hill.

- Seed, H. B., Woodward, R. J., and Lundgren, R. (1964). “Clay Mineralogical Aspects of the Atterberg Limits”. In: *Journal of the Soil Mechanics and Foundations Division* 90.4, pp. 107–131.
- Sharma, B. and Bora, P. K. (2015). “A Study on Correlation Between Liquid Limit, Plastic Limit and Consolidation Properties of Soils”. In: *Indian Geotechnical Journal* 2.45, pp. 225–230.
- Sharma, B. and Sridharan, a. (2018). “Liquid and plastic limits of clays by cone method”. In: *International Journal of Geo-Engineering* 9.22.
- Shibuya, S., Hwang, S. C., and Mitachi, T. (1997). “Elastic shear modulus of soft clays from shear wave velocity measurement”. In: *Géotechnique* 47.3, pp. 593–601.
- Shimobe, S. and Spagnoli, G. (2019). “Some relations among fall cone penetration, liquidity index and undrained shear strength of clays considering the sensitivity ratio”. In: *Bulletin of Engineering Geology and the Environment* 78, pp. 5029–5038.
- (2020). “Relationships between undrained shear strength, liquidity index, and water content ratio of clays”. In: *Bulletin of Engineering Geology and the Environment* 79, pp. 4817–4828.
- Simonini, P. and Cola, P. p. E. S. (2000). “Use of Piezocone to Predict Maximum Stiffness of Venetian Soils”. In: *Journal of Geotechnical and Geoenvironmental Engineering* 126, pp. 378–382.
- Sivapullaiah, P. V. and Sridharan, A. (1985). “Liquid Limit of Soil Mixtures”. In: *Geotechnical Testing Journal* 8.3, pp. 111–116.
- Skempton, A. W. (1957). *Discussion on airport paper NO. 35: The planning and design of the New Hong Kong Airport*. 2, p. 306.
- Skempton, A. W. and Jones, O. T. (1944). “Notes on the compressibility of clays”. In: *Quarterly Journal of the Geological Society* 100.1-4, pp. 119–135.
- Sorensen, K. and Okkels, N. (2013). “Correlation between drained shear strength and plasticity index of undisturbed overconsolidated clays”. In:
- Spagnoli, G. (2012). “Comparison between Casagrande and drop-cone methods to calculate liquid limit for pure clay”. In: *Canadian Journal of Soil Science* 92.6, pp. 859–864.
- Spagnoli, G. et al. (2018). “Statistical variability of the correlation plasticity index versus liquid limit for smectite and kaolinite”. In: *Applied Clay Science* 156, pp. 152–159.
- Sridharan, A. and Nagaraj, H. B. (2000). “Compressibility behaviour of remoulded, fine-grained soils and correlation with index properties”. In: *Canadian Geotechnical Journal* 37.3, pp. 712–722.
- Standardization, I. O. for (2017). *ISO 14688-2:2017; Geotechnical investigation and testing — Identification and classification of soil — Part 2: Principles for a classification*. International Organization for Standardization.
- Tanaka, H. and Tanaka, M. (1998). “Characterization of Sandy Soils Using CPT and DMT”. In: vol. 38. 3. Balkema; pp. 55–65.
- Terzaghi, K. and Peck, R. B. (1967). *Soil mechanics in engineering practice*. 2nd ed. New York: John Wiley & Sons Inc.
- Terzaghi, K., Peck, R. B., and Gholamreza, M. (1948). *Soil Mechanics in Engineering Practice*. 3rd ed. New York: John Wiley & Sons, Inc.
- Tiwari, B. and Ajmera, B. (2012). “New Correlation Equation for Compression Index of Remolded Clays”. In: *Journal of Geotechnical and Geoenvironmental Engineering, ASCE* 138.6, pp. 757–762.

- van Berkom, I. (2020). “An Automated System to Determine Constitutive Model Parameters from In Situ Test”. MA thesis. Delft University of Technology.
- Vardanega, P. and Haigh, S. (2014). “The undrained strength – liquidity index relationship”. In: *Canadian Geotechnical Journal* 51.9, pp. 1073–1086.
- Whyte, I. L. (1982). “Soil plasticity and strength - A new approach using extrusion”. In: *Ground Engineering* 15.1, pp. 16–20.
- Wood, D. M. (1990). *Soil behaviour and critical state soil mechanics*. Cambridge: Cambridge University Press.
- Wroth, C. P. (1979). “Correlations of some engineering properties of soils”. In: *Proc. 2nd International Conference on Behaviour of Offshore Structures*. Vol. 1. London, pp. 121–132.
- (1984). “The interpretation of in situ soil tests”. In: *Géotechnique* 34.4, pp. 449–489.
- Wroth, C. P. and Wood, D. M. (1978). “The correlation of index properties with some basic engineering properties of soils”. In: *Canadian Geotechnical Journal* 15.2, pp. 137–145.

Appendices

Appendix A

Collection of Correlations

A.1 Collection of Correlations

The correlation collection does not include the already implemented in thesis' database of Hauth (2020).

A.1.1 Small strain shear Modulus

1. Mayne and Rix (1993)

From 31 clay sites where a total of 481 paired observations of G_{max} and q_c , an equation is obtained. The data is log-log transformed to do a regression line:

$$G_{max} = 2.78 q_c^{1.335} \quad (\text{A.1})$$

The standard deviation of the logarithm of G_{max} is chosen as $\log(G_{max}) = 0.25$. Assuming normal distribution of the variability, the lower boundary is matched for a $CV = 0.34$. A lower value of G_0 is unfavourable for most of the cases.

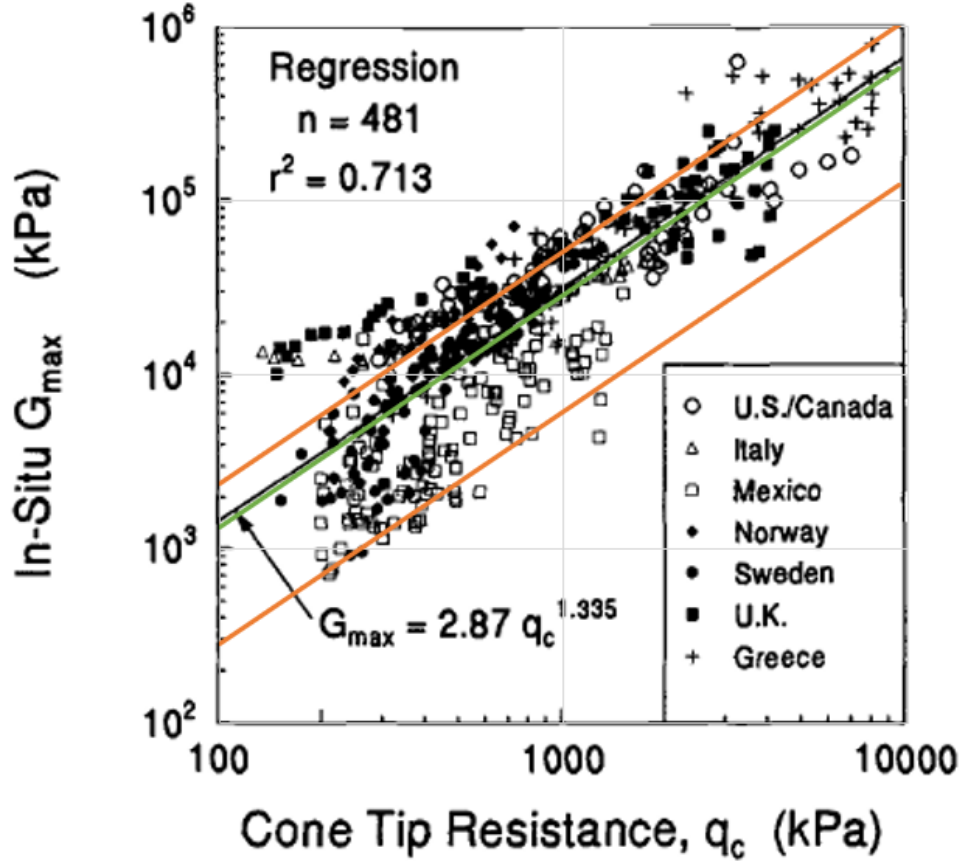


Figure A.1: Mayne and Rix (1993) G_0 apparent relation to cone tip resistance (q_c). The CV match the lower boundary.

The previous database was paired together with the void ratio (e_0). The multiple regression line is shown in figure A.1. The standard deviation of the logarithm of G_{max} is chosen as $\log(G_{max}) = 0.17$. The coefficient of variation of $CV = 0.27$ is chosen to match the lower boundary of a normal distribution of the error.

$$G_{max} = 99.5(p_a)^{0.305}(q_c)^{0.695}/e_0^{1.130} \quad (\text{A.2})$$

where p_a = atmospheric reference pressure in same units as G_{max} and q_c .

2. Mayne (2007)

Several relations based on Tanaka and Tanaka (1998) were explored to determine the stiffness of clays. The exponent m^* is 0.6 for clean quartz sands, 0.8 for silts, and 1.0 for intact clays of low to medium sensitivity.

$$G_0 \approx 50 \sigma_{atm} \cdot [(q_t - \sigma_{v0})/\sigma_{atm}]^{m^*} \quad (\text{A.3})$$

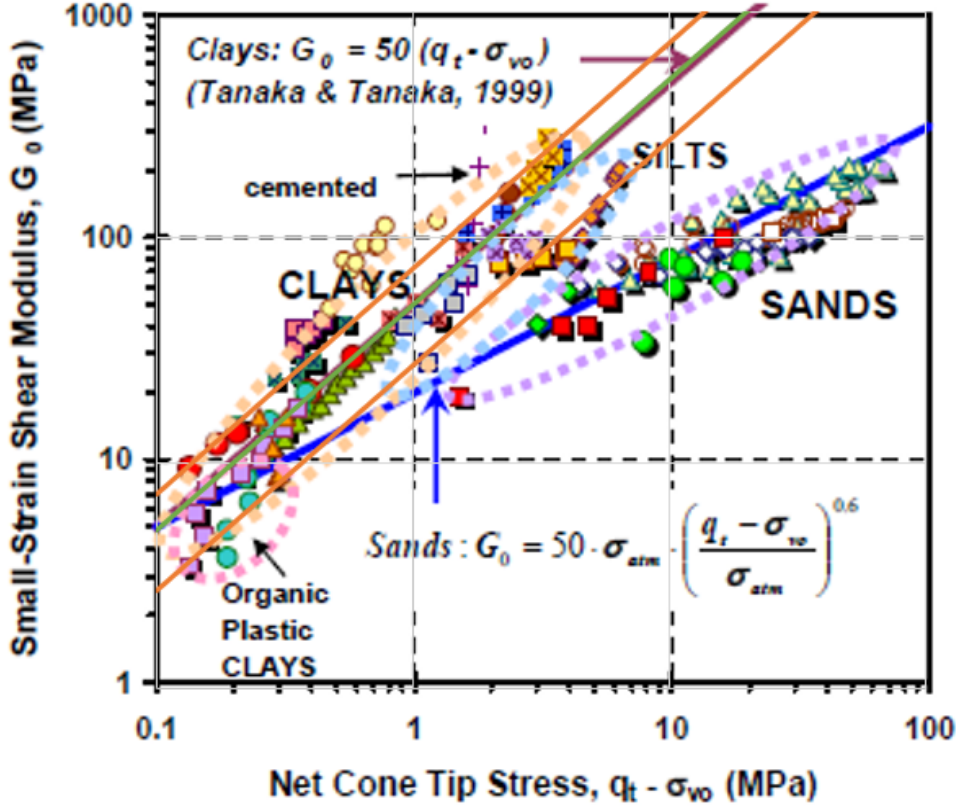


Figure A.2: Mayne (2007) relation for the net cone resistance ($q_t - \sigma_{v0}$) to G_0 .

The standard deviation of $\log G_0$ was chosen as $SD(\log G_{0(\text{clays})}) = 0.15$ for clays; $SD(\log G_{0(\text{silts})}) = 0.18$ for silts; $SD(\log G_{0(\text{sands})}) = 0.15$ for sands. The CV match the lower boundary for a normal distribution assumption and is chosen as $CV_{(\text{clays})} = 0.25$ for clays; $CV_{(\text{silts})} = 0.28$ for silts; $CV_{(\text{sands})} = 0.25$ for sands.

3. Shibuya et al. (1997)

From nine sites worldwide of normally consolidated soft clays, Shibuya et al. (1997) evaluate the results of laboratory Bender element test on reconstituted clay samples. The empirical expression found relates the void ratio (e_0) and the current effective stress state ($\sigma' - v$).

$$G_0 = A(1 + e_0)^{-2.4} \sigma'_v{}^{0.5} \quad (\text{in } kPa) \quad (\text{A.4})$$

where A has an average value of 24000. No statistical data is provided, neither a graph to estimate the overall match for the 9 sites. A coefficient of variation $CV = 0.25$ is chosen, similar to the estimated for Mayne and Rix (1993) equation.

4. Jamiolkowski et al. (1995)

Jamiolkowski et al. (1995) evaluates the small strain shear modulus G_0 for six different Italian natural clays on high-quality undisturbed samples. Different parameters for the equation were found for each clay, all of them having a $CV = 20\%$. Based on these results, Schnaid (2005) proposes the following equation:

$$G_0 = 480(e_0)^{-1.43}(\sigma'_v)^{0.22}(\sigma'_h)^{0.22}(p_a)^{1-2(0.22)} \quad (\text{A.5})$$

where σ'_v , σ'_h and p_a are in kPa.

Since the CV provided is site-specific and the equation used is not the aforementioned, a $CV = 0.27$ is chosen.

5. Simonini and Cola (2000)

On the Venetian Lagoon, several studies have been carried out. The authors estimate the small-strain shear modulus G_0 correlating piezocone measurements to different shear wave test results as cross-hole, seismic piezocone, bender element system, and resonant column test. Despite being a study of a specific soil, it can be useful in similar geological deposits. Two equations are summarised here; one only used the uncorrected cone resistance q_c while the other one includes the pore pressure ratio B_q with the intention of supply the void ratio e_0 . The unit of q_c is in MPa .

$$G_0 = 49.2 q_c^{0.51} \quad (MPa) \quad (A.6)$$

$$G_0 = 21.5 q_c^{0.79} (1 + B_q)^{4.59} \quad (MPa) \quad (A.7)$$

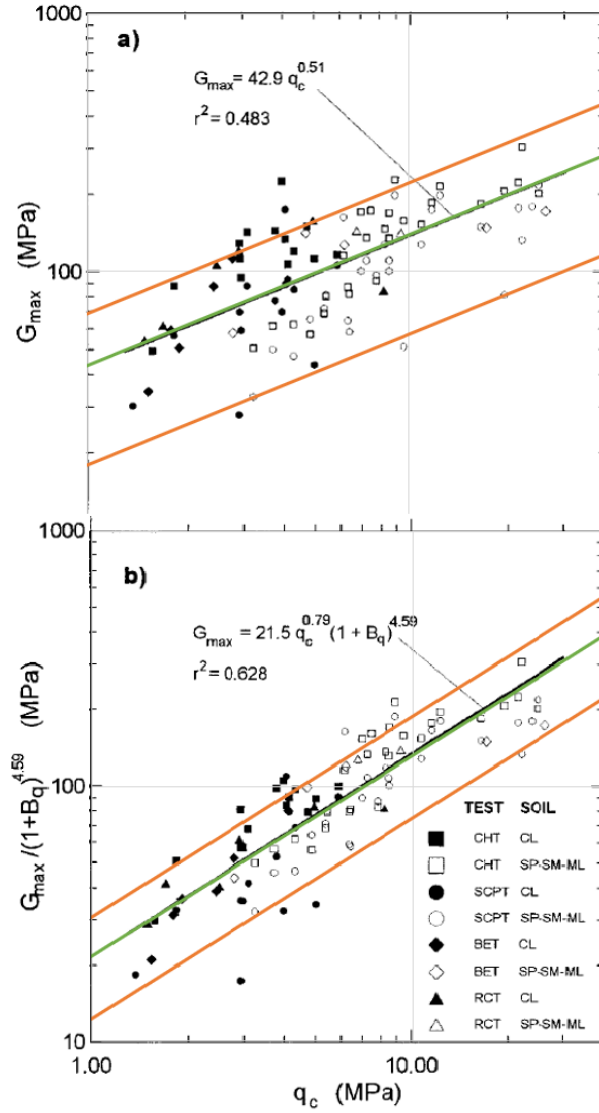


Figure A.3: Simonini and Cola (2000) relation for G_0 from CPTu measurements

The CV chosen for equation A.6 is 0.292 and for equation A.7 is 0.238, both of them match the lower boundary for a normal distribution assumption. The second equation has a better accuracy of the estimation, shown on the chosen CV .

A.1.2 Constrain elastic modulus

1. Robertson and Cabal (2014)

In his guide to Cone Penetration Testing, Robertson and Cabal (2014) summarised the empirical relationship used by many authors. Their recommendation is based on Robertson (2009):

$$E_{oed} = \alpha_M (q_t - \sigma_{v0}) \quad (\text{A.8})$$

The parameter α_M is defined as follows:

When $I_c < 2.2$ (fine-grained soils) use:

$$\begin{aligned}\alpha_M &= Q_t && \text{when } Q_t < 14, \\ \alpha_M &= 14 && \text{when } Q_t > 14\end{aligned}\tag{A.9}$$

When $I_c > 2.2$ (coarse-grained soils) use:

$$\alpha_M = 0.0188[10^{(0.55I_c+1.68)}]\tag{A.10}$$

No statistical data is provided for this correlation. However, it is remarked that the equation is less reliable in the region for fine-grained soils, and it is better for uncemented, predominately silica-based soils of Holocene and Pleistocene age.

Since the equation is exponential, a variability of the error is expected, and a coefficient of variation ($CV = 0.22$) is chosen.

A.1.3 Rigidity Index

1. Mayne (2016):

The rigidity index $I_R = G/s_u$ for clays is an important parameter for bearing capacity, pile driving, pore water pressure generation, and piezo-dissipation Mayne 2016. Using a spherical cavity framework, Mayne (2016) determine the rigidity index based on the pore water ratio parameter B_q . The minimum and maximum value of B_q is 0.5 and 0.7 correspondingly.

$$I_R = e^{\frac{2.93 \cdot B_q}{1 - B_q}}\tag{A.11}$$

No statistical data is provided. An arbitrary $SD = 5$ is assumed.

2. Mayne and Agaiby (2018):

Using a hybrid spherical cavity expansion - critical state framework, Mayne and Agaiby (2018) derived the operational rigidity index I_R . No statistical data is provided, and only a few profiles are compared to the framework, all of them having good results. A arbitrary $SD = 5$ is defined.

$$I_R = e^{\frac{1.5+2.925 \cdot M \cdot a_q}{M \cdot (1-a_q)}}\tag{A.12}$$

being

$$a_q = \frac{(u_2 - u_0)/\sigma'_{v0} - 1}{(q_t - \sigma_{v0})/\sigma'_{v0}}\tag{A.13}$$

$$M = (6 \sin\phi')/(3 - \sin\phi')\tag{A.14}$$

In the case of lacking ϕ , for soft to firm clays the effective friction angle needed for M is recommended as:

$$\phi' = 29.5 \text{ deg} \cdot B_q^{0.121} [0.256 + 0.336 \cdot B_q + \log(q_{net}/\sigma'_{v0})]\tag{A.15}$$

A.1.4 Overconsolidation ratio and effective preconsolidation stress

The OCR is defined as the ratio of the preconsolidation effective stress to vertical effective stress, $OCR = \sigma'_p / \sigma'_v$. Correlations for both are shown here since the OCR can be obtained from σ'_p correlations.

1. Kulhawy and Mayne (1990):

Lacking the pore water pressure, the following equation was presented:

$$\sigma'_p = 0.29q_c \quad (\text{A.16})$$

The standard deviation is provided as $SD = 2.31p_a$ being p_a the atmospheric pressure. However, it is difficult to believe that the dispersion follows an additivity shape. Instead, it can be seen that it is multiplicative in figure A.4. A Coefficient of Variation $CV = 0.30$ is chosen.

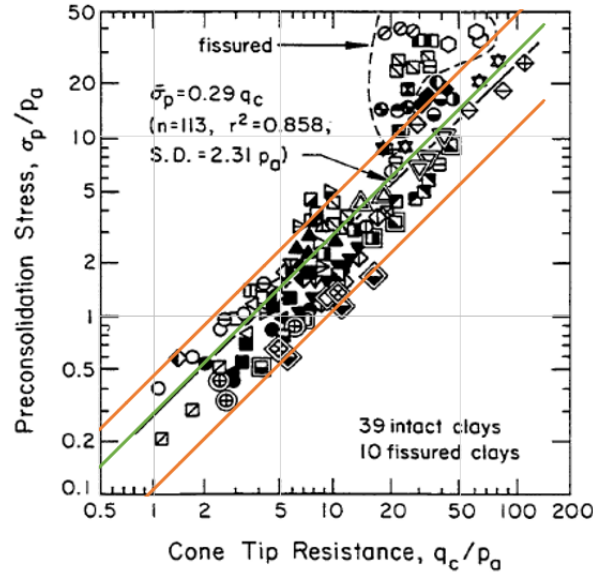


Figure A.4: Kulhawy and Mayne (1990) relation for σ'_p from q_c

Another relation is presented using the CPTu. The provided standard deviation does not seem to represent a multiplicative or additive error along the trendline. Based on an arbitrary lower boundary, a $CV = 0.271$ is chosen.

$$\sigma'_p = 0.33(q_t - \sigma_v) \quad (\text{A.17})$$

where σ_v is the total vertical stress and q_t the corrected cone resistance.

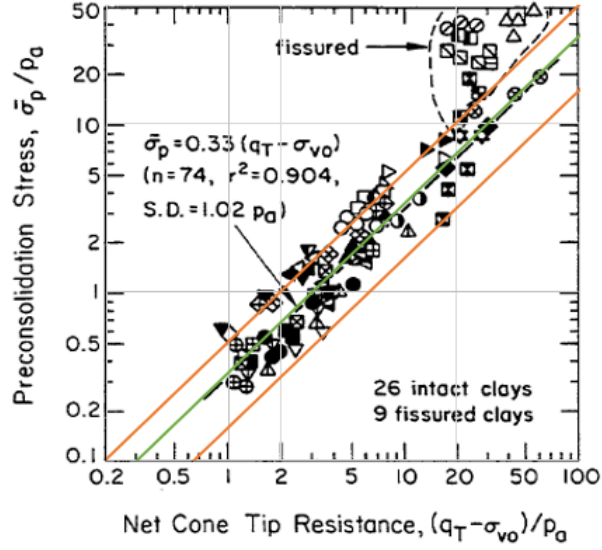


Figure A.5: Kulhawy and Mayne (1990) relation for σ'_p from q_t

2. Chen and Mayne (1996):

Different correlations were made based on worldwide samples and including different piezocones. The ones that are believed to be the most useful are shown. The equation has little difference with equation A.17, however, the database is larger. An estimation of the lower 95% confidence interval is made, obtaining a $CV = 0.282$, similar to the other equations. The correlation underestimate σ'_p for fissured clays. D'Ignazio et al. (2019) compared equation A.18 correlation to a database CLAY/9/249 and got a $CV = 0.20$.

$$\sigma'_p = 0.305(q_t - \sigma_v) \quad (\text{A.18})$$

A second equation was made including the plasticity index I_P . The statistics are not shown, a smaller variability was reported. Therefore, an arbitrary $CV = 0.25$ is chosen.

$$\sigma'_p = p_a \cdot 0.86 \cdot [(q_t - \sigma_v)/p_a]^{0.93} \cdot I_P^{-0.28} \quad (\text{A.19})$$

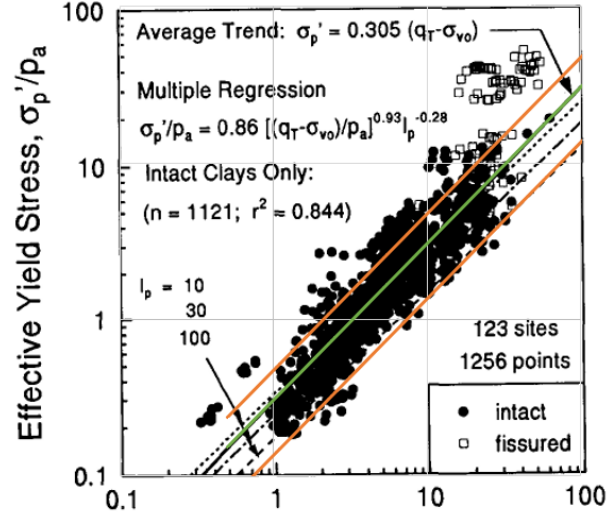


Figure A.6: Chen and Mayne (1996) relation for σ'_p from q_t and I_P

A second equation was made, including the plasticity index I_P . The statistics are not shown; therefore an arbitrarily $CV = 0.25$ is chosen.

$$\sigma'_p = 0.53(u_2 - u_0) \quad (\text{A.20})$$

$$\sigma'_p = 1.03p_a \cdot [(u_2 - u_0)/p_a]^{0.93} \cdot I_P^{-0.18} \quad (\text{A.21})$$

Only the sample number and the coefficient of determination is provided. An arbitrary lower 95% boundary is adopted. For equation A.20 the adopted $CV = 0.261$ and for equation A.21 $CV = 0.238$. D'Ignazio et al. (2019) evaluated equation A.20 to CLAY/9/249 database and got a $CV = 0.22$

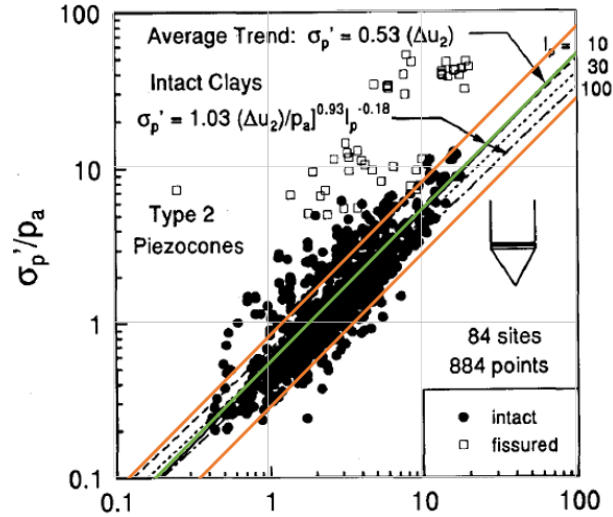


Figure A.7: Chen and Mayne (1996) relation for σ'_p from u_2 and I_P

A different evaluation was done comparing the differences between the corrected cone resistance q_t and the pore pressure behind the cone u_2 . Similar to the previous correlations, a general equation was made and another considering the plasticity

index I_P . Since no statistical data is provided, arbitrary 95% lower confidence interval is taken. For equation A.22 $CV = 0.261$ and for equation A.23 $CV = 0.261$. It must be noted that D'Ignazio et al. (2019) compared equation A.22 to the database CLAY/9/249 and gets a coefficient of variation $CV = 0.35$

$$\sigma'_p = 0.50(q_t - u_2) \quad (\text{A.22})$$

$$\sigma'_p = (q_t - u_2) \cdot I_P^{-0.20} \quad (\text{A.23})$$

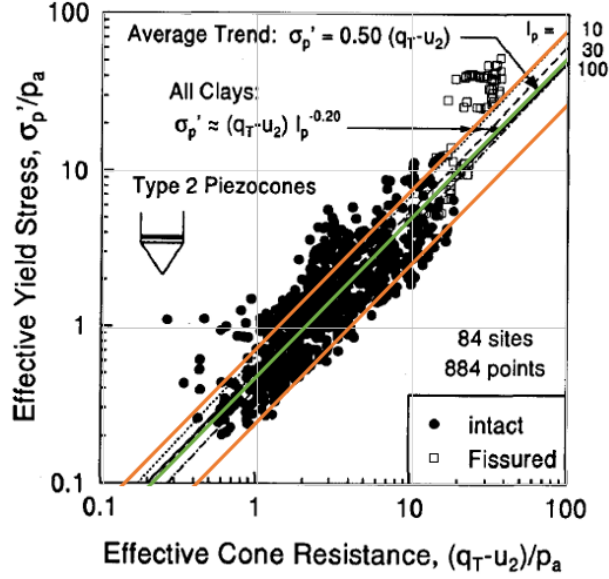


Figure A.8: Chen and Mayne (1996) relation for σ'_p from $q_t - u_2$ and I_P

The following equations for OCR made by Chen and Mayne (1996) have no statistics. However, D'Ignazio et al. (2019) evaluate them with a different database, CLAY/9/249, and their reported coefficient of variation is used in the APD database:

$$OCR = 0.317 \frac{q_t - \sigma_v}{\sigma'_v} \quad CV = 0.20 \quad (\text{A.24})$$

$$OCR = 0.259 \frac{q_t - \sigma_v}{\sigma'_v}^{1.107} \quad CV = 0.22 \quad (\text{A.25})$$

$$OCR = 0.545 \left(\frac{q_t - u_2}{\sigma'_v} \right)^{0.969} \quad CV = 0.34 \quad (\text{A.26})$$

$$OCR = 1.026 B_q^{-1.077} \quad CV = 0.25 \quad (\text{A.27})$$

3. Mayne (2014):

The effective yield stress σ'_y is taken as the effective preconsolidation stress σ'_p . However, technically σ'_p is associated with the mechanical unloading of stresses, whereas σ'_y includes additional effects as bonding, fabric and structure Mayne et al.

2009. To determine a quick first-order estimate of the yield stress, a unified approach was elaborated Mayne et al. 2009:

$$\sigma'_y = 0.33(q_t - \sigma_v)^{m'} \quad (\text{A.28})$$

where the exponent m' decreases with mean grain size. An equation for its function of the CPT material index I_c is expressed as Mayne 2014:

$$m' = 1 - \frac{0.28}{1 + (I_c/2.65)^{25}} \quad (\text{A.29})$$

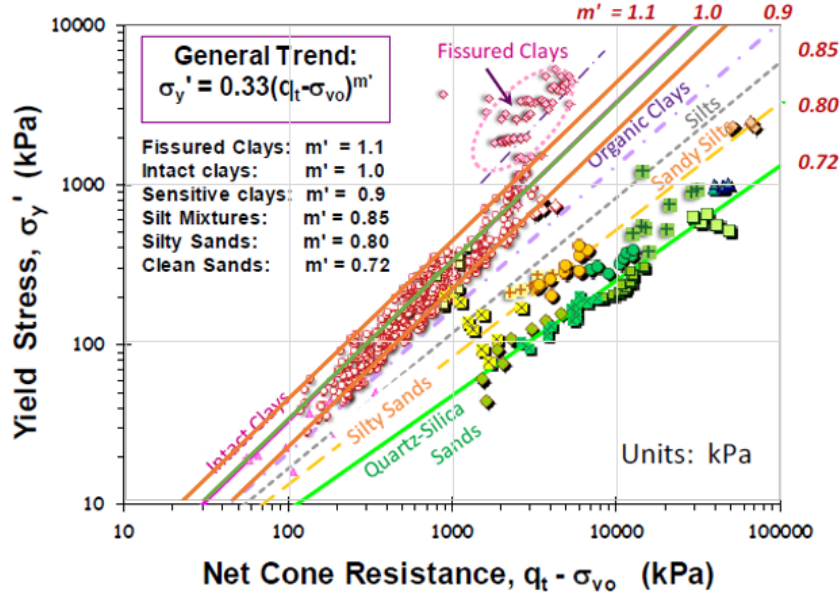


Figure A.9: Mayne (2014) relation for σ'_y from $q_t - \sigma_v$. Bounds for normal distribution of 95% confidence for clays ($m' = 1$) are shown.

For each exponent m' equation, meaning for each soil the lower boundary 95% confidence was estimated and the Coefficient of Variation. For clays $CV_{m'=1.0} = 0.199$, for silty sands and sandy silts $CV_{m'=0.80} = 0.185$, for organic clays $CV_{m'=0.9} = 0.185$ and for sands $CV_{m'=0.72} = 0.17$. For the variability of equation A.28 it is decided to take a single value $CV = 0.19$, while for equation A.29 a standard deviation $SD = 0.05$ is chosen.

4. Mayne (2017):

From Critical state soil mechanics and spherical cavity expansion solutions, a set of relations to the preconsolidation stress σ'_p are found:

$$\sigma'_p = \frac{q_t - \sigma_v}{M(1 + 1/3 \ln(I_R))} \quad (\text{A.30})$$

$$\sigma'_p = \frac{\Delta u}{1/3M \cdot I_R} \quad (\text{A.31})$$

$$\sigma'_p = \frac{q_t - u_2}{0.957M + 0.5} \quad (\text{A.32})$$

where M can be obtained with equation A.14, I_R with equation A.12. All these equations assume unitary plastic volumetric strain ratio $\Lambda = 1 - C_s/C_c$, C_s = swelling index and C_c = virgin compression index. The approximation works well for most clays and silts to have a first estimate. No statistical data is provided and a $CV = 0.2$ is adopted for the three of them.

5. Mayne (1991):

Using the cavity expansion and critical state soil mechanics concepts, a direct expression is determined:

$$OCR = 2 \left[\frac{1}{1.95M + 1} \left(\frac{q_t - u_2}{\sigma'_v} \right) \right]^{1.33} \quad (\text{A.33})$$

The exponent 1.33 results of adopting a plastic volumetric strain ratio $\Lambda = 1 - C_s/C_c = 0.75$. The parameter $M = 6 \sin \phi' / (3 - \sin \phi')$. No statistical data is provided from this theoretical equation. It is adopted a $SD = 0.5$.

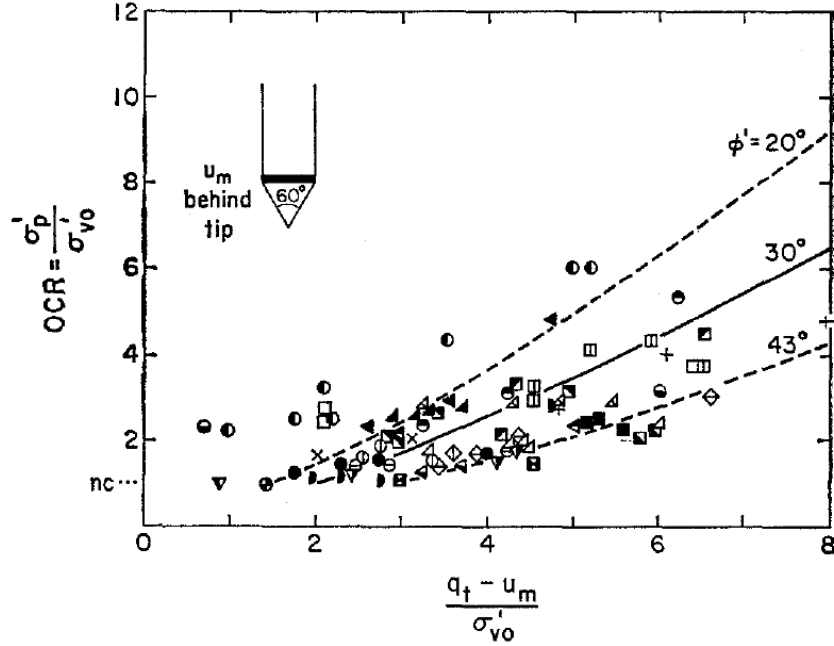


Figure A.10: Mayne (1991) relation for OCR from cavity expansion theory and critical state soil mechanics. Statistical data is not provided. Pore pressure in graph $u_m = u_2$.

6. Mayne and Agaiby (2018):

Following the cavity expansion theory and critical state soil mechanics, a new expression of OCR is proposed by Mayne and Agaiby 2018, where it was also proposed a rigidity index equation. It use $\Lambda = 1$ for natural clays at low OCR , if not it is recommended $\Lambda = 0.8$:

$$OCR = 2 \cdot \left(\frac{(2/M) \cdot (q_t - \sigma_v) / \sigma'_v}{(4/3) \cdot (\ln I_R + 1) + \pi/2 + 1} \right)^{\frac{1}{\Lambda}} \quad (\text{A.34})$$

where $M = 6 \sin \phi' / (3 - \sin \phi')$

7. Wroth (1984):

Derived from critical state soil mechanics for triaxial compression mode, Wroth (1984) proposed the following equation:

$$OCR = 2 \left[\frac{2(s_u/\sigma'_v)}{M} \right]^{\frac{1}{\Lambda}} \quad (\text{A.35})$$

where $M = 6 \sin \phi' / (3 - \sin \phi')$ and $\Lambda \approx 0.80$. No data was provided for this semi theoretical equation.

A.1.5 Shear wave velocity

Correlations are added to the database.

1. **Mayne and Rix (1995):** The relation of cone penetration tip resistance q_c to estimate the shear wave velocity V_s was studied. Different correlations are proposed from regression and it is observed that the inclusion of the void ratio, e_0 , increase the fitting. However, due to the stage of development of the APD, they are not included. The following correlations includes data from intact and fissured clays.

$$V_s = 1.75 \cdot q_c^{0.627} \quad (\text{m/s}) \quad (\text{A.36})$$

where q_c is introduced in kPa.

The standard deviation of the transformed variable is provided, $SD(\log V_s) = 0.146$ that is used to estimate a coefficient of variation $CV = 0.24$.

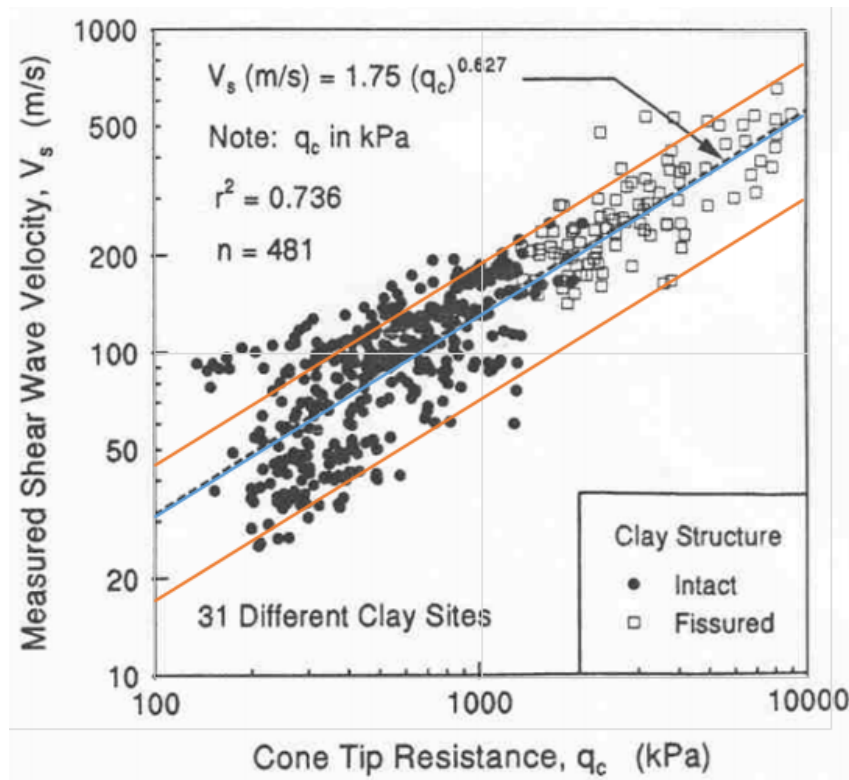


Figure A.11: Mayne and Rix (1995) relation for V_s from q_c . Estimated bounds for normal distribution of 95% are shown

2. Mayne (2007):

The shear wave V_s in m/s was compared from SCPT data to sleeve friction f_s in (kPa):

$$V_s = 51.6 \cdot \ln(f_s) + 18.5 \quad (m/s) \quad (A.37)$$

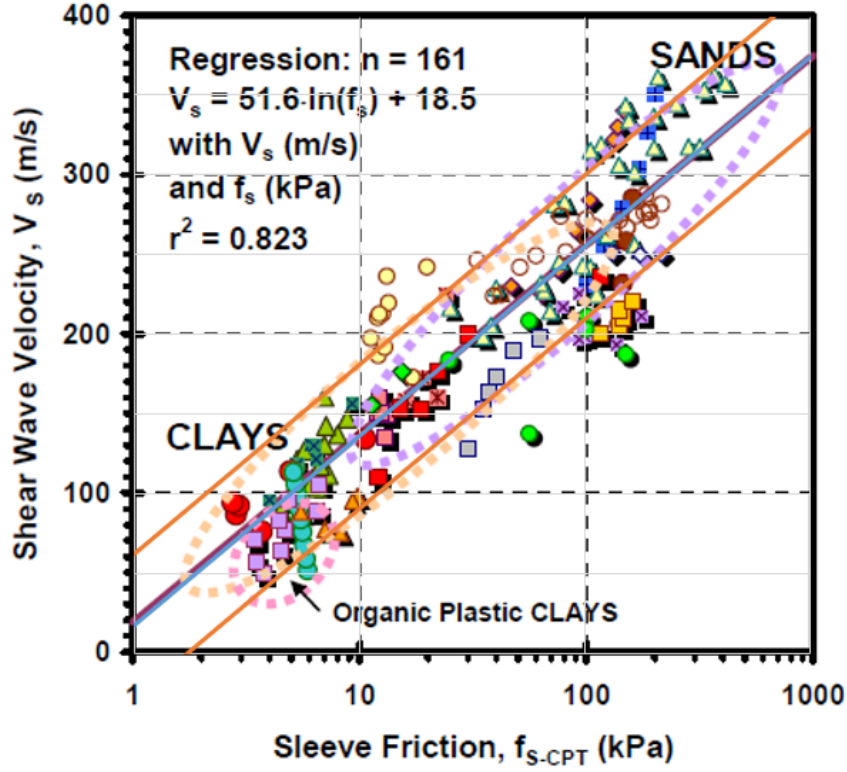


Figure A.12: Mayne (2007) relation for V_s from f_s . Bounds for normal distribution of 95%

The distribution of the samples follows a constant variability, estimated as $SD = 45 m/s$.

3. Robertson and Cabal (2014):

A general relation for the shear wave velocity based on SCPT data is provided for uncemented Holocene to Pleistocene age soils:

$$V_s = [\alpha_{vs}(q_t - \sigma_v)/p_a]^{0.5} \quad (m/s) \quad (A.38)$$

where $\alpha_{vs} = 10^{0.55I_c+1.68}$. No statistical data is provided, neither a graph. It is adopted a $SD = 45 m/s$.

A.1.6 Undrained shear strength ratio

The SHANSHEP approach relates the undrained shear strength, s_u , to a particular stress path and it calculates as:

$$s_u = \sigma'_v S (OCR)^m \quad (\text{A.39})$$

The parameter S , the undrained shear strength ratio will be included in the correlation's database. Since the APD framework estimates parameters for a specific soil location, it seems convenient to provide this ratio instead of s_u .

Moreover, since the correlations are taken from different test results, e.g., shear vane, triaxial compression, or DSS, the user should decide which ones to include or remove. It is believed that for a first estimation, the result can be taken as an average s_u .

1. Wroth (1984):

For normally consolidated soils (NC), Mayne (2013) summarised equations for the undrained shear strength ratio. An approximation was made for laboratory triaxial compression test, based on critical-state soil mechanics Wroth 1984.

$$S_{CIUC\&CK_0UC} = \frac{\phi'}{100} \quad (\text{A.40})$$

No statistical data is provided; it is assumed a constant variability $SD = 0.051$ based on Mayne 2013 recommendation: if no data is available, assume $\phi' = 28.6$ deg (mean value) with a standard deviation $SD = 5.1$ deg.

2. Mayne (2013):

Mayne (2013) summarised the work done on correlating the plasticity index, I_P , to undrained shear strength. He reached an exponential equation relating the I_P and the undrained shear strength ratio, S . The vane shear test, VST, was used for this correlation.

$$S_{VST} = 0.0611 \cdot I_P^{0.419} \quad (\text{A.41})$$

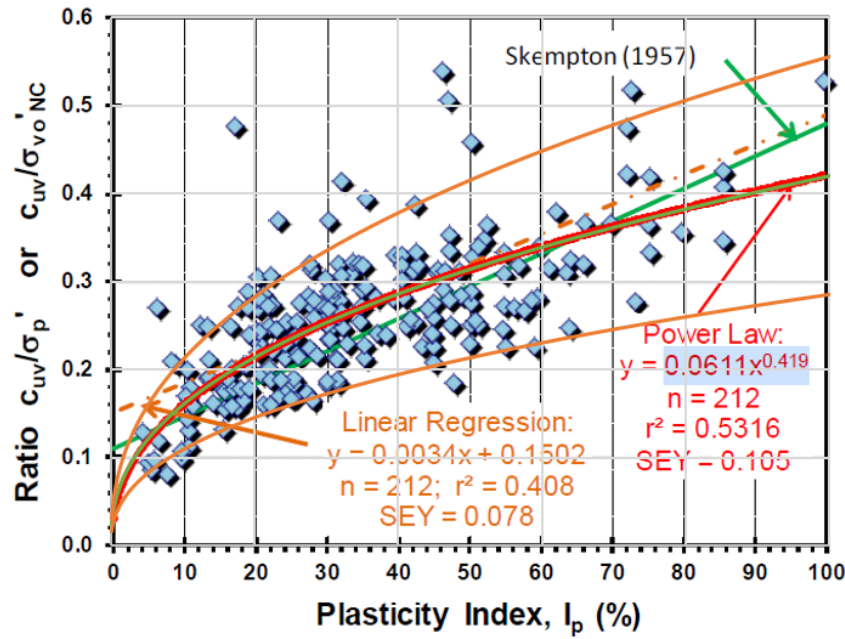


Figure A.13: Mayne (2013) relation for S_{DSS} from PI . Bounds for normal distribution of 95%

Using the provided $S.E.Y.$ the confidence intervals are drawn in figure A.13. To match the lower one for a normal distribution, the $CV = 0.192$ is chosen.

3. Mayne (2013):

It is summarised in Mayne (2013) the research done by Wroth (1984) and the undrained shear strength ratio for normally-consolidated clays in direct simple shear (DSS) based on the Critical State Soil Mechanics, CSSM, can be:

$$S_{DSS} = (S_u/\sigma'_v)_{NC} = \sin\phi'/2 \quad (A.42)$$

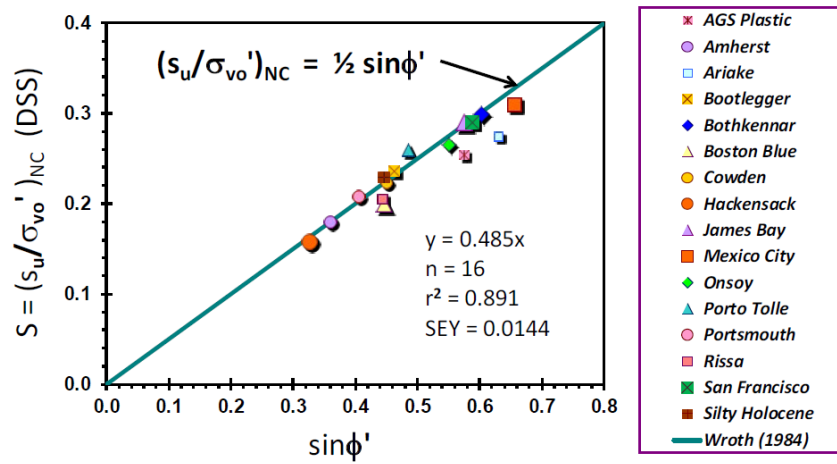


Figure A.14: Mayne (2013) relation for S from $\sin\phi'$. Statistical data is provided and since no transformation of the variable was used, it can be used directly.

A reported constant variability of $SD = 0.0144$ is used in the APD database.

The stress history is included in the CSSM and in the general case of DSS can be Mayne 2013:

$$S_{DSS} = (s_u/\sigma_{vo}')_{OC} = \frac{\sin \phi'}{2} OCR^\lambda \quad \lambda = 1 - C_s/C_c \approx 0.8 \quad (A.43)$$

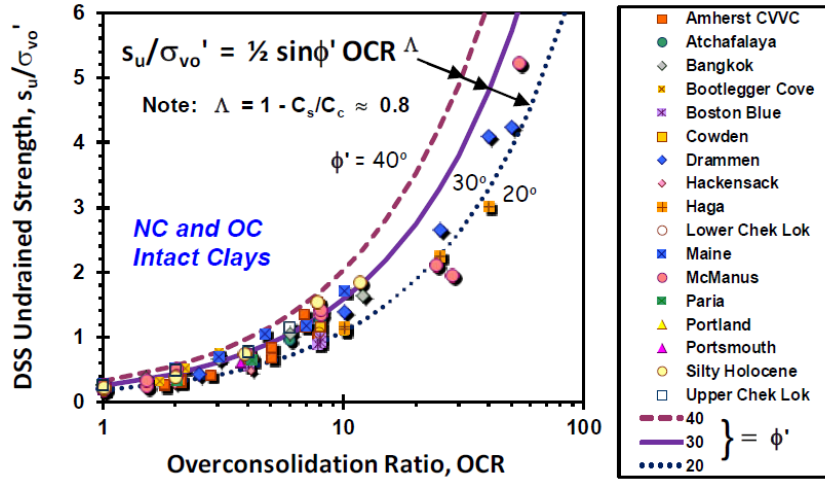


Figure A.15: Mayne (2013) relation for S from $\sin \phi'$ and OCR . Statistical data is not provided.

The equation A.43 do not have statistic data. To introduce the variability of the equation in the APD framework, the figure A.15 is used. Since equation A.43 have two independent variables, $\sin \phi'$ and OCR , the variability depends on both and no database is provided of the soils sample to analyse the variability. Instead, a fix value of $\sin \phi' = 0.25$ is chosen, base on $\phi = 30$ deg and in this way a 95% lower boundary can be selected from figure A.15 matching $\phi' = 20$ deg. This results in a $CV = 0.177$.

4. Levesque et al. (2007):

The correlation is reported in Mayne 2014, and it could not be accessed to the original report. It relates the undrained shear strength s_u to the shear wave velocity, V_s , and it is believed to be useful since it is entirely different from the others. However, no information was found about the test type to what s_u was compared. The log-log transformed data reported standard deviation is $SD_{logY} = 0.15$, and it was used to estimate a $CV = 0.29$. **leve**

$$s_u = \left(\frac{V_s}{7.93}\right)^{1.59} \quad (kPa) \quad (A.44)$$

where the shear wave velocity, V_s must be introduced in m/s

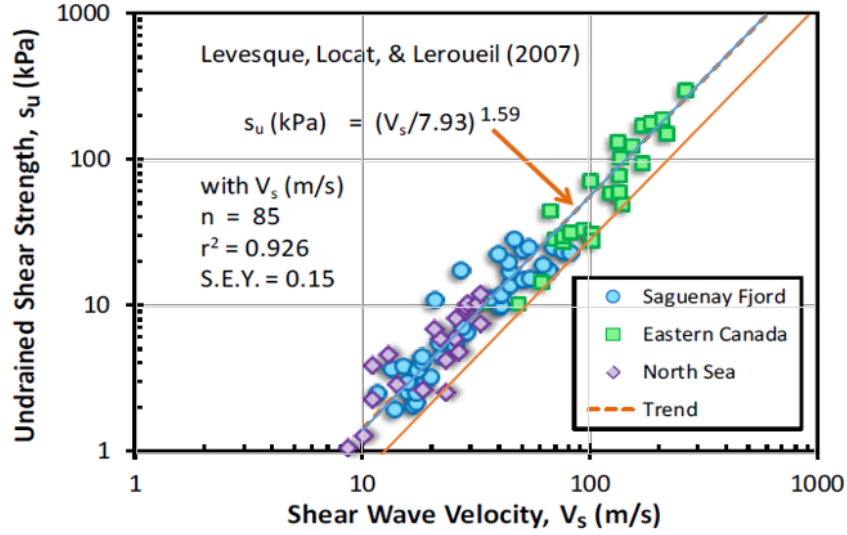


Figure A.16: Levesque et al. (2007) relation for s_u from V_s , retrieved from Mayne 2014 . CV estimated from the provided statistics.

A.1.7 Undrained shear strength factors

Different correlations are known that relate CPTu parameters to the undrained shear strength s_u . The following parameters are considered here:

Pore pressure factor:

$$N_{\Delta u} = \frac{u_2 - u_0}{s_u} \quad (\text{A.45})$$

Normalised expression for corrected cone resistance q_t :

$$N_{kt} = \frac{q_t - \sigma_v}{s_u} \quad (\text{A.46})$$

Expression relating tip resistance and pore pressure:

$$N_{ke} = \frac{q_t - u_2}{s_u} \quad (\text{A.47})$$

1. Karlsrud et al. (2005):

From 17 different sites of Norway, correlations were made comparing CPTu results against undrained triaxial compression strength and preconsolidation pressure. The soil samples are of very high quality and range from soft to medium stiff clays with plasticity index from 10 to 50% and sensitivity from 3 to 200. One of the study's conclusions is that the measured excess pore pressure gives the best and most consistent correlation to the measured undrained strength Karlsrud et al. 2005.

For low sensitive clays ($S_t < 15$)

$$N_{\Delta u} = 6.9 - 4.0 \log(OCR) + 0.07(I_p) \quad I_p \text{ in } \% \quad (\text{A.48})$$

For high sensitive clays ($S_t > 15$)

$$N_{\Delta u} = 9.8 - 4.5 \log(OCR) \quad (\text{A.49})$$

The reported variability of the undrained shear strength using this correlation is $\pm 10-15\%$. Since the estimation of s_u from the definition of the factors is analytical, e.g., [A.49](#), the inclusion of the reported variability is introduced in APD on the factors' correlations and not in the s_u one. Therefore, the equations [A.48](#) and [A.49](#) will be introduced with a $CV = 0.0625$. Similar approach is used for the factors N_{kt} and N_{ke} from this publication.

For low sensitive clays ($S_t < 15$)

$$N_{kt} = 7.8 + 2.5 \log(OCR) + 0.082I_P \quad (\text{A.50})$$

For high sensitive clays ($S_t > 15$)

$$N_{kt} = 8.5 + 2.5 \log(OCR) \quad (\text{A.51})$$

The reported variability is of $\pm 15\%$ for equation [A.51](#) and $\pm 30\%$ for equation [A.50](#). Therefore a $CV = 0.075$ and $CV = 0.15$ for equations [A.51](#) and [A.50](#) is adopted correspondingly.

For low sensitive clays ($S_t < 15$) with $N_{ke} = 2.0$ as a lower limit

$$N_{ke} = 11.5 - 9.05B_q \quad (\text{A.52})$$

For high sensitive clays ($S_t > 15$) with $N_{ke} = 2.0$ as a lower limit

$$N_{ke} = 12.5 - 11.0B_q \quad (\text{A.53})$$

The equations report a non constant variability depending on B_q . The variation in strength increase from $\pm 15\%$ at $B_q = 0.6$ to $\pm 33\%$ at $B_q = 0.9$. However, due to the impossibility of adding a variability based on the independent variable, a $CV = 0.25$ is chosen.

2. Mayne and Peuchen (2018):

The parameter N_{kt} is correlated to the pore pressure ratio B_q and shows a decrease of N_{kt} when B_q increases. The proposed equation is:

$$N_{kt} = 10.5 - 4.6 \ln(B_q + 0.1) \quad (\text{A.54})$$

The equation is also used by the Fugro company's software, allowing a bandwidth of $0.8N_{kt}$ and $1.15N_{kt}$. The complete soil data set includes normally consolidates, overconsolidated, and fissured clays; the reported variability is $CV = 0.256$. These statistics are given comparing the CPTu s_u to anisotropically-consolidated triaxial s_u . As the factor will be used with the theoretical equation [A.50](#), caution should be applied when using this on fissured clays [Mayne and Peuchen 2018](#).

Appendix B

Validation of plasticity index and liquid limit proposition

The identification number is referred to the published in Cetin and Ozan 2009. The header of the summarised data has the following denomination:

- q_t : Corrected cone tip resistance
- f_s : Sleeve resistance
- w_L : Liquid limit
- I_P : Plasticity index
- FC : Fines content
- Soil type: Classification under unified soil classification system (USCS)
- γ : volumetric unit weight calculated using Robertson 2010 equation.
- e_0 : calculated void ratio, assuming $G_s = 2.6$ and complete saturation
- w_0 : natural water content, assuming $G_s = 2.6$ and complete saturation
- I_L : liquidity index, estimated from Wood 1990 equation and assuming $s_{ur} = f_s$

Summary of equations

Estimation of volumetric weight, Robertson 2010

$$\gamma/\gamma_w = 0.27[\log(fs/qt)] + 0.36[\log(q_t/pa)] + 1.236 \quad (\text{B.1})$$

Assuming that $\gamma = \gamma_{sat}$ in equation B.1, complete saturation and a modification of the soil's volumetric weight of 2 kN/m^3 :

$$e_0 = \frac{\gamma_{sat} + 2 - G_s \gamma_w}{\gamma_w - \gamma_{sat} + 2} \quad (\text{B.2})$$

Assuming complete saturation:

$$w_0 = \frac{100\%e_0}{G_s} \quad (\text{B.3})$$

Liquidity index is defined as:

$$I_L = \frac{w_L - w}{I_P} \quad (\text{B.4})$$

Adapting Wood 1990 equation $s_{ur} \sim f_s$:

$$I_L = 1 - \log(f_s/2)/\log(100) \quad (\text{B.5})$$

Favre 1980 unique relation for I_P :

$$I_P = 0.73(w_L - 13) \quad (\text{B.6})$$

Rearranging the definition of I_L and equation B.6:

$$w_L = \frac{-0.73 I_P + I_P 0.73 I_P + w_0}{1 - 0.73 + I_P 0.73} \quad (\text{B.7})$$

Original Data from Cetin and Ozan 2009								Estimated Data					
Identification	Depth (m)	q_t (Mpa)	f_s (kPa)	w_L %	I_P %	FC	Soil type	γ (kN/m ³) modified	e_0 [-]	w_0 %	I_L [-]	w_L %	I_P %
2	2.91	0.69	24.75	65	35	100	CH	18.9	0.86	32.4	0.45	45.3	23.6
3	3.67	0.78	24.79	46	23	87	CL	18.9	0.85	32.0	0.45	44.6	23.1
10	2.85	0.75	25.51	51	23	100	CH	18.9	0.84	31.9	0.45	44.6	23.1
11	3.6	0.64	12.52	49	25	85	CL	18.0	1.05	39.6	0.60	50.5	27.4
13	5.26	0.74	11.31	43	20	95	CL	18.0	1.07	40.2	0.62	50.5	27.4
19	10.8	1.68	74.64	62	40	10	CH	20.5	0.57	21.5	0.21	32.8	14.5
26	3.56	0.96	36.61	74	45	99	CH	19.5	0.74	28.0	0.37	40.9	20.4
32	4.59	0.75	24.24	48	27	91	CL	18.9	0.86	32.3	0.46	45.0	23.3
33	5.39	1.23	23.03	42	18	100	CL	19.0	0.83	31.3	0.47	42.9	21.8
35	2.86	1.05	39.88	64	42	99	CH	19.6	0.72	27.1	0.35	39.9	19.6
38	2.76	0.7	31.98	45	22	99	CL	19.2	0.80	30.1	0.40	43.4	22.2
39	4.89	1.22	25.14	40	15	88	CL	19.1	0.81	30.5	0.45	42.3	21.4
41	7.98	1.6	29.34	67	36	98	CH	19.4	0.75	28.5	0.42	39.9	19.7
44	3.6	0.69	12.71	35	12	95	CL	18.1	1.04	39.2	0.60	50.0	27.0
47	1.38	0.9	5.97	33	14	81	CL	17.3	1.26	47.4	0.76	54.6	30.4
49	3.01	0.31	5.23	50	26	99	CH	16.7	1.45	54.6	0.79	62.1	35.8
54	4.09	2.86	22.49	31	12	96	CL	19.3	0.77	29.1	0.47	39.1	19.0
59	4.77	0.88	26.61	61	33	95	CH	19.1	0.82	31.0	0.44	43.5	22.3
64	4.73	1.5	17.96	33	13	81	CL	18.8	0.87	33.0	0.52	43.6	22.4
66	9.3	1.54	29.46	53	27	100	CH	19.4	0.76	28.5	0.42	40.1	19.8
67	10.29	2.04	34.12	48	29	98	CL	19.7	0.70	26.6	0.38	37.7	18.0
71	7.75	1.48	29.66	58	31	99	CH	19.4	0.76	28.6	0.41	40.2	19.9
72	8.81	1.25	23.67	40	18	95	CL	19.1	0.82	31.0	0.46	42.6	21.6
73	9.76	1.18	28.84	48	24	99	CL	19.3	0.78	29.5	0.42	41.5	20.8
74	11.24	1.4	38.82	51	30	98	CH	19.7	0.70	26.6	0.36	38.6	18.7
76	1.81	1.26	8.86	41	16	97	CL	17.9	1.09	41.0	0.68	49.6	26.7
79	4.28	1.09	10.89	53	33	97	CH	18.1	1.04	39.2	0.63	48.8	26.1
80	5.05	2.99	21.38	37	25	78	CL	19.3	0.78	29.4	0.49	39.2	19.1
84	1.39	0.53	25.08	43	23	75	CL	18.8	0.88	33.1	0.45	46.5	24.5
85	3.3	0.65	13.42	43	17	98	CL	18.1	1.03	38.8	0.59	49.9	27.0
86	4.13	0.75	15.74	70	37	100	CH	18.4	0.97	36.6	0.55	48.0	25.6
87	5.23	1.97	32.65	36	17	90	CL	19.6	0.72	27.0	0.39	38.2	18.4
89	6.86	1.83	25.82	41	21	90	CL	19.3	0.77	29.2	0.44	40.2	19.8
90	7.6	1.64	30.84	49	22	99	CL	19.5	0.74	28.0	0.41	39.5	19.3

Original Data from Cetin and Ozan 2009								Estimated Data					
Identification	Depth (m)	q_t (Mpa)	f_s (kPa)	w_L %	I_P %	FC	Soil type	γ (kN/m^3) modified	e_0 [-]	w_0 %	I_L [-]	w_L %	I_P %
92	11.29	1.52	53.34	70	46	98	CH	20.1	0.64	24.0	0.29	35.9	16.7
93	1.29	0.93	33.85	73	48	99	CH	19.4	0.76	28.8	0.39	41.6	20.9
96	5.1	3.04	40.11	43	33	94	CL	20.0	0.65	24.4	0.35	34.7	15.8
103	4.34	0.82	30.66	75	44	99	CH	19.2	0.79	30.0	0.41	42.9	21.8
105	8.8	1.16	33.72	66	40	100	CH	19.4	0.75	28.2	0.39	40.5	20.1
109	3.96	0.65	18.51	55	29	96	CH	18.5	0.94	35.4	0.52	47.6	25.3
110	4.7	1.16	33.21	62	32	94	CH	19.4	0.75	28.3	0.39	40.6	20.2
112	1.39	0.65	24.19	46	23	99	CL	18.8	0.87	32.8	0.46	45.7	23.9
115	4.9	0.81	21.98	46	21	98	CL	18.8	0.87	33.0	0.48	45.3	23.6
117	1.27	0.68	19.84	46	24	77	CL	18.6	0.92	34.6	0.50	46.9	24.7
123	1.49	0.94	47.68	63	39	99	CH	19.8	0.69	26.0	0.31	39.2	19.1
124	2.51	0.83	25.82	40	26	88	CL	19.0	0.83	31.5	0.44	44.0	22.7
125	3.27	0.98	31.86	40	27	88	CL	19.3	0.77	29.1	0.40	41.8	21.0
127	5.2	0.79	23.34	39	21	94	CL	18.9	0.86	32.5	0.47	45.0	23.3
134	3.19	0.77	23.49	48	26	98	CL	18.9	0.86	32.5	0.47	45.1	23.4
137	6.42	1.49	31.97	34	22	72	CL	19.5	0.74	28.0	0.40	39.7	19.5
140	9.63	1.05	50.29	68	44	99	CH	19.9	0.67	25.3	0.30	38.2	18.4
141	3.65	0.62	12.61	41	18	78	CL	18.0	1.05	39.7	0.60	50.6	27.5
143	2.49	1.03	42.71	58	35	98	CH	19.7	0.71	26.6	0.34	39.5	19.3
145	4.84	1.01	45.58	79	51	97	CH	19.7	0.69	26.2	0.32	39.1	19.1
146	5.79	2	85.09	75	50	99	CH	20.7	0.54	20.2	0.19	30.8	13.0
147	7.36	1.26	46.01	65	43	100	CH	19.8	0.68	25.5	0.32	37.9	18.2
148	8.36	0.97	24.37	44	25	99	CL	19.0	0.83	31.5	0.46	43.7	22.4
150	1.29	0.69	26.95	73	48	99	CH	19.0	0.84	31.6	0.44	44.7	23.1
153	5.08	2.71	37.29	43	33	94	CL	19.9	0.67	25.2	0.36	35.8	16.6
161	5.29	0.78	27.62	54	30	92	CH	19.1	0.82	31.0	0.43	43.9	22.5
166	3.54	2.03	20.81	39	14	98	CL	19.1	0.81	30.7	0.49	41.2	20.6
169	6.19	1.24	22.14	40	18	96	CL	19.0	0.84	31.6	0.48	43.1	22.0
170	7.04	1.33	30.67	40	16	97	CL	19.4	0.76	28.6	0.41	40.5	20.1
171	9.34	1.18	31.5	54	27	98	CH	19.4	0.76	28.7	0.40	40.9	20.4
172	1.28	0.65	42.64	64	36	95	CH	19.5	0.74	27.9	0.34	41.9	21.1
173	2.15	0.6	21.32	70	44	99	CH	18.6	0.91	34.3	0.49	47.0	24.8
174	3.18	1.07	14.89	33	16	88	CL	18.5	0.95	35.9	0.56	46.6	24.5
175	4.33	1.04	16.76	39	22	86	CL	18.6	0.92	34.8	0.54	45.9	24.0
180	1.3	1.47	58.88	64	38	97	CH	20.2	0.62	23.4	0.27	35.4	16.3
185	7	1.89	19.75	48.5	22	98	CL	19.0	0.83	31.4	0.50	41.9	21.1
186	8.35	0.79	25.14	65	40	100	CH	18.9	0.84	31.8	0.45	44.5	23.0
190	3.2	0.9	18.71	35	15	90	CL	18.7	0.91	34.2	0.51	45.9	24.0
195	1.29	0.45	19.3	42	20	89	CL	18.4	0.96	36.2	0.51	49.2	26.5
197	3.41	2.15	17.65	69	40	99	CH	18.9	0.85	32.0	0.53	42.1	21.2
198	4.19	0.73	19.66	34	12	92	CL	18.6	0.91	34.4	0.50	46.6	24.5
203	9.38	2.77	37.62	57	28	99	CH	19.9	0.66	25.1	0.36	35.6	16.5
204	1.26	0.54	25.16	39	19	87	CL	18.8	0.87	33.0	0.45	46.4	24.4
206	4.33	0.69	27.69	47	25	89	CL	19.0	0.83	31.4	0.43	44.5	23.0
213	4.95	0.74	38.49	59	35	97	CH	19.4	0.75	28.3	0.36	41.9	21.1
216	8.59	3.35	44.04	35	18	96	CL	20.2	0.62	23.5	0.33	33.6	15.0
217	1.2	0.63	27.51	53	30	98	CH	19.0	0.84	31.7	0.43	45.0	23.4
219	3.95	0.86	25.81	55	28	100	CH	19.0	0.83	31.3	0.44	43.9	22.5
223	8.29	1.19	42.42	60	36	100	CH	19.7	0.70	26.3	0.34	38.8	18.8
224	9.37	1.2	49.96	65	38	99	CH	19.9	0.66	25.0	0.30	37.6	18.0
261	4.15	0.52	9.58	45	23	89	CL	17.7	1.16	43.6	0.66	53.7	29.7
262	6.12	0.6	8.82	41	18	99	CL	17.6	1.17	44.0	0.68	53.6	29.6
263	4.36	0.58	11.04	39	17	93	CL	17.9	1.10	41.4	0.63	52.0	28.5
264	5.05	0.54	13.11	39	19	96	CL	18.0	1.05	39.7	0.59	51.1	27.8
265	10.07	1.68	106	39	19	82	CL	20.9	0.51	19.2	0.14	29.8	12.3
266	4.13	0.38	4.36	57	32	96	CH	16.6	1.50	56.5	0.83	62.6	36.2

Original Data from Cetin and Ozan 2009								Estimated Data					
Identification	Depth (m)	q_t (Mpa)	f_s (kPa)	w_L %	I_P %	FC	Soil type	γ (kN/m^3) modified	e_0 [-]	w_0 %	I_L [-]	w_L %	I_P %
267	5.23	0.38	5.98	58	32	86	CH	17.0	1.36	51.5	0.76	59.6	34.0
268	7.34	0.44	8.16	56	32	96	CH	17.4	1.23	46.4	0.69	56.0	31.4
269	8.55	0.46	8.91	55	34	96	CH	17.5	1.19	45.0	0.68	55.0	30.7
281	8.71	2.02	26.54	31	19	56	CL	19.4	0.76	28.6	0.44	39.5	19.4
282	9.65	1	14.17	35	17	90	CL	18.4	0.97	36.7	0.57	47.3	25.1
283	10.64	0.87	16.36	36	18	80	CL	18.5	0.95	35.7	0.54	47.0	24.8
289	9.25	0.69	21.33	41	21	77	CL	18.7	0.90	33.8	0.49	46.3	24.3
290	9.97	0.82	20.59	43	24	72	CL	18.7	0.89	33.6	0.49	45.7	23.8
295	18.3	1.7	57.88	52	25	99.8	CH	20.2	0.61	23.2	0.27	34.8	15.9
296	3.3	0.47	11.06	47	25	85.2	CL	17.8	1.12	42.3	0.63	53.1	29.3
297	5.26	0.46	5.69	44	22	84.8	CL	17.0	1.36	51.3	0.77	58.9	33.5
298	6.3	0.98	14.19	37	16	94.9	CL	18.4	0.97	36.7	0.57	47.4	25.1
299	7.8	1.19	26.88	42	19	91.5	CL	19.2	0.80	30.0	0.44	42.0	21.1
301	1.85	0.65	17.35	42	27	77	CL	18.4	0.96	36.1	0.53	48.1	25.6
302	3.85	1.74	60.73	30	11	68	CL	20.3	0.60	22.8	0.26	34.3	15.5
304	7.85	0.72	19.92	48	33	86	CL	18.6	0.91	34.3	0.50	46.6	24.5
313	5.8	1.01	48.2	35	15	74	CL	19.8	0.68	25.7	0.31	38.7	18.8
318	1.85	0.95	80.26	35	17	88	CL	20.4	0.59	22.2	0.20	35.3	16.3
322	1.8	1.07	54.24	70	50	95	CH	20.0	0.66	24.7	0.28	37.6	17.9
325	1.8	0.78	37.11	74	52	98	CH	19.4	0.76	28.5	0.37	41.9	21.1
326	3.85	2.1	33.87	45	29	88	CL	19.7	0.70	26.6	0.39	37.6	18.0
329	1.85	0.74	47	61	40	95	CH	19.7	0.71	26.7	0.31	40.5	20.1
330	3.85	0.69	42.02	40	24	76	CL	19.5	0.74	27.8	0.34	41.6	20.9
331	1.85	0.86	46.69	40	22	80	CL	19.7	0.70	26.4	0.32	39.8	19.5
332	3.85	0.74	29.65	44	25	88	CL	19.1	0.81	30.6	0.41	43.7	22.4
333	5.85	1.21	70.53	40	25	75	CL	20.3	0.60	22.6	0.23	35.0	16.0
336	1.8	0.82	68.57	33	15	70	CL	20.1	0.63	23.7	0.23	37.3	17.7
337	3.8	0.65	33.64	38	20	70	CL	19.2	0.79	29.8	0.39	43.5	22.2
346	2.73	1.42	35	36	9	80	ML	19.6	0.72	27.4	0.38	39.3	19.2
350	12.23	2.27	46.67	31	8	95	CL	20.1	0.64	24.0	0.32	35.0	16.0
369	4.78	0.95	30	30	8	N/A	CL	19.2	0.79	29.7	0.41	42.3	21.4
375	11.73	1.77	68.33	32	11	N/A	CL	20.4	0.58	21.9	0.23	33.3	14.8
376	12.73	1.99	75	32	11	N/A	CL	20.6	0.56	21.1	0.21	31.9	13.8
377	13.73	2.27	98.33	33	12	N/A	CL	21.0	0.51	19.1	0.15	28.9	11.6
378	14.78	2.3	108.3	28	13	N/A	CL	21.1	0.49	18.5	0.13	27.9	10.9
379	16.73	2.36	31.67	22	6	N/A	CL-ML	19.6	0.71	26.8	0.40	37.6	17.9
391	16.24	2.86	58.33	24	7.9	72	CL	20.4	0.58	21.9	0.27	32.2	14.0
392	17.74	2.26	33.33	28.2	10.5	76	CL	19.7	0.70	26.5	0.39	37.4	17.8
393	19.29	2.21	26.67	28.1	11.3	82	CL	19.4	0.75	28.4	0.44	39.1	19.0
394	20.79	2.55	46.67	34.5	14	90	CL	20.1	0.63	23.7	0.32	34.4	15.6
395	23.74	2.52	31.67	33.3	12.3	85	CL	19.7	0.71	26.6	0.40	37.3	17.7
397	26.79	3.5	66.67	30.8	11.2	78	CL	20.7	0.55	20.6	0.24	30.1	12.5
398	1.28	1.43	61.67	36.5	17.5	87	CL	20.2	0.61	23.1	0.26	35.1	16.2
399	5.73	1.71	38.33	33.1	11.6	60	CL	19.7	0.69	26.2	0.36	37.7	18.1
400	7.23	1.19	41.67	47.6	22.1	98	CL	19.7	0.70	26.4	0.34	38.9	18.9
401	8.75	0.91	18.57	37.2	15.9	98	CL	18.6	0.91	34.3	0.52	45.9	24.0
402	10.23	0.97	23.33	41.2	20.2	99	CL	18.9	0.85	31.9	0.47	44.0	22.6
403	11.78	0.7	8.33	23.8	6.8	90	CL	17.6	1.17	44.1	0.69	53.2	29.4
408	12.27	1.25	26.67	31.9	10.4	96	CL	19.2	0.79	30.0	0.44	41.8	21.0
409	13.32	1.33	20	30.6	11.3	80	CL	18.9	0.86	32.3	0.50	43.5	22.2
410	14.77	2.25	95	30.9	10.9	80	CL	20.9	0.51	19.3	0.16	29.2	11.9
411	16.27	3.41	128.3	32.4	13.9	85	CL	21.4	0.44	16.7	0.10	24.0	8.0
422	17.75	1.53	60	29.9	11.1	75	CL	20.2	0.61	23.1	0.26	35.0	16.1
423	19.23	2.03	55	41.9	16.3	96	CL	20.2	0.61	23.1	0.28	34.3	15.5
427	2.78	0.82	10	36.9	14.3	95	CL	17.9	1.09	41.3	0.65	50.9	27.7
429	10.28	1.88	28.33	35.3	14.3	97	CL	19.4	0.75	28.3	0.42	39.4	19.3

Original Data from Cetin and Ozan 2009								Estimated Data					
Identification	Depth (m)	q_t (Mpa)	f_s (kPa)	w_L %	I_P %	FC	Soil type	γ (kN/m^3) modified	e_0 [-]	w_0 %	I_L [-]	w_L %	I_P %
433	20.75	1.59	44.29	41.5	16.2	93	CL	19.9	0.67	25.2	0.33	37.1	17.6

Appendix C

Oedometer and Triaxial simulation results

C.1 Oedometer simulation

The simulated oedometer test is compared with the laboratory one. Two simulations are run, one with the merged layer resulted from the stratification algorithm and another one with local CPT data corresponded to a small layer that includes the sample depth. The reported effective stress is also shown. It can be seen that in the proximity of the effective stress, a good approximation is obtained if the slopes are compared. The model Hardening soils with small strain stiffness, HSsmall is used in the simulations.

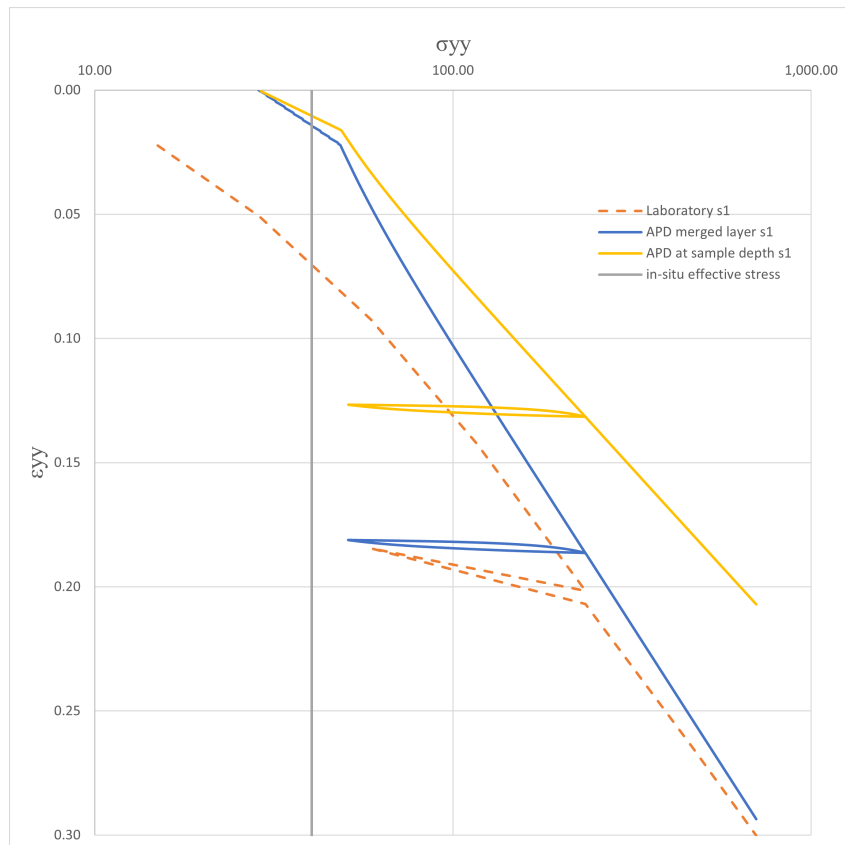


Figure C.1: Oedometer simulation of sample number 1

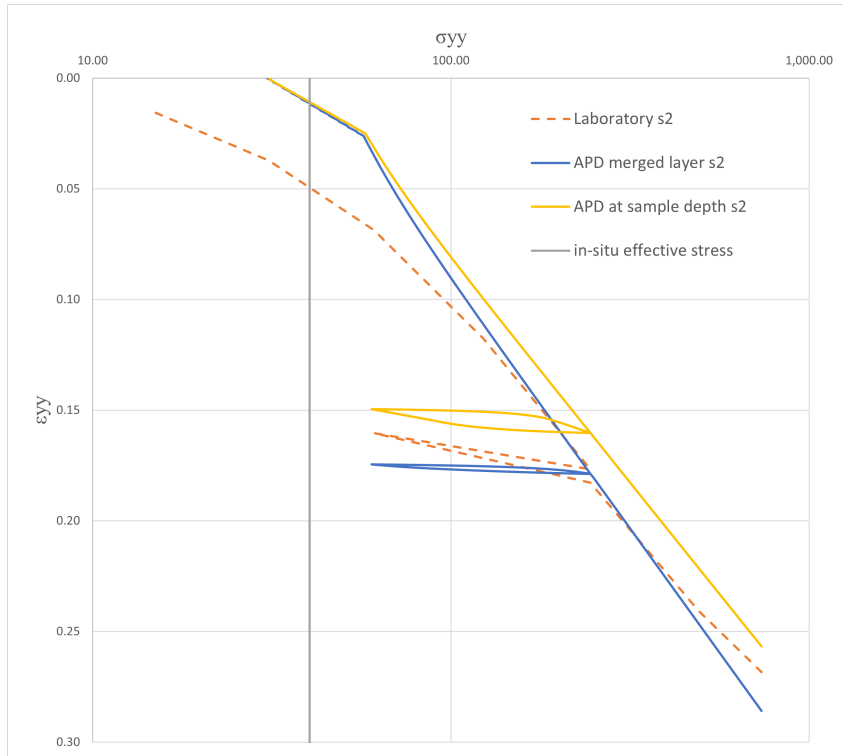


Figure C.2: Oedometer simulation of sample number 3

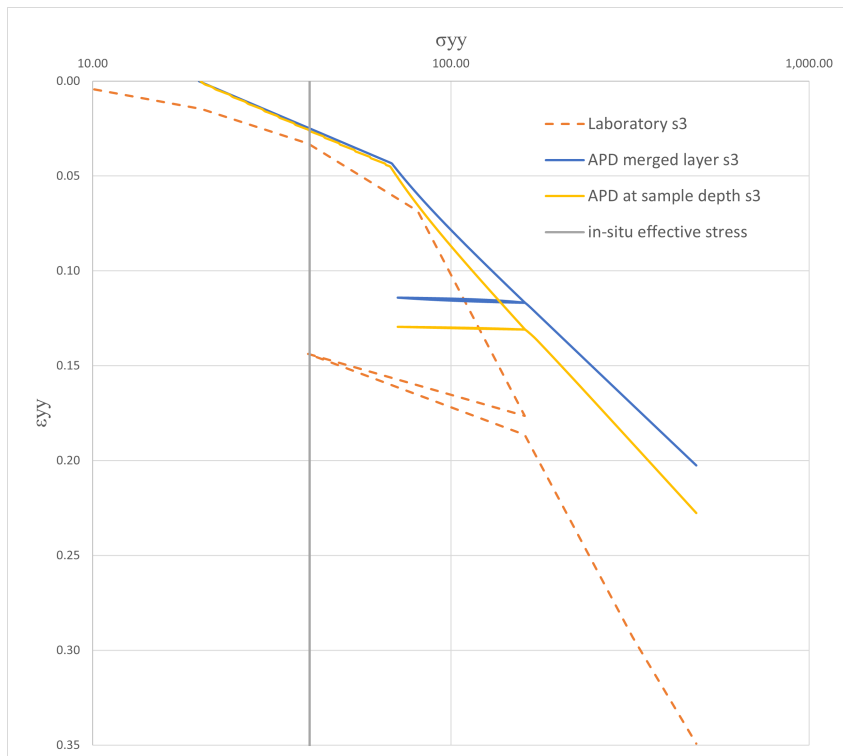


Figure C.3: Oedometer simulation of sample number 3

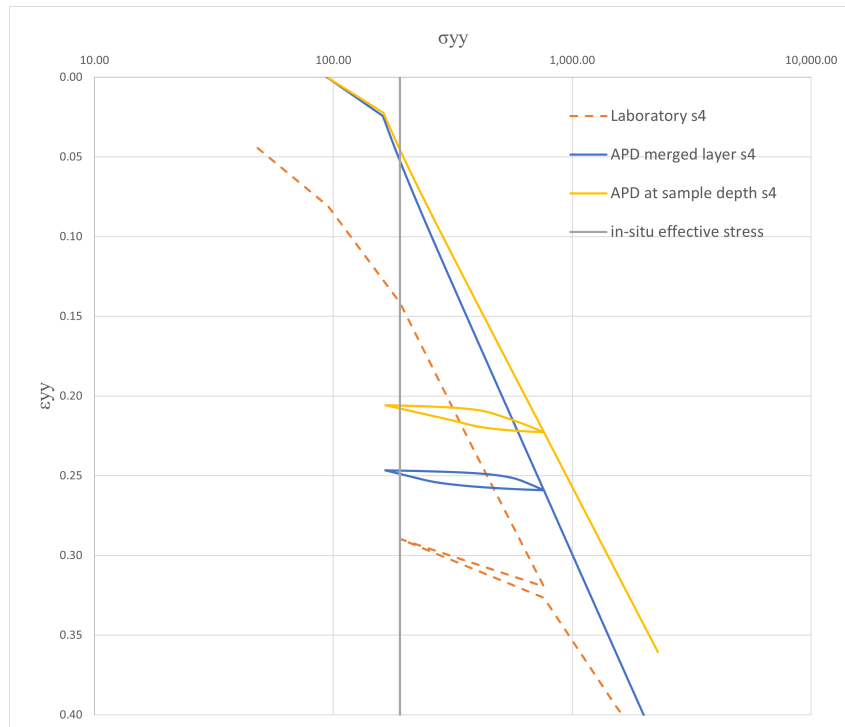


Figure C.4: Oedometer simulation of sample number 4.

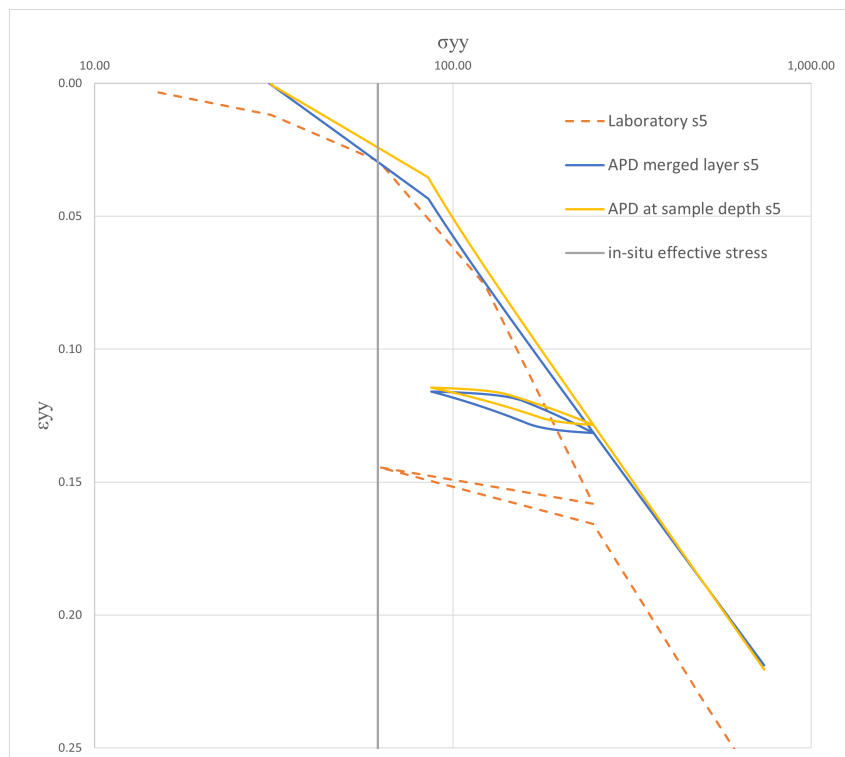


Figure C.5: Oedometer simulation of sample number 5.

C.2 CAU simulation

The same initial effective stress are used in the simulation and the laboratory CAU test. Similar to the oedometer simulation, the model Hardening soils with small strain stiffness, HSsmall is used in the simulations.

In this case, no modification of the friction angle is applied to show the underprediction of the existing correlations in the bibliography. The reported ϕ' is above 35° , and the existing correlations for clays do not surpass the 30° .

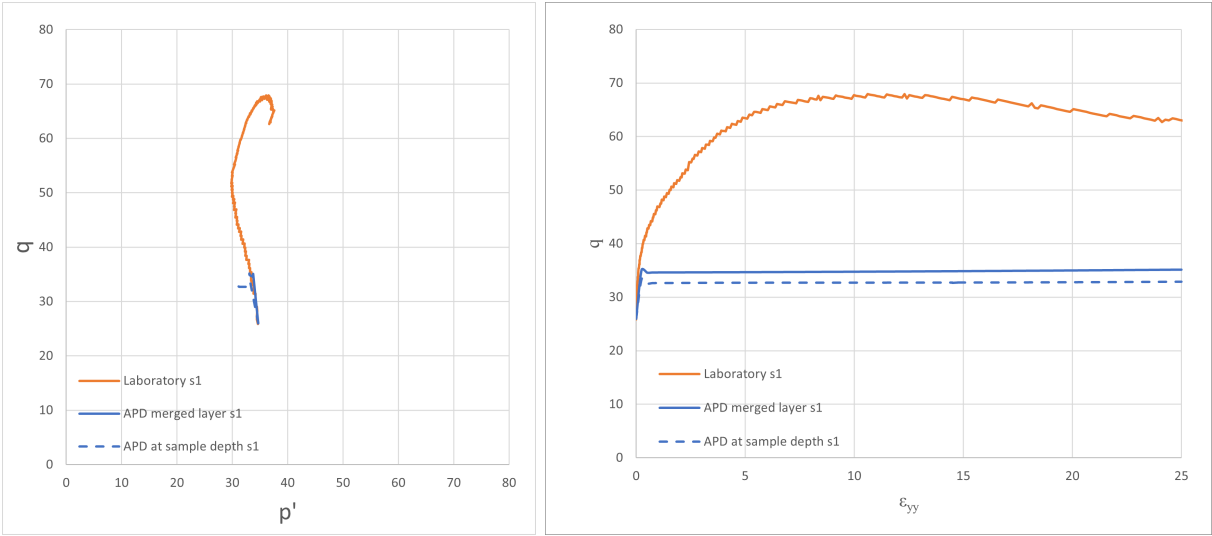


Figure C.6: CAU triaxial simulation using APD framework compared to laboratory test for sample s1.

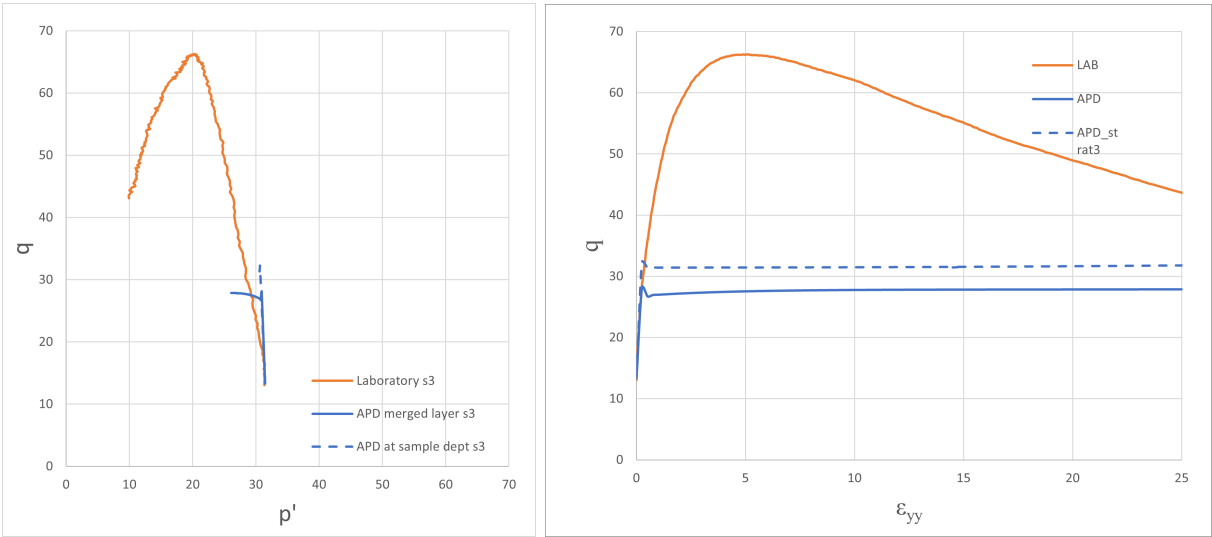


Figure C.7: CAU triaxial simulation using APD framework compared to laboratory test for sample s3.

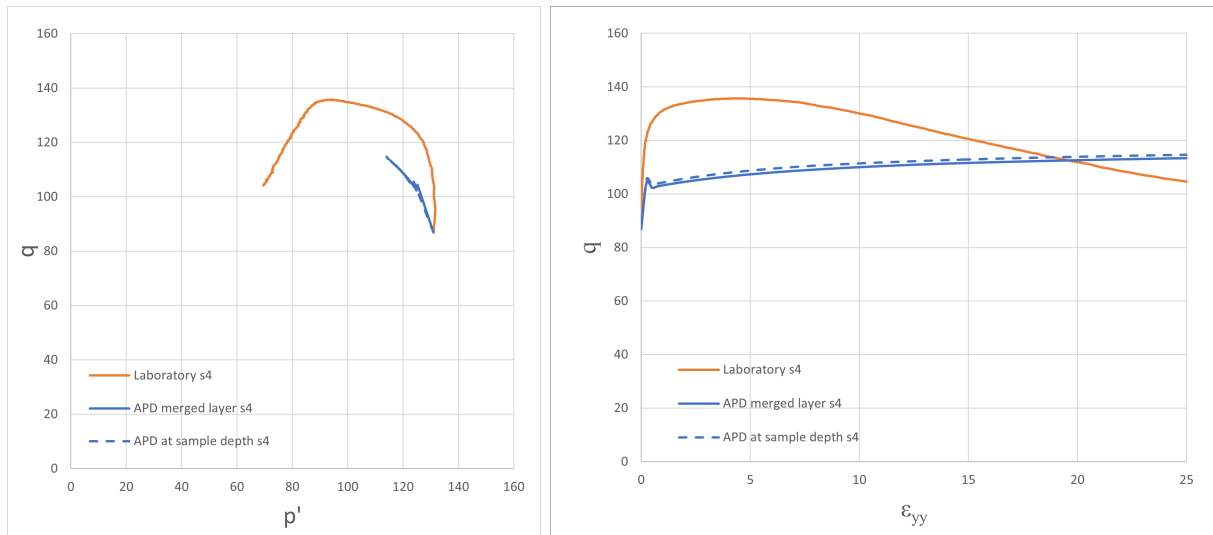


Figure C.8: CAU triaxial simulation using APD framework compared to laboratory test for sample s4.

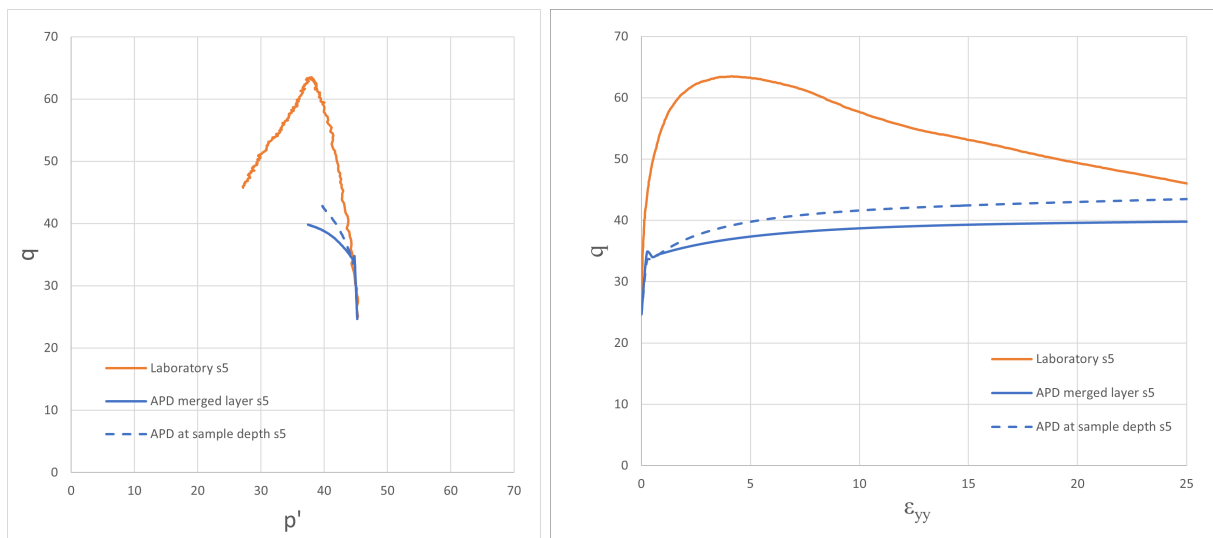


Figure C.9: CAU triaxial simulation using APD framework compared to laboratory test for sample s5.

C.3 Summary of APD's parameters output

The more relevant parameters resulting from the APD framework are summarised in table C.3. In the table, is noted as *Layer* the resulted parameter of a layer that includes the Oedometer and Triaxial samples, but they are not necessarily thin enough to only include that soil layer, e.g. the layer thickness is one meter but the samples are taken from 30 cm soil-layer. The column that is denominated *Local*, it only accounts for a soil layer of dimensions 30 - 50 cm, that includes the triaxial and oedometer samples.

	s1			s2			s3			s4			s5		
	LAB	Layer	Local	LAB	Layer	Local	LAB	Layer	Local	LAB	Layer	Local	LAB	Layer	Local
q_c [kPa]	545	740	446	545	446	446	481	546	654	860	472	386	472	386	386
q_t [kPa]	556	752	458	556	458	458	483	547	662	868	523	435	523	435	435
f_s [kPa]	33.56	59.62	17.47	33.56	17.47	17.47	16.43	33.18	27.25	53.52	12.05	9.27	12.05	9.27	9.27
u_2 [kPa]	47.14	45.30	48.33	47.41	48.33	48.33	4.78	0.64	19.00	19.45	201.17	196.10	201.17	196.10	196.10
R_f [%]	5.40	7.89	3.81	5.40	3.81	3.81	3.16	5.67	4.14	5.57	2.13	2.14	2.13	2.14	2.14
Q_{tm} [-]	10.50	15.26	8.18	10.50	8.18	8.18	10.62	13.76	2.08	3.12	6.81	5.61	6.81	5.61	5.61
F_r [-]	6.36	8.90	4.70	6.36	4.70	4.70	3.74	6.49	6.61	7.95	2.70	2.84	2.70	2.84	2.84
U_2 [-]	0.14	0.16	0.15	0.14	0.15	0.15	-0.93	-0.96	-0.07	-0.07	2.44	2.53	2.44	2.53	2.53
Bq [-]	0.02	0.01	0.02	0.02	0.02	0.02	-0.09	-0.08	-0.04	-0.03	0.40	0.45	0.40	0.45	0.45
u_0 [kPa]	38.50	40.90	38.44	42.50	41.39	41.39	35.20	34.13	33.44	33.64	48.80	47.56	48.80	47.56	47.56
γ_{sat} [kN/m ³]	16.10	14.61	13.11	16.10	15.98	15.98	13.30	14.51	16.64	15.66	16.50	15.23	16.50	15.23	15.23
w_0 [%]	72.60	56.44	84.06	64.50	40.25	40.25	112.50	57.91	34.37	43.53	59.10	48.39	59.10	48.39	48.39
e_0 [-]	1.92	1.50	2.23	1.71	1.07	1.07	2.98	1.53	0.91	1.15	1.57	1.28	1.57	1.34	1.28
z_{top} [m]	-3.13	-2.96	-3.06	-3.53	-3.34	-3.34	-3.52	-3.23	-4.06	-2.96	-6.05	-5.52	-6.05	-4.90	-5.52
z_{bot} [m]	-3.13	-3.94	-3.34	-3.53	-3.66	-3.66	-3.52	-4.91	-3.71	-4.20	-6.05	-6.52	-6.05	-8.00	-6.52
σ_{eff} [kPa]	58.50	45.22	43.89	45.22	45.31	45.31	38.03	34.86	203.85	204.39	61.70	58.59	61.70	60.84	58.59
σ_{tot} [kPa]	86.11	82.33	86.70	86.11	86.70	86.70	77.94	68.99	237.29	238.03	112.63	106.16	112.63	112.63	106.16
OCR [-]	0.87	3.62	5.24	3.62	2.90	2.90	4.09	5.12	1.13	1.54	1.41	1.94	1.41	2.38	1.94
σ_p [kPa]	51.0	165.02	224.7	59.50	165.02	134.15	71.00	168.47	196.73	264.72	87.00	108.00	87.00	134.85	108.00
E_{50}^{ref} [kPa]	1034	1053	1053	1034	1154	1154	1293	1124	1343	1150	1271	2010	1271	1271	2010
E_{ood}^{ref} [kPa]	1034	1053	1053	1034	1154	1154	1293	1124	806	690	1271	1206	1271	1271	1206
E_{ur}^{ref} [kPa]	6664	6814	6814	6664	6961	6961	7891	7825	6093	5620	5908	7305	5908	5908	7305
G_0 [kPa]	19075	25550	25550	19075	14916	14916	14830	19055	22451	31492	10513	8548	10513	10513	8548
V_s [m/s]	109	131	94	109	94	94	97	109	112	134	92	83	92	92	83
G_0^{ref} [kPa]	46212	52323	40209	46212	40209	40209	42278	51986	26954	32092	23909	21651	23909	23909	21651
k_0 [-]	0.91	1.11	0.82	0.91	0.82	0.82	0.92	1.05	0.41	0.48	0.72	0.67	0.72	0.72	0.67
LL [-]	73.73	110.2	55.32	73.73	55.32	55.32	59.51	72.24	78.48	86.91	58.03	57.73	86.91	58.03	57.73
PI [-]	46.79	64.9	37.11	46.79	37.11	37.11	36.87	44.94	61.19	63.75	36.19	37.04	63.75	36.19	37.04
ϕ_{CV} [deg]	26.87	26.0	27.74	26.87	27.74	27.74	27.98	27.15	25.71	25.30	28.00	27.81	25.30	28.00	27.81
ϕ_p [deg]	26.87	26.0	27.74	26.87	27.74	27.74	27.98	27.15	25.71	25.30	28.25	27.87	25.30	28.25	27.87
s_u [kPa]	33.95	51.40	41.05	51.40	41.05	41.05	33.15	54.02	57.84	79.31	31.75	27.37	79.31	33.09	27.37
C_c [-]	0.61	0.89	0.46	0.61	0.46	0.46	0.48	0.59	0.74	0.79	0.47	0.47	0.79	0.47	0.47
S [-]	1.14	1.64	0.91	1.14	0.91	0.91	0.83	1.55	0.28	0.39	0.51	0.47	0.39	0.54	0.47

Table C.1: Summary of five clay Calais A layers compared to the resulted *Layer* of the stratification program and the customised layer *Local* correspondent to a small layer at the sample depth *LAB*